DEVELOPMENT OF FOAM GENERATORS FOR ALUMINIUM FOAM PRODUCTION FOR AUTOMOTIVE APPLICATIONS

YOK NUSOM

A THESIS SUBMITTED IN PARTIAL FULFILLMENT

OF THE REQUIREMENT FOR THE DEGREE OF

MASTER OF ENGINEERING IN AUTOMOTIVE ENGINEERING

(INTERNATIONAL PROGRAM)

INTERNATIONAL COLLEGE

KING MONGKUT'S INSTITUTE OF TECHNOLOGY LADKRABANG

2010

KMITL-2010-IC-M-004-004

Thesis Title	Development of Foam Generators for Aluminium foam Production for Automotive Applications
Student	Mr. Yok Nusom
Student ID.	50061922
Degree	Master of Engineering
Program	Automotive Engineering (International Program)
Thesis Advisor	Dr. Nattawoot Depaiwa
	Dr. Sompong Srimanosaowapak
	Prof. Dr. Tadaharu Adachi

ABSTRACT

This work was carried out to develop foam generators for aluminium foam production based on the gas injection method. Physical water model and Computational Fluid Dynamics simulation were used to understand the physics of foam generated by various designed impellers. Based on numerous foaming experiments and simulation using water as a testing fluid, three foam generators with different impeller and foam vessel designs were developed. Experimental results of foaming in water show that the size of bubbles and the extent of foams were controlled by the gas flow rate, impeller rotation speed and impeller design. The foam extent increased with increasing gas flow rate whereas all impellers gave approximately identical bubble sizes. The impeller equipped with a stator was found to reduce the rotational momentum of water. The water within the vessel was split into stationary and rotating portions by the stator resulting in a shear and vortex free liquid surface and hence permitting bubbles to accumulate. Bubble diameter in the range of 3-7 mm and the foam extent in the range of 0-160 mm were produced. Two foam generators having a rectangular foam vessel with side exit and a tri-cylindrical foam vessel were developed for sheet and mold aluminium foams respectively. Aluminium foam samples can be successfully produced using the latter foam generator. At one operation, this foam generator can simultaneously produce three identical aluminium foams with cylindrical shape. The bubble size and foam extent of the produced aluminium foams were 2-4 times larger and up to 2.5 times smaller, respectively, than those of water. All in all, it is suggested that the foam generator comprising of an impeller and a stator is most favourite for foaming.

ACKNOWLEDGEMENTS

This thesis could not be completed without the assistance of many persons to whom I would like to express my sincere appreciation.

First, I would like to sincerely thank my advisor, Dr. Sompong Srimanosaowapak , who has given me many helpful suggestions, useful advice and fruitful discussion during the undertaken research.

I would also like to sincerely thank Dr. Nattawoot Depaiwa and Prof. Dr. Tadaharu Adachi for Suggestions and Discussion.

Moreover, I would like to acknowledge National Metal and Materials Technology Center (MTEC) for providing laboratory equipments and instruments as well as a financial supporting.

Some of this work has already been presented at conferences or filed for patents as follows:

1. Y. Nusom, N. Depaiwa, T. Adachi and S. Srimanosaowapak, "Comparative Study of Bubble Formation between Water and Molten Aluminium for Manufacturing of Aluminium Foam", *ICMAT 2009 - International Conference on Materials for Advanced Technologies*, 28 June - 3 July 2009, Singapore, p. 28 – 29 (Oral).

2. Y. Nusom, N. Depaiwa, T. Adachi and S. Srimanosoawapak, "Aluminium Foams towards Automotive Industry Implementation in Thailand", Published in CD Proceeding of *ICAE – 5 – International Conference on Automotive Engineering*, 30 March – 2 April 2009, Bangkok, Thailand, 2:1 – 7 (Oral).

3. S. Srimanosaowapak and Y. Nusom, "Foam Generator with Controllable Bubble Feeding Direction", Patent Application No. 0901005077, Thailand Department of Intellectual Property, Filed on 13 November 2009.

4. S. Srimanosaowapak, Y. Nusom and P. Wattanapornphan, "Apparatus for Metallic Foam Component Production in a Multi-Cavity Mold", Patent Application No. 1001000069, Thailand Department of Intellectual Property, Filed on 15 January 2010.

I am grateful to National Science and Technology Development Agency (NSTDA), which provided the full scholarship for my Master degree study.

Finally, I am very grateful to my family for all love, caring, understanding and motivation throughout my life.

Yok Nusom

CONTENTS

CONTENTS (CONT.)

CONTENTS (CONT.)

CONTENTS (CONT.)

LIST OF TABLE

LIST OF FIGURE

LIST OF FIGURE (CONT.)

LIST OF FIGURE (CONT.)

LIST OF FIGURE (CONT.)

LIST OF FIGURE (CONT.)

LIST OF FIGURE (CONT.)

LIST OF FIGURE (CONT.)

LIST OF FIGURE (CONT.)

LIST OF FIGURE (CONT.)

LIST OF FIGURE (CONT.)

LIST OF FIGURE (CONT.)

CHAPTER 1

INTRODUCTION

1.1 Background

At present, the amount of fossil fuel is continuously reduced because of the highly increased demand and its limited existence. Fossil fuel is the main energy source used in automotive vehicles, it is therefore vital to improve fuel consumption efficiency of the automotive vehicles. Apart from the requirement of fuel efficiency improvement, safety is also another issue necessary to be concerned. Light weight materials with good crashworthiness behaviour are therefore being developed worldwide.

Aluminium foam is an interesting candidate material for using as a structural material in future automotive vehicles. It has a combination of good properties required for the automotive vehicles such as high energy absorption, light weight and good thermal efficiency. An automotive vehicle with structures made of aluminium foam will undoubtedly consume less fuel. The ability of high energy absorption of aluminium foam is also especially promising for impact absorption applications in the automotive vehicles.

While good properties of aluminium foam provide automotive manufacturers wider alternative designs. Irregular microstructures, which lead to inhomogeneous mechanical behaviour, and high material price, however, impede aluminium foam to overcome existing materials. Thus, there is a challenging requirement for producing a finer and more uniform cell structure aluminium foam in order to capture the intrinsic average in mechanical behaviour and to receive more commercial incentive. In Thailand, there is no any aluminium foam manufacturer, the development of low cost foaming process with controllable microstructures of aluminium foam is therefore required.

There are many processes for metal foam production, e.g. powder and melt routes. For aluminium foam, the melt route process using a gas injection into molten metal has been known as the most cost effective process for large scale production. However, small cell size and uniform structure are rather difficult to be obtained, and a near net shape automotive component

has not yet been produced by using this method. These obstructions are required to solved in order to increase the use of aluminium foam in automotive industries.

This research aims to develop a gas injection device and investigate related physical parameters of foaming in order to receive aluminium foams with a controllable structure. Physical model based on water and numerical simulation are used for designing the device and studying foam formation to receive essential design parameters for the development of the gas injection device for actual aluminium foam production. Impeller configuration, impeller rotation speed and gas flow rate are main parameters concentrated in this work.

1.2 Objectives

1.2.1 To investigate effects of physical parameters of fluid on foaming behaviour.

1.2.2 To investigate effects of gas injection parameters on foaming behaviour of water.

1.2.3 To develop a gas injection device for aluminium foam production.

1.3 Scopes of Research

1.3.1 Physical model using water as a testing fluid was used to investigate the effects of processing parameters on foaming behaviour of different impeller. Impeller configuration, impeller rotation speed and gas flow rate are main parameters focused in this research. Behaviours of fluid under rotation of impellers were studied using, COSMOSFloWork, a computational fluid dynamic software.

1.3.2 Results of foaming in water were used to design a gas injection device for foaming.

1.4 Benefits

1.4.1 To receive essential information on device design and processing parameters affecting foaming.

1.4.2 To understand the differences of foaming behaviour between water and molten aluminium.

1.4.3 To obtain a prototype of gas injection device for aluminium foam production.

1.4.4 To provide a low cost method for producing aluminium foam to be used as an alternative material for automotive industries.

CHAPTER 2

LITERATURE REVIEW

2.1 Aluminium Foam

Aluminium foam is an interesting material for automotive industries because it has a combination of various good properties such as high energy absorption, light weight and good thermal management. Based on structure, it can be classified into two groups: closed cell and open cell. Aluminium and its alloys are most used metals for making metallic foams owing to their light weight, excellent strength and high stiffness to weight ratios, recyclability and low melting temperature.

2.1.1 Aluminium Foam Productions

There are a number of methods for producing aluminium foam. Based on raw material type, aluminium foam production can be classified into two groups: liquid and solid state, as shown in **Figure 2.1** (Banhart, 2001). The list of the current manufacturers for aluminium-based foams is given in **Table 2.1**. Details, advantages and disadvantages of the production methods are described below.

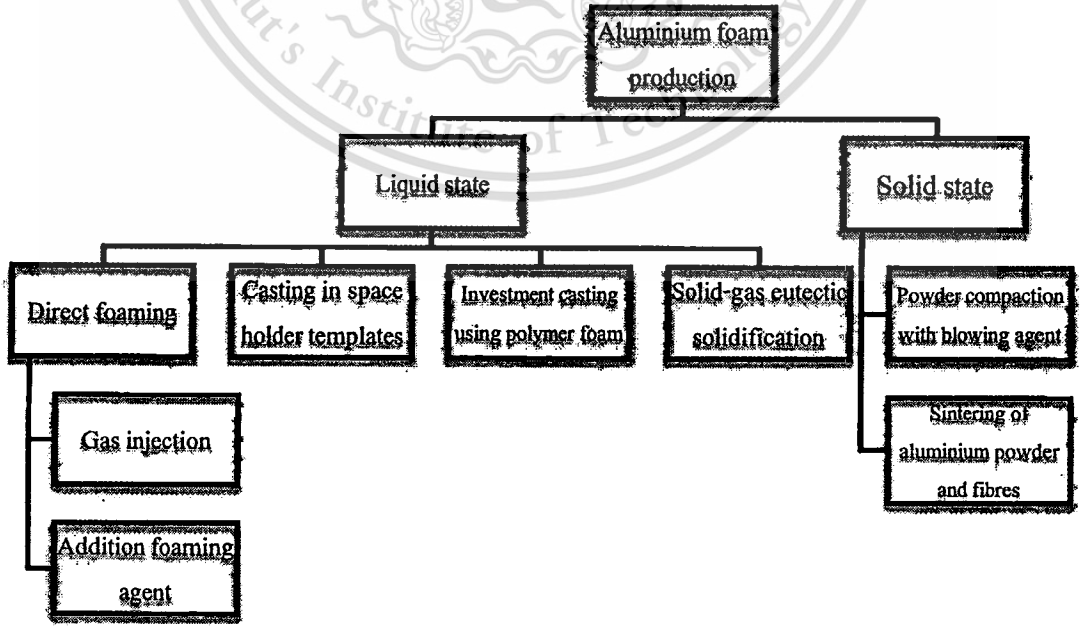

Figure 2.1 Aluminium foam production routes (Banhart, 2001).

Table 2.1 Basic foaming routes for metallic foams and current manufacturers for aluminium-based foams (Banhart, 2007).

Direct foaming	Melt alloy make alloy foamable create gas bubbles collect foam solidify foam	Indirect foaming	Prepare foamable precursor remelt precursor create foam solidify foam
Manufacturers *(products)*	Cymat, Canada *(SAF)* Foamtech, Korea *(Lasom)* Hütte Kleinreichenbach (HKB), Austria *(Metcomb)* Shinko-Wire, Japan *(Alporas)* (Distributor: Gleich, Germany)	Manufacturers *(products)*	alm, Germany *(AFS)* Alulight, Austria *(alulight)* Gleich-IWE, Germany Schunk, Germany

2.1.1.1 Direct Foaming in Molten Metal

Direct foaming is the method for producing metallic foam by generating bubbles in molten metal. The generated bubbles are required to be stabilised with the addition of ceramic powders or alloying elements to increase the viscosity of the molten metal (Babcsan *et al.*, nd). This foaming method can be used for producing aluminium, magnesium and zinc foam (Banhart, 2001). Nowadays, bubbles can be generated in a molten metal by direct gas injection or foaming agent addition

2.1.1.1.1 Direct Gas Injection

This foaming method has been used for producing aluminium and its alloys foam. Silicon carbide, aluminium oxide and magnesium oxide particles are ceramic powders currently used for viscosity enhancement in aluminium melt (Banhart, 2001). The foaming production, as summarised in **Figure 2.2**, starts with the injection of gas such as air, nitrogen or argon into the viscous aluminium melt through a specially designed impeller or vibrating nozzle for generating fine bubbles. The bubbles accumulating on the top surface of the melt are then taken out and solidified into a solid foam. **Figure 2.3-Figure 2.4** show examples of commercial direct gas injection processes for producing aluminium foams namely "Cymat" and "Metcomb", respectively. **Figure 2.5** shows another direct gas injection process being developed in a laboratory for producing a near net shape aluminium foam prototype. Advantages of these direct gas injection processes are low cost compared to other foaming methods and continuous foam production ability. However, size and distribution of gas bubbles are difficult to be controlled by using these foaming processes.

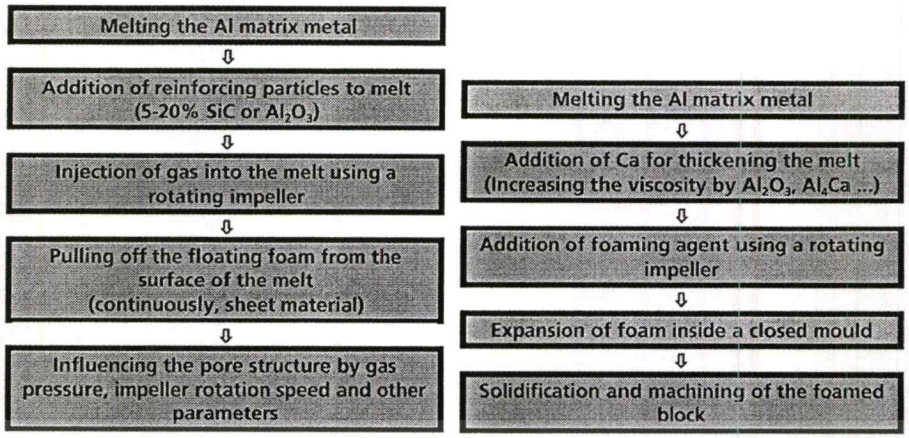

Figure 2.2 Diagram of direct foaming of melts: (a) MMC foams and (b) Alporas (Banhart, n.d.).

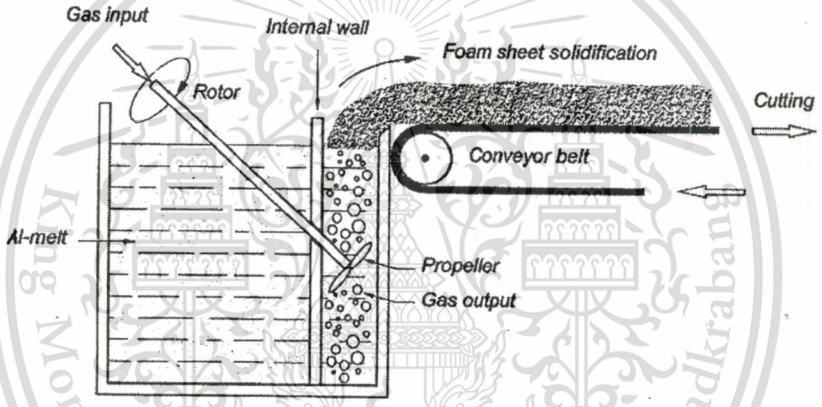

Figure 2.3 Schematic of "Cymat" direct gas injection (Banhart, 2001).

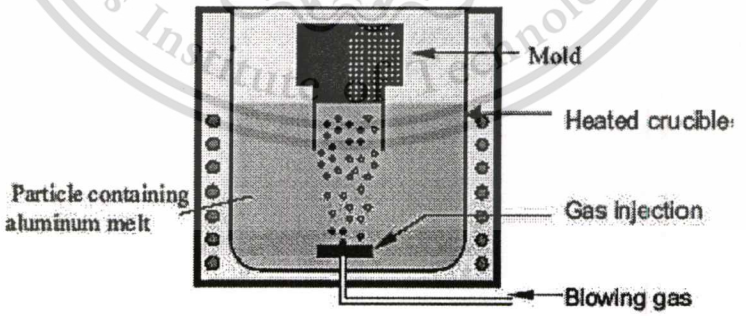

Figure 2.4 Schematic of "Metcomb" direct gas injection foaming method (Banhart, 2006).

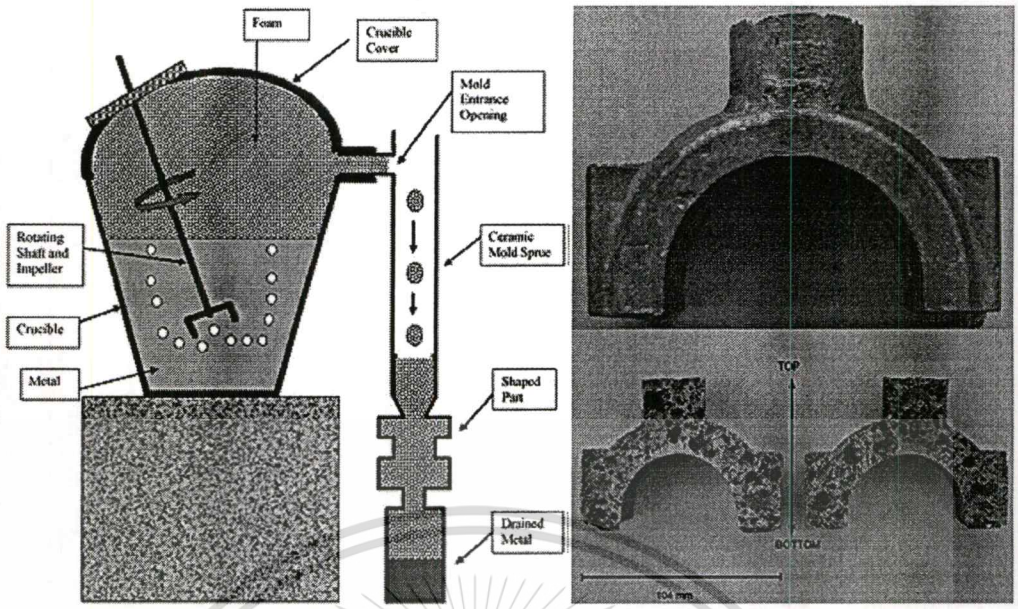

Figure 2.5 Diagram of Celal Cingi *et al.*'s aluminium foam production and a foam prototypes (Cingi *et al.*, 2009).

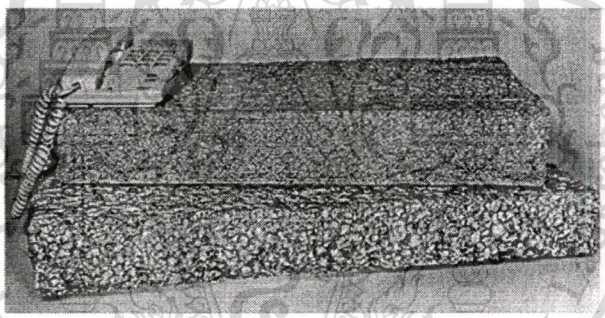

Figure 2.6 Foam slabs of two different densities and cell sizes produced by the direct gas injection method (Banhart, 2001).

The direct gas injection foaming method can produce aluminium foams with densities 0.07-0.54 g/cm^3, average cell sizes 3-25 mm and wall thicknesses 50-85 μm (Banhart, 2001; Deqing *et al*, 2006). **Figure 2.6** shows an example of aluminium foam slabs with different densities and cell sizes produced by the direct gas injection method.

A number of parameters, such as foam vessel volume, gas injection (Deqing *et al.*, 2006), melt properties and impeller design (Oak *et al.*, 2002), have been found to affect the final structure of aluminium foams produced by the direct gas injection foaming method. Viscosity enhancement of molten metal is necessary in order to restrict bubbles from too quickly rising and breaking, and hence make the foam structure more uniform. Diameter and distribution of gas

bubbles in the melt depend on the type and speed of impeller, and the flow rate of the injected gas. Cell size of closed cell aluminium foam has been found to increase with increasing gas flow rate and impeller speed and decrease with increasing melt viscosity (Deqing *et al.*, 2006).

2.1.1.1.2 Foaming Agent Addition

Metallic melts can be foamed by adding a foaming agent to generate bubbles (Cingi *et al*, 2009 and Babcsan *et al.*, n.d.). Bubbles can be generated by the release of gas of the foaming agent (Babcsan *et al.*, n.d.). The first step of the production of aluminium foam is to increase the viscosity of aluminium melt by the addition of 1.5 wt. % calcium at 680 °C (Banhart, 2001) follow by stirring for 5-10 minutes with an impeller at the rotation speed of 400-500 rpm (Cingi *et al.*, 2009). The effect of stirring time and the amount of calcium addition on the viscosity enhancement in aluminium melt is shown in **Figure 2.7** (Babcsan *et al.*, n.d.). After that, 1.6 wt% titanium hydride (TiH_2) is added into the melt as a foaming agent for bubble generation. The melt soon starts to expand slowly and gradually in the foaming vessel as shown schematically in **Figure 2.8**. After cooling the vessel below the melting temperature of the aluminium, the liquid foam turns into solid and can be taken out of the vessel for further processing. A commercial aluminium produced by this method is called "Alporas" giving more uniform structure but more expensive than that of the direct gas injection method (Banhart, 2000). Magnesium and its alloy foams can also be produced using $CaCO_3$ as a foaming agent (Yang *et al.*, 2007).

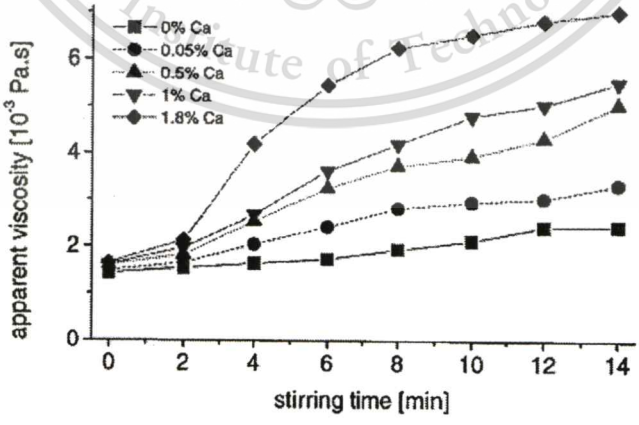

Figure 2.7 Influence of stirring time on the viscosity of an aluminium melt after admixture of calcium metal (Babcsan *et al.*, n.d.).

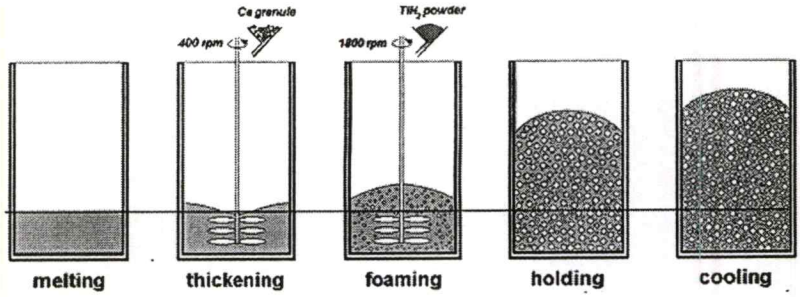

Figure 2.8 Direct foaming of melts using TiH_2 as a foaming agent (Song and Nutt, 2007).

2.1.1.2 Solid-Gas Eutectic Solidification ("Gasar/Lotus")

The principle of this foaming method is based on the difference of gas solubility of liquid and solid metals. A melt with saturated is dissolved gas, e.g. hydrogen or nitrogen, under high pressure (up to 50 bar), forms a foam after solidification at a low pressure as a result of the precipitation of gas at the solidification front. The full foaming process is summarised in **Figure 2.9**. **Figure 2.10** shows, for example, the pore structure of a Gasar foam produced by this method.

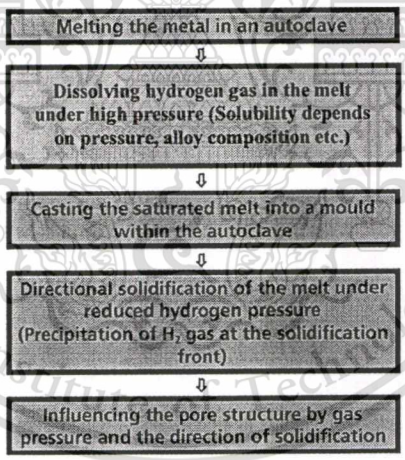

Figure 2.9 Diagram of foaming metals by the Gasar process (Banhart, n.d.).

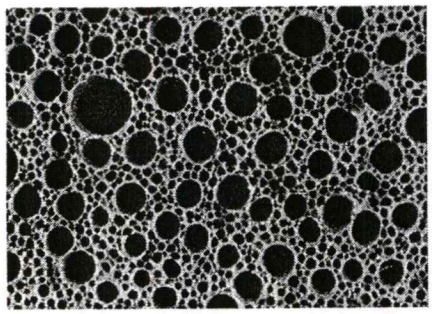

Figure 2.10 Pore structure of a "Gasar" foam (Banhart, 2001).

2.1.1.3 Casting in Space Holder Templates

Aluminium foam can be produced by casting molten metal in inorganic or even organic granules or hollow spheres. The granules remained in the metallic product after casting can then be removed by solvents, acids or thermal treatments (see **Figure 2.11**).

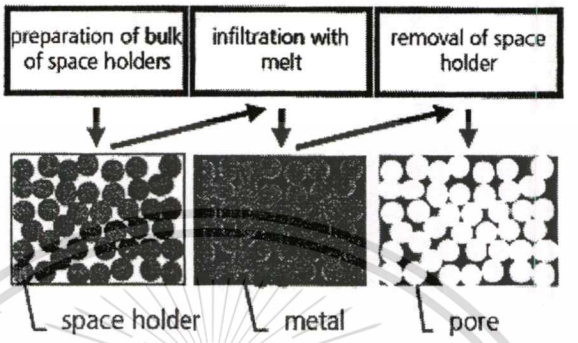

Figure 2.11 Production of cellular metallic materials using a space-holder template (Banhart, 2001).

Fired clay pellets, soluble salts, loose bulks of expanded clay granules, sand pellets, foamed glass spheres and aluminium oxide hollow spheres can be used as inorganic space holder templates and polymer spheres can be used as organic space holder template (Banhart, 2000; Banhart, 2001).

Figure 2.12 shows a possible way for making "syntactic foams". In this case, commercially available alumina hollow spheres diameters of 2.1–3.6 mm are used. The bulk of spheres are infiltrated by magnesium melts at about 700 °C. The structure of the produced foam is very uniform and the foam properties are nearly isotropic. Sandwich panels can also be made by this method.

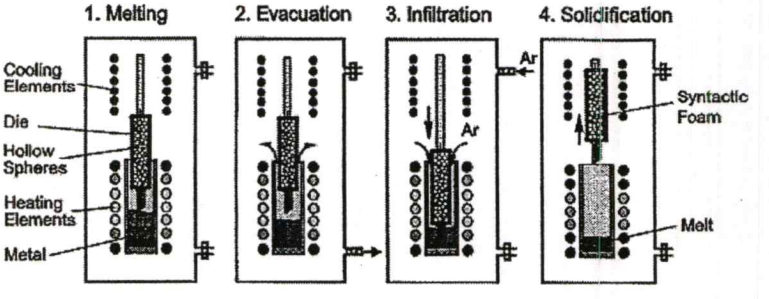

Figure 2.12 Process steps for making a syntactic foam (Banhart, 2001).

One of the main advantages of using space holder template is the close control of the pore size distribution which is given by the distribution of particle sizes of the filler granules. However, the maximum porosities which can be achieved are limited to values below 80% (Banhart, 2001).

2.1.1.4 Investment Casting using Polymer Foam

Foams can be manufactured from a molten metal without direct foaming the metal. Polymer foam, e.g. polyurethane foam, can be used as a template material for metallic foam production as shown in **Figure 2.13** and **Figure 2.14**. If the polymer foam has closed pores, it has to be transformed into an open porous one by a reticulation treatment. Slurry of sufficiently heat resistant material, e.g. a mixture of mullite, phenolic resin and calcium is filled in the polymer foam and the foam is removed by thermal treatment. Molten metal is subsequently cast into the resulting open voids which replicate the original polymer foam structure. After the removal of the mould material, e.g. by pressurised water, a cellular material is obtained. Difficulties of this process include the achievement of a complete filling of the slurry, the control of the directional solidification and the removal of the mould material without damaging the foam structure.

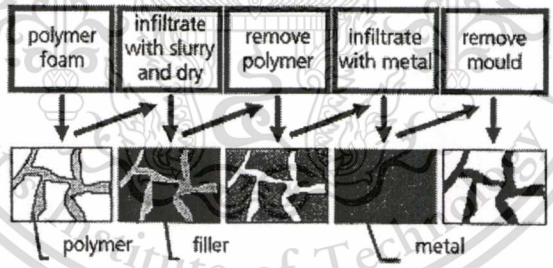

Figure 2.13 Production of cellular metals by investment casting (Banhart, 2001).

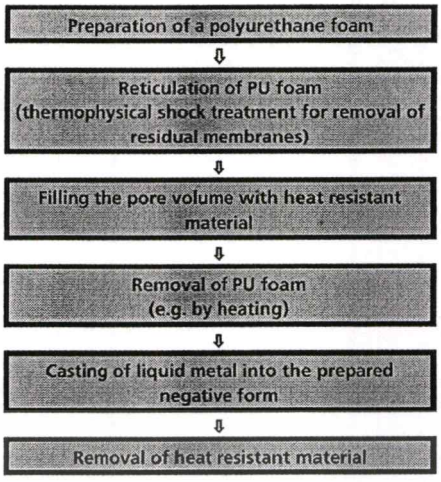

Figure 2.14 Diagram of making metallic foams by investment casting (Banhart, n.d.)

Figure 2.15 shows a micrograph of an aluminium foam made by investment casting technique. Commercial aluminium foams produced by this method is called ''Duocel'' which is developed by a Japanese company. The numbers of cell are ranging from 2-16 pores/cm (5–40 ppi). Aluminium alloys such as 6101 or AlSi7Mg (A356) and other metals, such as copper and magnesium can be used to produce metallic foams using this method.

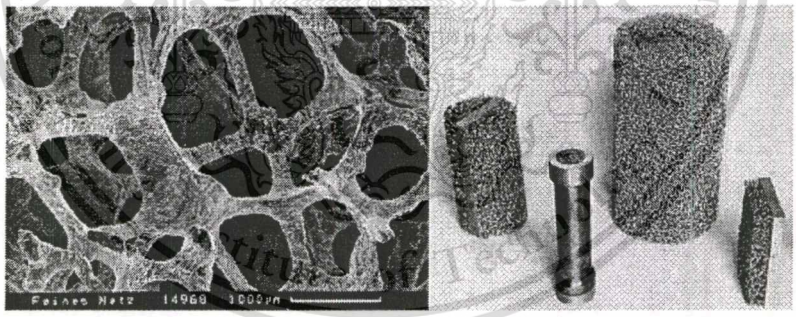

Figure 2.15 Left: SEM image of "Duocel", right: some aluminium foam products made by investment casting (Banhart, 2001).

2.1.1.5 Powder Compaction Technique

This foaming method is often called "powder metallurgical process" whose processing steps are shown in **Figure 2.16**. The production process begins from the mixing of metal powders with a foaming agent, followed by compaction the mixture into a dense material called a precursor material. Several methods can be used for the compaction such as hot uniaxial or isostatic compressing and extrusion, as shown in **Figure 2.17**. However, the extrusion method

seems to be the most economical method (Banhart, 2001; Babcsan *et al.*, n.d.). "Foam-in-Al" and "Alulight" are commercial aluminium foams made by this method (Babcsan *et al.*, n.d).

After heating the precursor material at a temperature near the melting temperature of the base metal, the foaming agent will release gas and forces the compacted precursor material to expand and form to a foam (Banhart, 2001; Koza *et al.*, 2003). The advantage of this foaming method is the possibility to produce near net shape lightweight parts. The foaming method itself combined with the excellent energy absorption ability, makes the produced foams especially attractive for automotive industries, i.e. a lifting and conveying systems of a truck (Koza *et al.*, 2003).

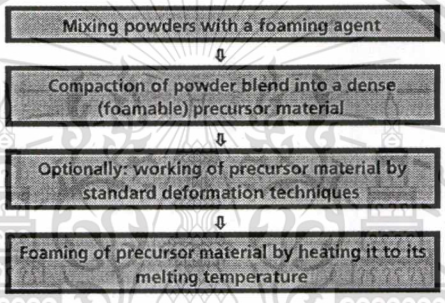

Figure 2.16 Diagram of powder metallurgical process for making metallic foams (Banhart, n.d.).

There are several factors influencing this foaming method. A key of the method is the use of an appropriate foaming agent which releases gas at the right temperature to ensure high expansion and the formation of a uniform porosity (Matijasevic and Banhart, 2006). Expansion and density of foam can be controlled by adjusting the heating temperature and the heating rate. For this method, titanium or zirconium hydride can be used as a foaming agent for making zinc and aluminium alloy foam. Aluminium, tin, zinc, brass, lead, gold and other metals can be foamed by using this foaming method provided that a right foaming agent is used. (Banhart, 2001; Babcsan *et al.*, n.d.). **Figure 2.18** and **Figure 2.19** show expansion of aluminium foams. Foam expansion starts at about 590–640 °C depending on the pre-treatment conditions of TiH_2.

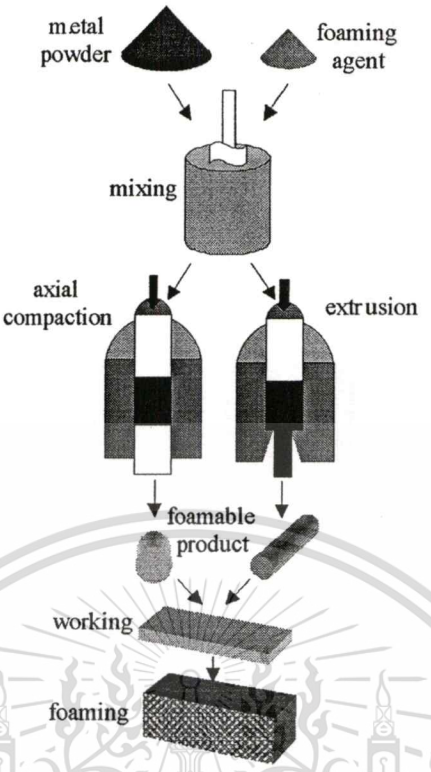

Figure 2.17 Powder compaction process for making foam (Srivastava and Sahoo, 2007).

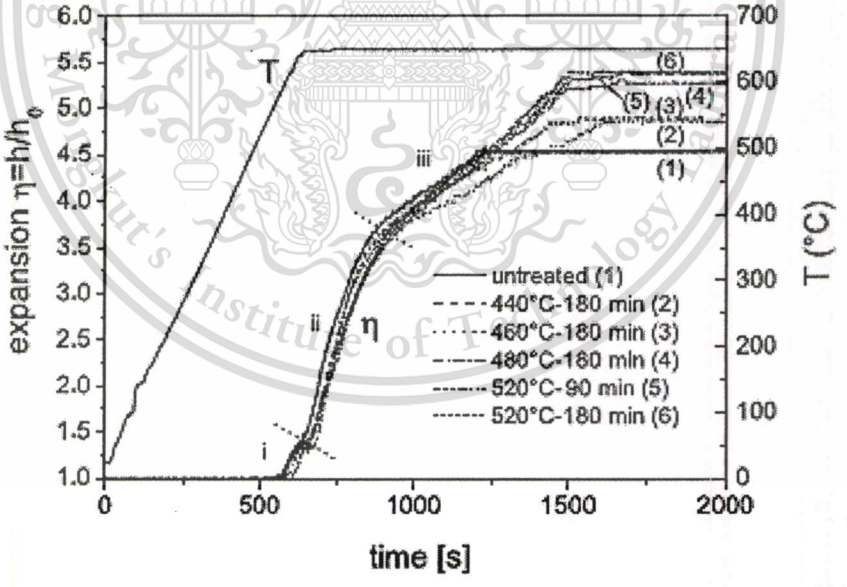

Figure 2.18 Expansion curves of precursors based on six different modifications of TiH_2 (Matijasevic and Banhart., 2006).

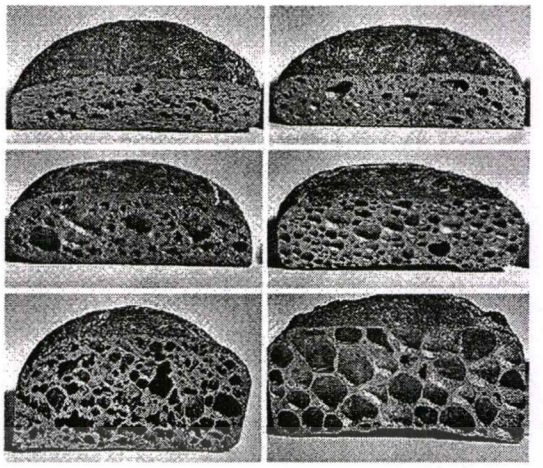

Figure 2.19 Aluminium foams after expansion to a height of approx. 2, 2.5 and 4 times of the height of the original precursor (from top to bottom). Foams with, left column: untreated TiH_2, right: TiH_2 treated at 520 °C for 180 min. Sample width is 36 mm (Matijasevic and Banhart, 2006).

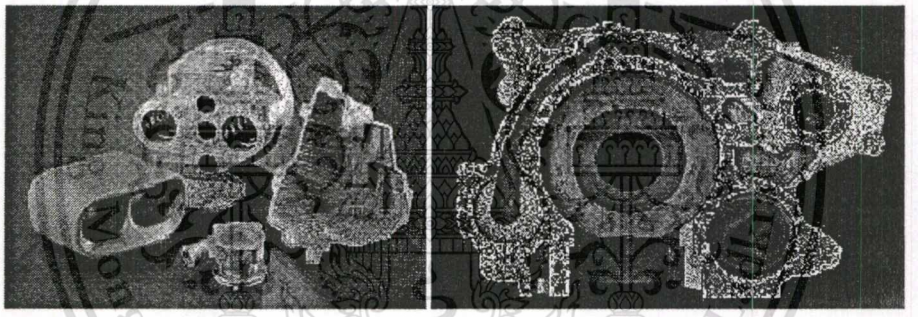

Figure 2.20 Various complex shaped aluminium foam products (Simancik and Schoerghuber, 1998).

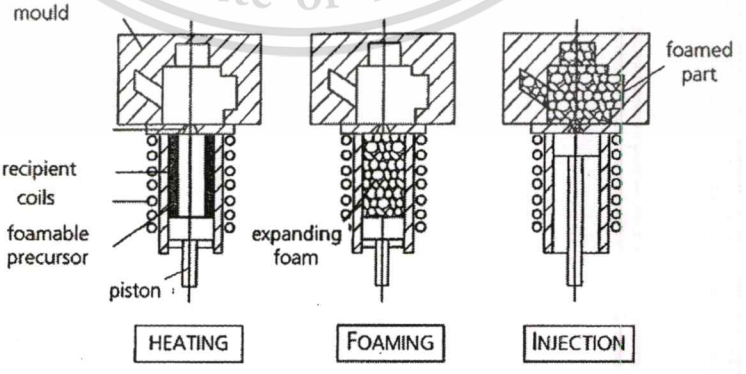

Figure 2.21 Foam injection process

Complex shaped aluminium foam products, as shown in **Figure 2.20**, can be produced by injection moulding technique, as shown in **Figure 2.21**, which is a combination process between the powder metallurgical and casting method (Simancik and Schoerghuber, 1998). The key aspect of this combined process is the rapid cool of the mould to prevent collapse of the foamed structure (Simancik, 2001).

2.1.1.6 Sintering of Aluminium Foam Powders

This foaming method is simple as metallic powder are only compacted and sintered. This foaming method is mostly used for bronze (Cu89Sn11) by sintering at around 820 °C to obtain porosities between 20 and 50% with comparatively low strength. An example of a bronze foam produce by this method is shown in **Figure 2.22**.

Making aluminium foam from alloy powders or granules by this method is more difficult because aluminium is usually covered by a dense oxide layer which prevents the powders or granules from sintering together. To avoid this problem, the powders or granules have to be pressed to break up the oxide films and to create metallic bonding between the powders. **Table 2.2** summarises all available processes for metallic production.

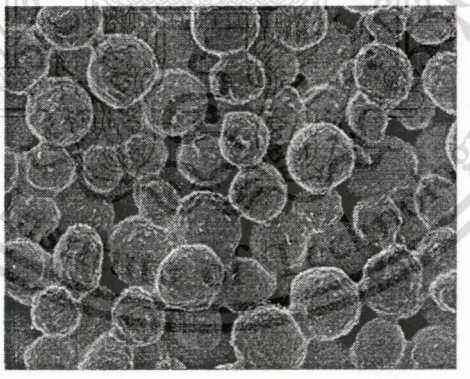

Figure 2.22 Porous sintered bronze made from particles with about 100 μm in diameter (Banhart, 2001).

Table 2.2 All available production processes for making metallic foam (Banhart, 2001).

Category	Process	Achievable porosity (%)	Metal	Commercially available
Liquid state processing	-Direct foaming by gas injection	80 – 97.5	Al, Zn	Yes
	-Direct foaming with blowing agents	91 – 93	Al, Zn	Yes
	-Gasars	5 – 75	Ni, Cu, Al, Mg	No
	-Powder compact melting	60 – 90	Al, Zn, Pb	Yes
	-Investment casting using polymer foams	80 – 97	Al, Zn	Yes
	-Lattice block materials		Al	No
	-Casting around space holders	<65	Al, Zn, Pb, Cu	Yes
	-Spray foaming	<60	Steel, Cu	No
Solid state processing	-Sintering of powders and fibres	20 – 80	Bronze, steel	Yes
	-Gas entrapment	<45	Ti	No
	-Foaming of slurries	<93	Al	No
	-Powder pressing around space holders	<70	Ti	No
	-Hollow sphere structures	<80	Steel	No
	-Powder/binder techniques		Fe, Cu	No
	-Reaction sintering	<50	TiAl, FeAl	No
Electro-deposition	Electro-deposition	92 - 95	Ni, Cu	Yes
Vapour deposition	Vapour deposition	93 - 97	Ni, Ni-Cr, Cu	Yes

2.1.2 Properties of Closed Cell Aluminium Foam

Aluminium foam has a combination of good properties such as high energy absorption, light weight and sound absorption. In automotive industries, aluminium foam has been interested due to its good energy absorption and light weight properties. **Table 2.3** shows properties of commercial aluminium foams. Properties of aluminium foam depend on production method, cell size and density, as shown in **Figure 2.23-Figure 2.29**. Service temperature also affects the mechanical properties of the foam, as shown for example in **Figure 2.30**, in that the compressive strength of ALPORAS foams decreases with increasing service temperatures (Aly, 2007).

Table 2.3 Properties of commercial aluminium foams (Andrews *et al*,. 1999).

	Alporas	Cymat	Alulight	Incofoam	Duocel
Relative density	0.07-0.2	0.03-0.2	0.1-0.35	0.03-0.04	0.05-0.1
Young's modulus (GPa)	0.4-1	0.02-2.0	1.7-12	0.4-1.0	0.06-0.3
Poisson's ratio	0.31-0.34	0.31-0.34	0.31-0.34	0.31-0.34	0.31-0.34
Elastic limit (MPa)	1.6-1.8	0.04-7.0	2.0-20	0.6-1.1	0.9-2.7
Tensile strength (MPa)	1.6-1.9	0.05-8.5	2.2-30	1.0-2.4	1.9-3.5
compressive strength (MPa)	1.3-1.7	0.04-7.0	1.9-14	0.6-1.1	0.9-3.0
Thermal conductivity (W/m.K)	3.5-4.5	0.3-10	3.0-35	0.2-0.3	6.0-11
Thermal expansion (10-6/K)	21-23	19-21	19-23	12-14	22-24

Energy absorption is one of the most required the most properties of automotive material. **Figure 2.23-Figure 2.24** show the dependency of density, cell size and stress level on the energy absorption capacity of aluminium foams. The absorption of energy can be calculated by integrating the area under the stress-strain curve as given by the equation 2.1 (Miyoshi *et al.*, 1999; Ramanurty and Paul, 2004; Yu *et al.*, 2007).

$$W = \int_0^{\epsilon} \sigma(\varepsilon) d\epsilon \qquad (2.1)$$

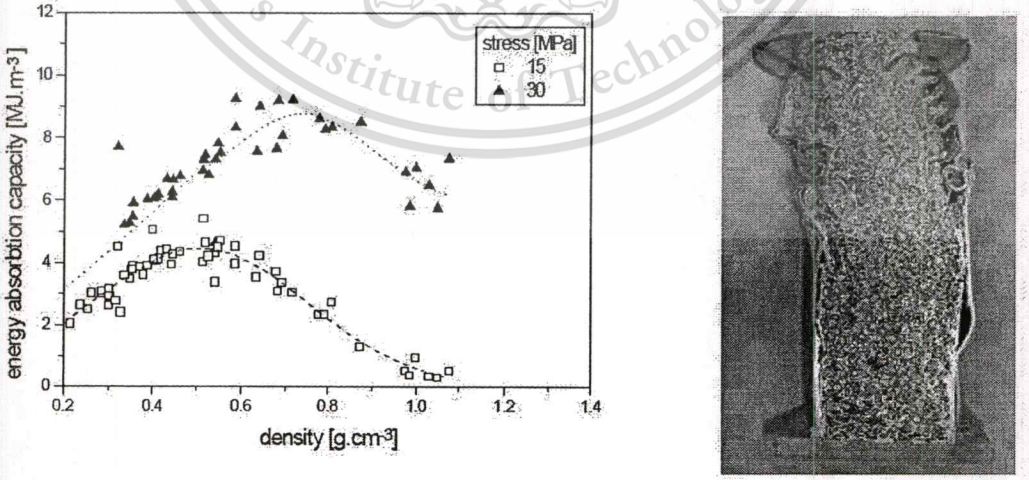

Figure 2.23 The foam density giving maximum energy absorption depends on allowed stress level (left). The foamed motor carrier after frontal impact (right) (Simancik, 2001).

Another interesting property of Aluminium foam is sound absorption. **Figure 2.28** shows the close match of the sound absorption coefficient of Aluminium foam with PU-foam and glass fibre materials, and the possibility to increase the sound absorption coefficient at particular sound frequencies.

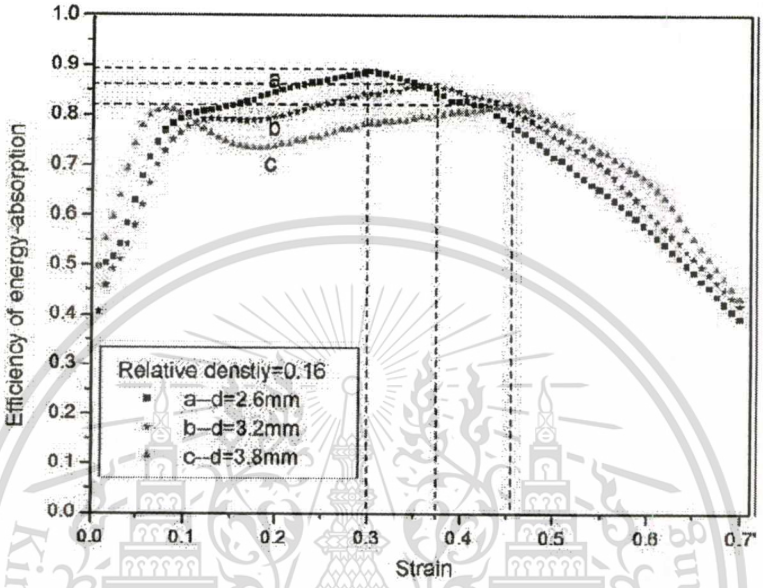

Figure 2.24 Effect of cell size on the efficiency of energy absorption of aluminium foam (Yu *et al.*, 2007).

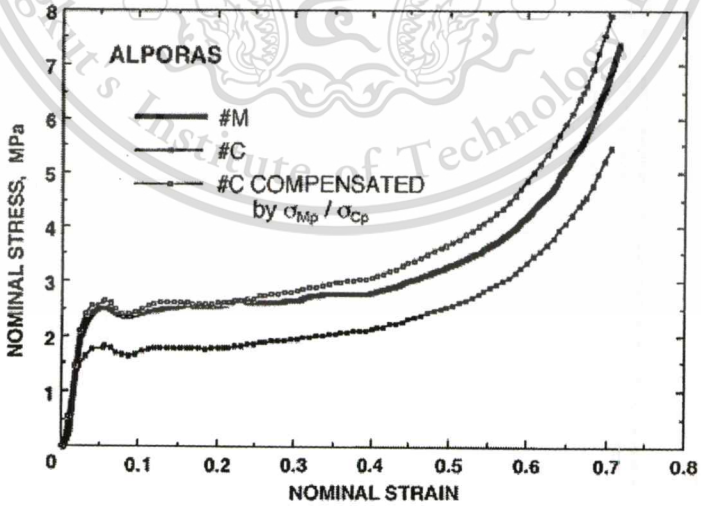

Figure 2.25 Nominal stress-strain curves at a quasi-static strain rate of $1x10^{-3}s^{-1}$ of ALPORAS (Miyoshi *et al.*, 1999).

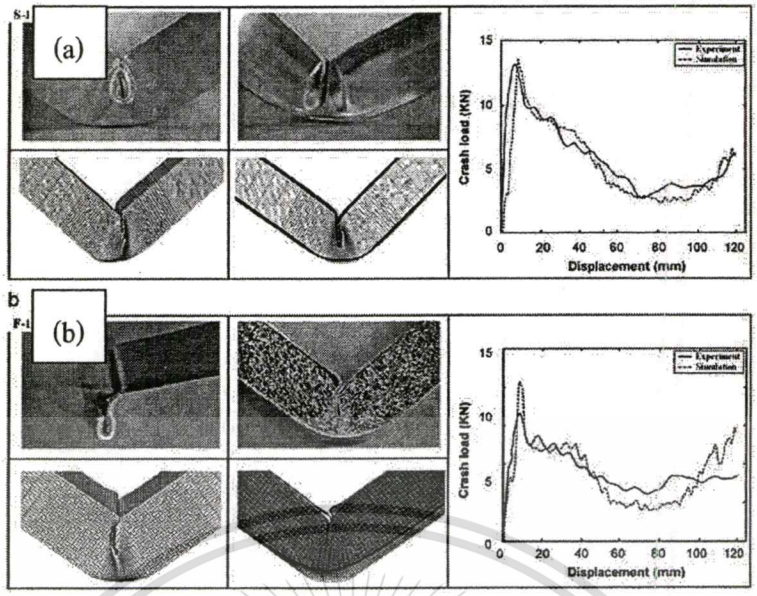

Figure 2.26 Experimental and numerical prediction of crash pattern and crash load–displacement curves of (a) empty and (b) foam-filled tubes (Simancik, 2001).

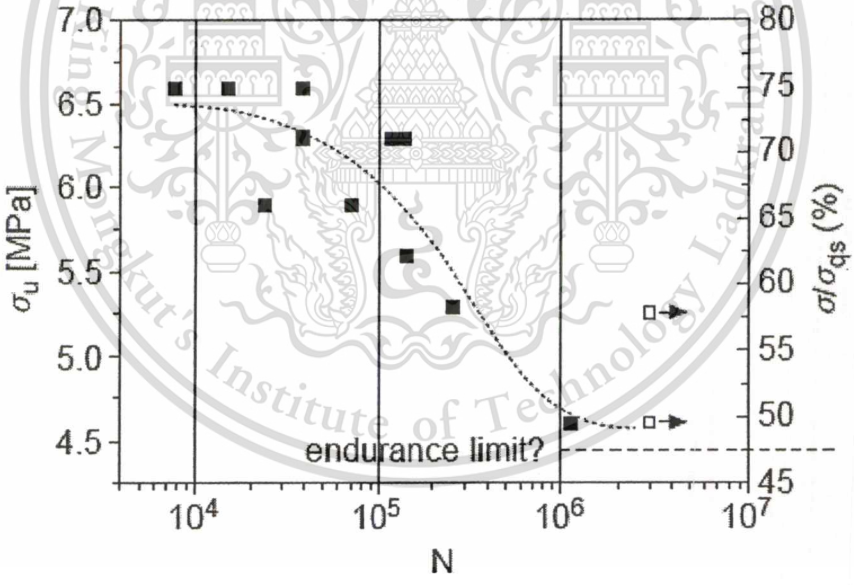

Figure 2.27 Results of fatigue tests on AlSi7 foams with a density of 0.63 g/cm^3. Full squares : <3x10^6 cycles; open squares: no failure after 3x10^6 cycles (Banhart and Brinkers, 1999).

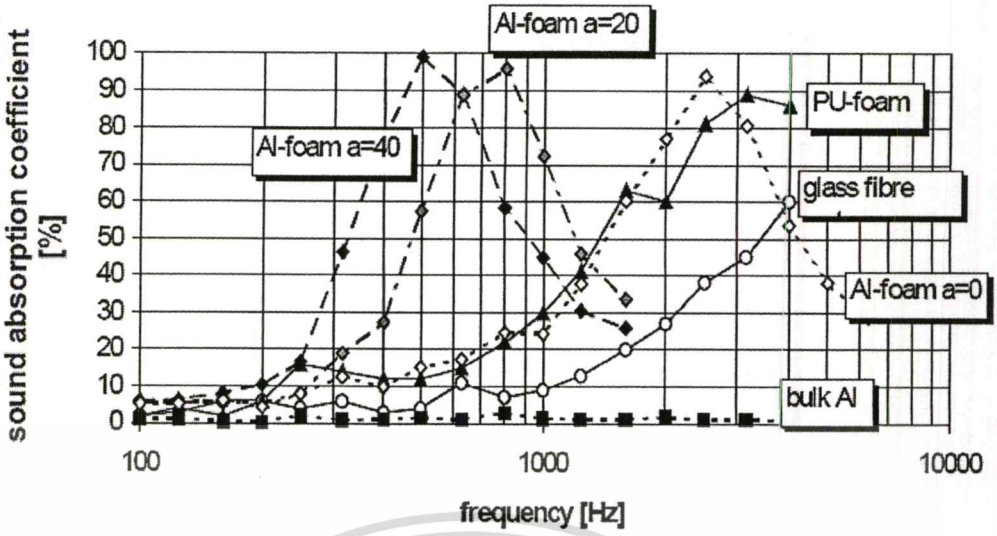

Figure 2.28 Sound absorption coefficient of 0.5 g/cm^3 open cell aluminium foams with different air gap between the sample and solid background compared with bulk aluminium, PU-foam and glass fibre material (Simancik *et al.*, 1995).

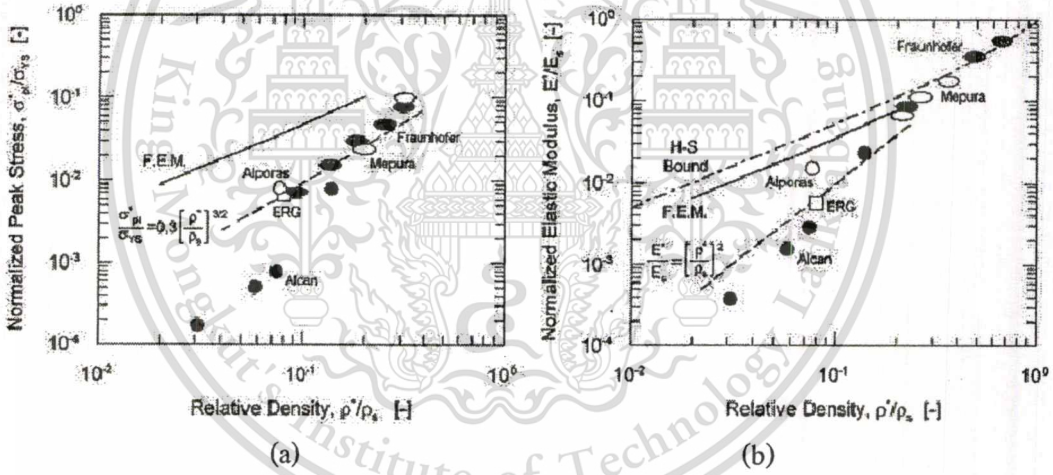

(a) (b)

Figure 2.29 Properties of aluminium foam: (a) Stress and (b) Young's modulus (Andrews *et al.*, 1999).

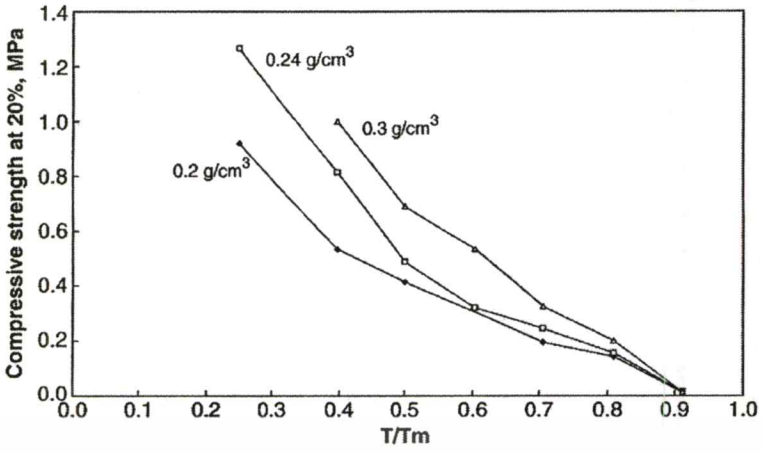

Figure 2.30 Influence of service temperature on the compressive strength of ALPORAS foams having densities of 0.22, 0.24 and 0.3 g/cm^3 (Aly, 2007).

2.1.3 Automotive Applications of Aluminium Foam

In automotive industries, aluminium foam is becoming a candidate material because of its light weight, good energy absorption and excellent damping insulation properties as shown in **Figure 2.31**.

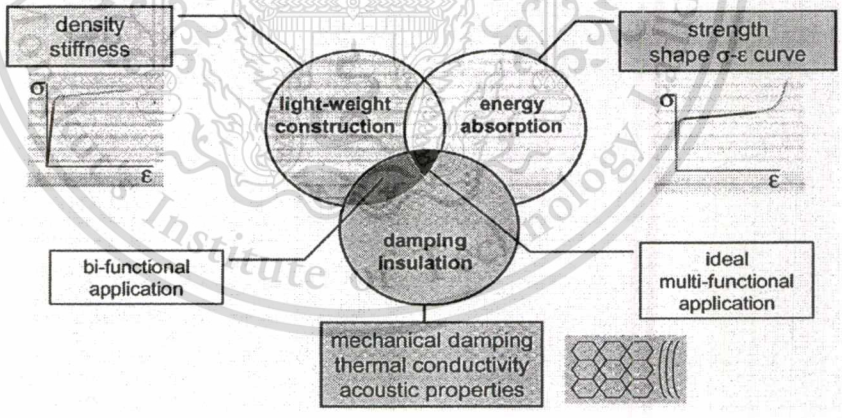

Figure 2.31 Application ranges of metallic foam in automotive industries (Banhart, 2005).

Aluminium foams can be used for automotive structures such as frame, pillar, door, bonnet, roofs, floors, lifting arm, crash box and bumper, as shown in **Figure 2.32-Figure 2.38**. Crash box and bumper are most potential components to be produced by aluminium foams, which are required to have a high crash energy absorption for protecting passengers and pedestrians, as well as car bodies, during crashes (Ito and Kobayashi, 2006).

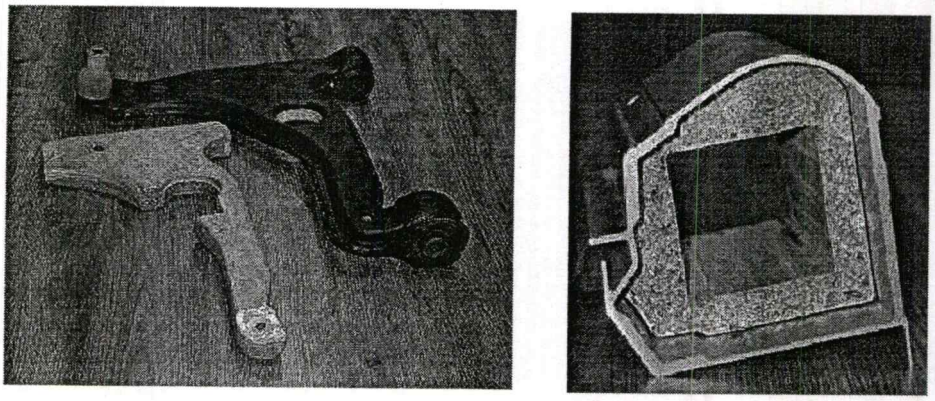

Figure 2.32 Suspension and structural part reinforced with inserted aluminium foams (Simancik, 2001).

Figure 2.33 Crash box (Cymat).

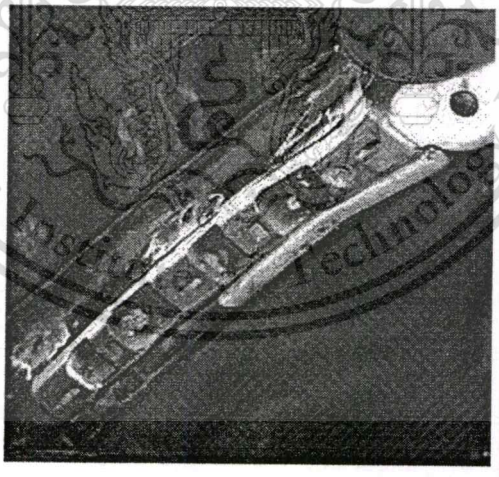

Figure 2.34 Prototype of aluminium foam inserted in A-pillar (Kretz *et al.*, 2002).

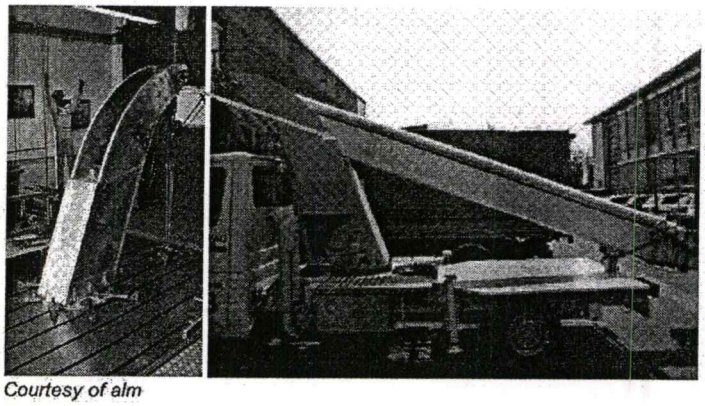

Courtesy of alm

Figure 2.35 Base of a lifting arm made from AFS sandwich panels (Banhart, n.d.).

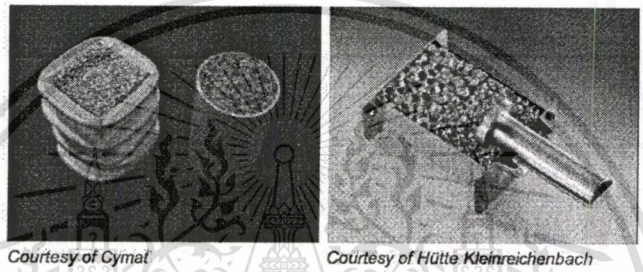

Courtesy of Cymat

Courtesy of Hütte Kleinreichenbach

(a) (b)

Figure 2.36 Prototypes of crash absorbers: (a) Cymat aluminium foam, and (b) Metcomb aluminium foams (Banhart, n.d.).

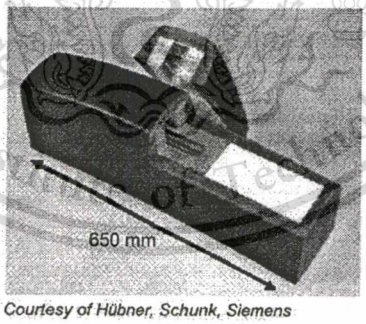

Courtesy of Hübner, Schunk, Siemens

Figure 2.37 Crash energy absorber for a tram built for the COMBINO vehicle system (Banhart, n.d.).

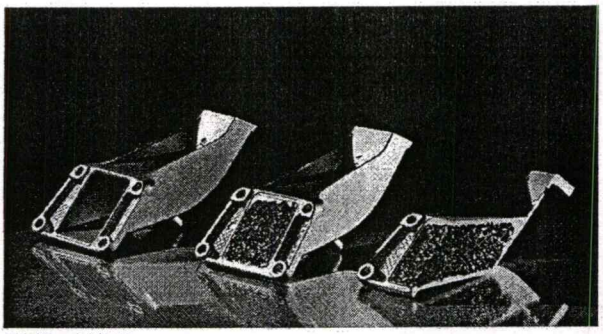

Courtesy of LKR

Figure 2.38 Prototype of a BMW engine mounting bracket manufactured by LKR Ranshofen. Fromleft: empty casting, composite part consisting of foam core and cast shell, and section through composite part (Banhart, n.d.).

2.1.4 Characterisations of Aluminium Foams

Testing of aluminium foam properties can be classified into two groups: destructive and Non destructive testings.

2.1.4.1 Non-Destructive Characterisations

Density, acoustic absorption and thermal conductivity are properties which can be characterised using non-destructive methods. The density of aluminium foam can be measured using Archimedes' principle which can be calculated by equation 2.2.

$$D_{foam} = \frac{W_{air}}{W_{air} - W_{water}} \tag{2.2}$$

where D_{foam} is the foam density,

W_{air} is the weight of the foam measured in air,

W_{water} is the weight of the foam measured in water.

X-ray radiography and computed tomography can also be used to observe the evolution of foam structure during foaming in real time.

2.1.4.2 Destructive Characterisations

Mechanical properties testing such as fatigue, energy absorption and strength are measured using destructive methods. Microstructure of foam material can be simply characterised using

image analysis method. Size, shape, and distribution of cell can be measured using commercial image analysis software. The analysis is carried out on clear images normally taken from a well polished section specimen using an optical microscope. Cell membranes and the interior of the cells should appear in different brightness, for example by embedding black resin in cells as shown in **Figure 2.39**. .

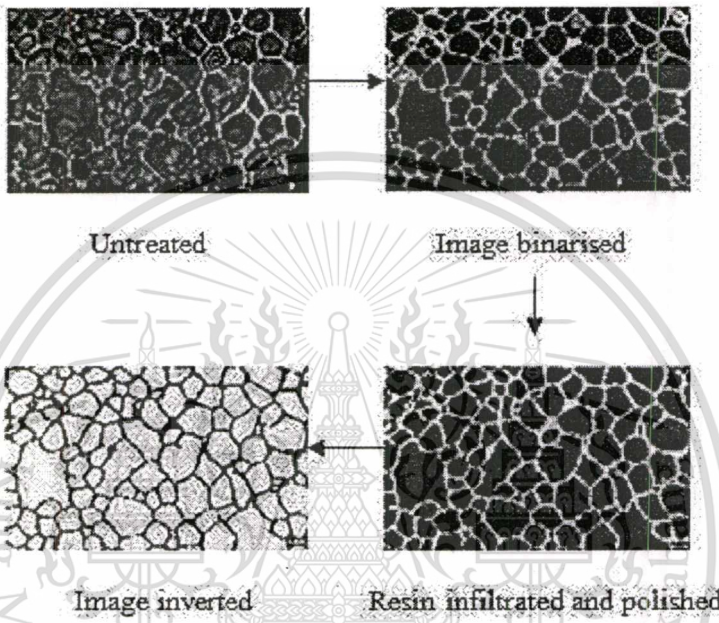

Figure 2.39 Image analysis in aluminium foam images taken from optical microscope (Banhart, 2001).

2.2 Theories of Foam

Liquid foams are known as non-Newtonion fluid (Larmignate *et al.*, 2008). They are bubbles separated by thin liquid films (Bogdanovic *et al.*, 2009). The foams consist of three structural elements: cell face, Plateau border and vertex as shown in **Figure 2.40** (Gergely and Clyne, 2004). Foaming behaviour is affected by liquid properties such as surface tension, viscosity and ionic strength. To form a metallic foam, the gas phase needs to be dispersed prior to rise to the melt surface, and the foam begins to form. The foam column starts to form when the number of bubbles arriving at the liquid/gas interface exceeds the number of rupturing bubbles (Malysa and Lunkenheimer, 2008). Surfactants are used to reduce surface tension in liquid to stabilise the foam (Bogdanovic *et al.*, 2009).

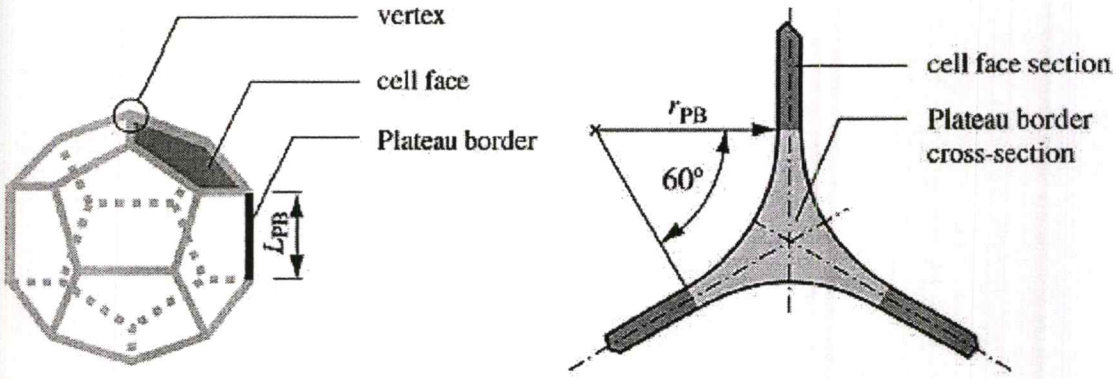

Figure 2.40 Structure of a foam bubble (Gergely and Clyne, 2004).

Figure 2.41 shows the schematic of foaming behaviour in a vertical tube, which represents three stages. Foam starts to form when the superficial velocity of gas phase, j_g, more than the superficial velocity of minimum conditions for onset of foaming, j_m.

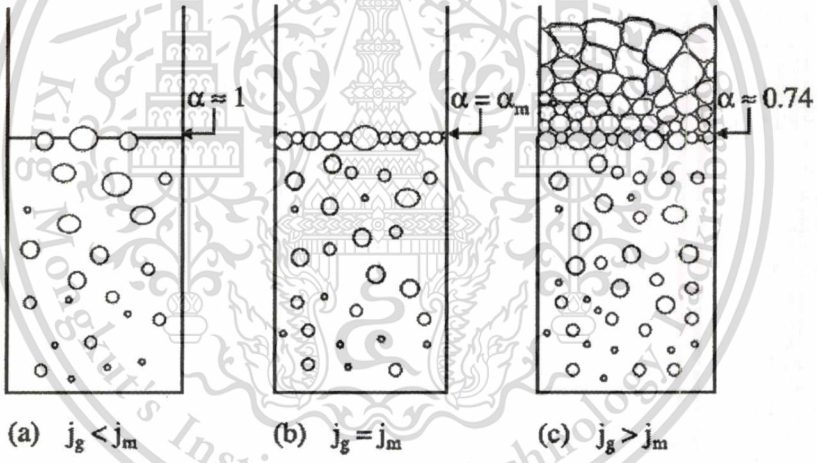

Figure 2.41 Schematic of the behaviour of a foaming solution as the superficial gas velocity is increased (a) bubbly flow without foam, (b) onset of foaming and (c) development foam layer (Pilon and Viskanta, 2004).

The mean bubble size in flowing foam is influenced by several factors including gas flow rate, liquid viscosity, and foam generator design. **Figure 2.42** and **Figure 2.43** show the mean radius/diameter of bubbles which are generated by single orifices and a sparger.

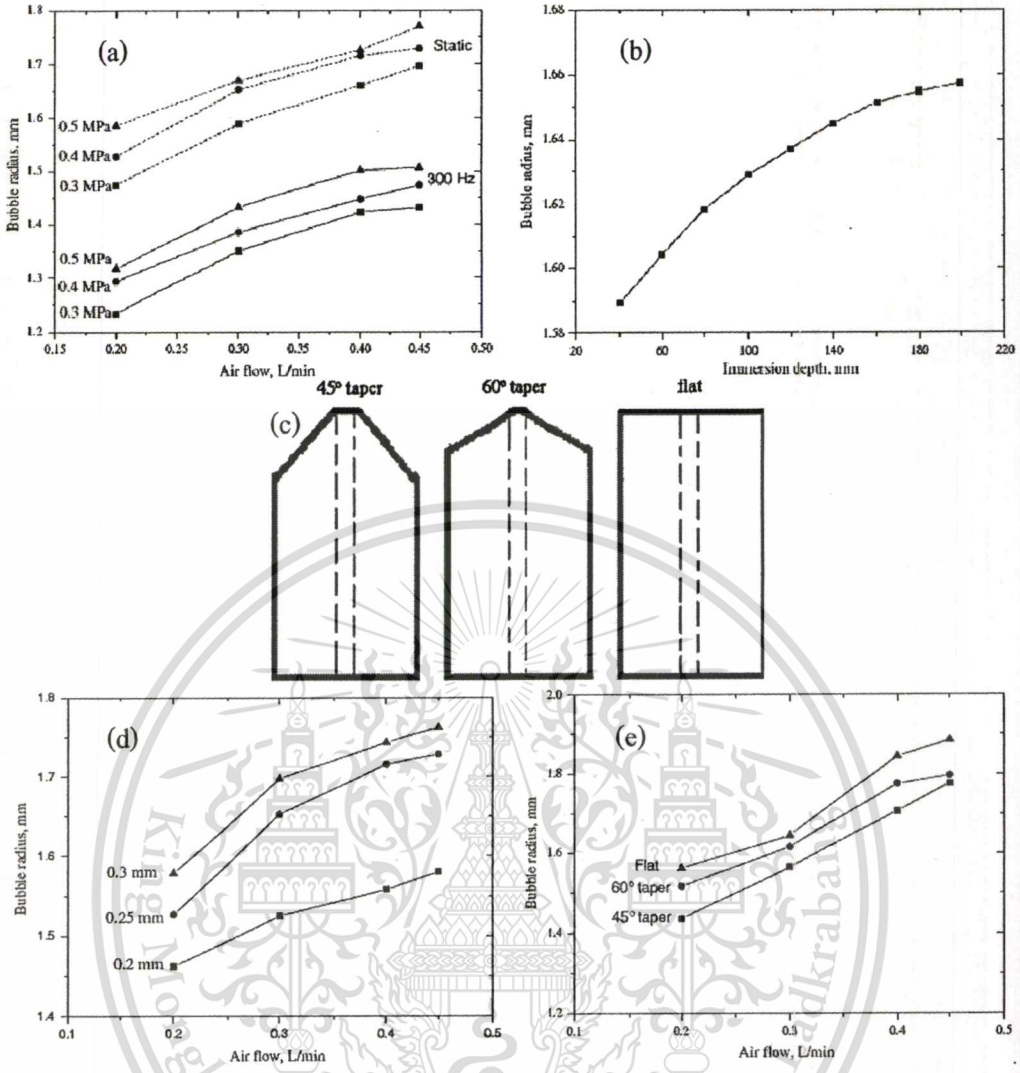

Figure 2.42 The depending of bubble radius on (a) air flow rate, air supplied pressure and nozzle movement, (b) immersion depth, (c) orifices, (d) air flow rate and nozzle size, and (e) air flow rate and orifice shape (Deqing and Chengxin, 2008).

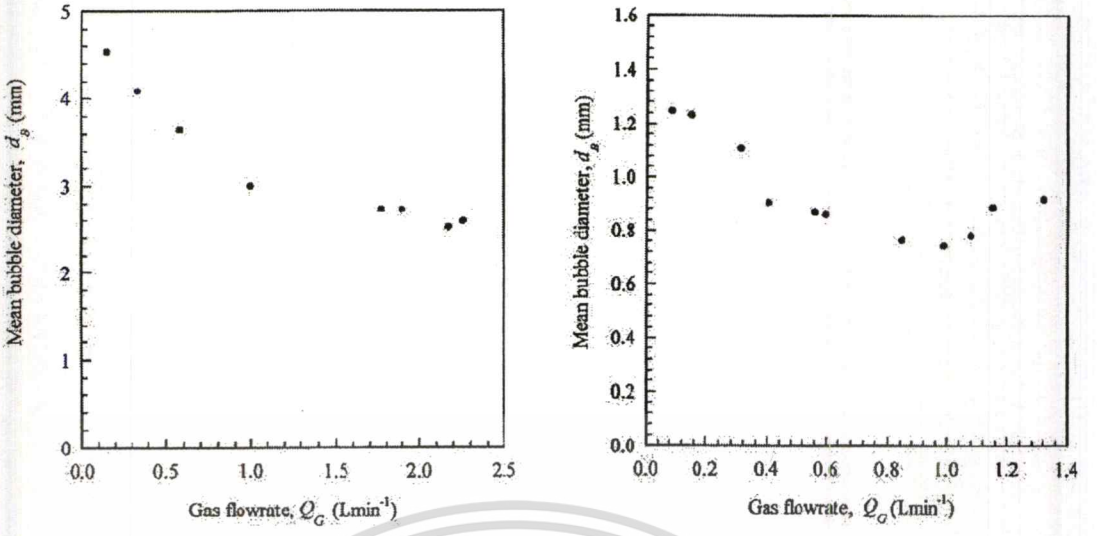

Figure 2.43 Mean bubble diameter of foam in a vertical tube generated by: (a) generated by a single orifice (1.5 mm) and (b) generated by a disc sparger (100-160 μm) (Deshpande and Brigou, 2000).

2.2.1 Bubble Formation

There are three systems of bubble formation: gas-liquid, gas-solid and gas-liquid-solid. In this review, only the gas-liquid system is considered since it is identical to the occurrence of foam produced by the gas injection. The formation of single and multi bubbles is determined as described below.

2.2.1.1 Single Bubble

Generally, a single bubble is generated by an orifice, a tube or a gas injector. There are two mechanical arrangements which are orifice connected and unconnected to a gas chamber. In the case of the orifice without the gas chamber, the gas flow through the orifice is always constant. The gas flow rate generated from the orifice connected to the gas chamber varies with gas injection conditions which are characterised by capacitance number, N_c.

$$N_c = \frac{4V_c g \rho_l}{\pi d_o^2 P} \tag{2.3}$$

where N_c is the dimensionless capacitance number,

V_c is the volume of gas chamber,

g is the gravitational acceleration,

ρ_l is the liquid density,

d_o is the orifice diameter,

P is the system pressure.

When N_c is smaller than 1, the gas flow rate through the orifice is constant but if larger than 1, the gas flow rate is not constant (Yang *et al.*, 2006; Gerlach *et al.*, 2007). **Figure 2.44** shows the force balance of single bubble during formation and its equation can be written as

$$F_B + F_M = F_D + F_\sigma + F_{BA} + F_{I,g} + F_C + F_{I,m} \tag{2.4}$$

where F_B is the buoyancy force,

F_M is the gas momentum force,

F_D is the liquid drag force,

F_C is the particle-bubble collision force,

F_σ is the surface tension force,

F_{BA} is the Basset force,

$F_{I,g}$ is the bubble inertial force,

$F_{I,m}$ is the liquid-solid suspension inertial force.

The theoretical descriptions of the forces (Zhang and Shoji, 2001) are stated as:

$$F_B = V_b(\rho_l - \rho_g)g \tag{2.5}$$

$$F_M = \rho_g \frac{{Q_g}^2}{(\pi/4)d_o^2} \tag{2.6}$$

$$F_D = \frac{1}{2}\rho_l \frac{\pi}{4} {D_b}^2 C_D \left(\frac{ds}{dt}\right)^2 \tag{2.7}$$

$$F_\sigma = \pi d_0 \sigma_l \tag{2.8}$$

$$F_I = F_{I,g} + F_{I,m} = \left(\rho_g + \xi_1 \rho_l\right) \frac{d}{dt}\left(V \frac{ds}{dt}\right) \tag{2.9}$$

where V_b is the bubble volume,

D_b is the bubble diameter,

ρ_g is the density of gas,

Q_g is the gas flow rate,

C_D is the drag force coefficient,

σ_l is the surface tension,

ds/dt is bubble center velocity,

ξ_1 is the added mass coefficient.

In order to understand the influencing forces acting on the bubble during formation, non-dimensional quantities are derived and their importance in the range of parameters considered here is discussed. At low gas flow rates, the bubble volume at detachment,V_b, can be estimated by the balance of the buoyancy and surface tension forces, i.e.,

$$2\pi r_o \sigma \approx V_b(\rho_l - \rho_g)g \tag{2.10}$$

The ratio of buoyancy and surface tension is characterised by the Bond number,Bo_b, (Gerlach *et al.*, 2007; Higuera and Medina, 2006; Jamialahmadi *et al.*, 2001) and the ratio of viscous to capillary forces is described by the capillary number,Ca_b (Gerlach *et al.*, 2007), as given by the below equations.

$$Bo_b = \frac{\rho_l g r_o^2}{\sigma} \tag{2.11}$$

$$Ca_b = \frac{\mu_l \dot{Q}}{\sigma_l r_o^2} \tag{2.12}$$

where Bo_b is the Bond number of bubble,

Ca_b is the capillary number of bubble,

$\dot{Q}$ is the orifice flow rate,

r_o is the orifice radius,

μ_l is the liquid viscosity.

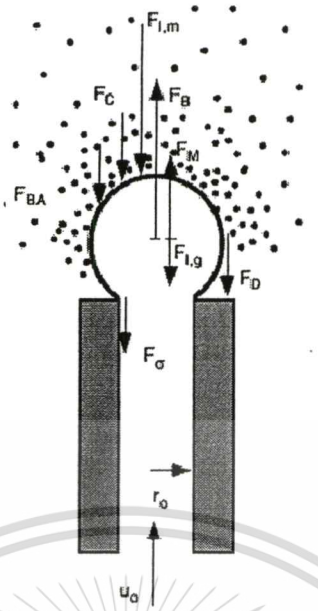

Figure 2.44 Forces on a single bubble at the outlet of an orifice (Yang *et al.*, 2007).

The bubble growth is affected by the pressure in the bubble and liquid container (Valencia *et al.*, 2002). In principle, bubble size depends on orifice size, gas flow rate and fluid properties (fluid viscosity, liquid surface tension, liquid density, gas density, orifice configuration) and bubble diameter can be calculated by equations given in **Table 2.4**. Apart from above factors, fine bubbles can be produced by using a vibration nozzle as shown in **Figure 2.45**. For bubbles generated by a gas injector, i.e. an orifice or a nozzle, frequency and amplitude of the gas injector are important factors controlling the formation of bubble as shows in **Figure 2.46**. When the frequency increases, bubble size becomes small. However, when the frequency higher than 100 Hz, the bubble size remains constant.

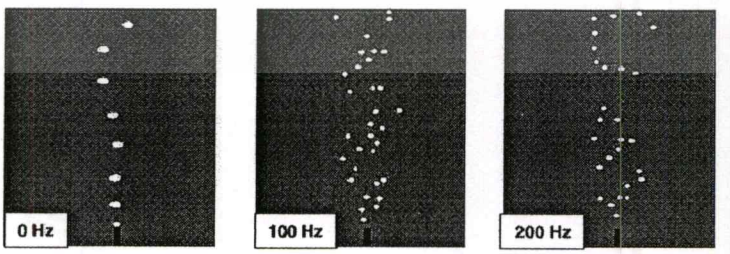

Figure 2.45 Bubble generation at different nozzle vibration (Krishna and Ellenberger, 2003).

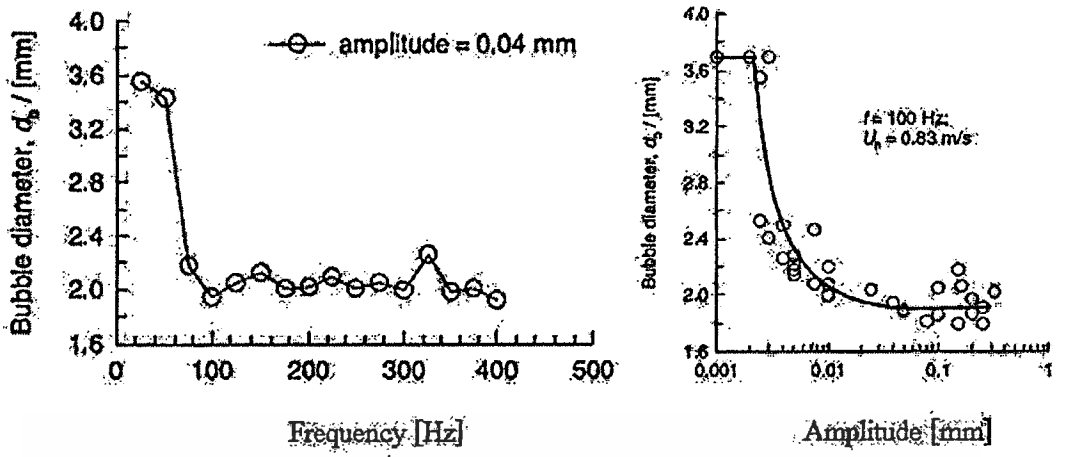

Figure 2.46 Effects of frequency and amplitude of gas injector on bubble diameter (Krishna and Ellenberger, 2003).

Table 2.4 Equations of bubble diameter generated by a single orifice.

Author	Bubble diameter	Remark
Cho and Laskowski, 2002	$d_b = \left[\frac{6d_o\sigma_l}{g(\rho_l - \rho_g)}\right]^{1/3}$	For low gas flow rate.
Deqing *et al.*, 2006	$d_b = \frac{p_o Q_g^{0.3} H^{0.5} d_0^{0.5}}{(1.56\times10^4 - 804\sigma)n^{0.3}\mu^{0.545}\rho_l^{0.33}}$	
Forrester *et al.*, 1998	$d_b = \left(\frac{16r_o\sigma_l}{C_D U_o^2 \rho_l}\right)^{0.5}$	
	$d_b = 0.7\left(\frac{\sigma_l^{3/5}}{\rho_l^{1/5} 2\varepsilon^{2/5}}\right)\left(\frac{\mu_l}{\mu_g}\right)^{0.1}$	For Non-Newtonian fluid.
	$d_b = 2.4(Q_o/U_o)^{0.5}$	Jet-break up model.
Jamialahmadi *et al.*, 2001	$d_b = d_o\left(\frac{5}{Bd_o^{1.08}} + \frac{9.261Fr^{0.36}}{Ga^{0.39}} + 2.147Fr^{0.51}\right)^{\frac{1}{3}}$	
Kantarci *et al.*, 2005	$d_b = 0.9d_o^{04.8}Re_o^{0.32}$	$Re_o = \frac{4Q\rho_g}{\pi d_o \mu_g}$
	$d_b = 0.18d_o^{1/2}Re_o^{1/3}$	For Re < 2000.
	$d_b = 3.23d_o\left(\frac{4\rho_l Q}{\pi\mu_l d_o}\right)^{-0.1}\left(\frac{Q^2}{d_o^5 g}\right)^{0.21}$	
Kogawa *et al.*, 2008	$d_b = \left(\frac{6M\sigma d_o}{\sigma_l g}\right)^{1/3}$	
Nahra and Kamotani, 2003	$d_b = 2\left(\frac{Q_g t_d + V_{B0}}{4/3\,\pi}\right)^{1/3}$	For Non-Newtonian fluid.
	$d_b = 2\left(\frac{9Q_g^2}{8\pi^2 g}\right)^{1/5}$	For Non-Newtonian fluid.

Table 2.4 (Cont.) Equations of bubble diameter generated by a single orifice.

Ruzicka *et al.*, 2009	$r_b = z_d - 2r_o$	
	$r_b = r_o/sin\theta$	
Sam *et al.*, 1996	$d_b = \left[\frac{6d_o\sigma_l cos(\theta_c)}{g(\rho_l - \rho_g)}\right]^{1/3}$	
Stevenson, 2006	$r_b = r/(1.2\varepsilon^{0.46})$	For Non-Newtonian fluid..
Tsuge *et al.*, 2006	$d_b = 0.821Q_g^{0.4}$	
	$d_b = \left(\frac{6Q_g t_d}{\pi}\right)^{1/3} = \left(\frac{6V_b}{\pi}\right)^{1/3}$	
Valencia *et al.*, 2002	$d_b = 0.794d_o^{0.8}u_o^{0.4}$	
Zhang *et al.*, 2003	$d_b = 2\left(\frac{3r_c\sigma\, cos\theta}{2\Delta\rho g}\right)^{1/3}$	For low gas flow rate.
Zhang *et al.*, 2005	$d_b = \left(\frac{V_g}{n}.\frac{6}{\pi}\right)^{\frac{1}{3}}$	

Where d_b is the bubble diameter, r_b is the bubble radius, d_o is the orifice diameter, r_o is the orifice radius, g is the gravitational acceleration, ρ_l is the liquid density, ρ_g is the density, u_o is the gas orifice velocity, Re_o is the orifice Reynolds number, Q is the heat flux, θ is the bubble angle, C_D is the drag coefficient, σ_l is the liquid surface tension, U_o is the liquid velocity over orifice, ms^{-1}, Bd_o is the Bond number in terms of bubble diameter, Fr the is the Froude number, Ga is the Galileo number, M is the constant value 0.79-9.145, Q_o is the gas flow rate through a single orifice, m^3s^{-1}, μ_l is the liquid viscosity, Q_g is the gas flow rate, t_d is the time interval of bubble formation, z_d is the bubble distance over orifice, V_g is the injected gas volume, n is the number of bubble generated in some interval, ε is the volumetric liquid fraction in foam, dimensionless, r is the radius of curvature of Plateau border wall, n is the orifice number, $p_o$is the gas pressure at orifice, kg/m3, H is the total height of simulation liquid, r_c is the radius of capillary, and θ is the contact angle.

Three dimensionless parameters, the bubble Reynolds number (Re), the bubble Eötvös number (Eo), and the bubble Morton number (Mo), are commonly used to characterise the shape and the rising behaviour of bubbles (Yang *et al.*, 2006; Andreussi *et al.*, 1999; Salman *et al.*,

2006; Zhang *et al.*, 2005; Parkinson *et al.*, 2008; Vitankar *et al.*, 2002 and Zhang *et al.*, 2000). They are defined as

$$Re_b = \frac{\rho_l u_b d_b}{\mu_l} \tag{2.13}$$

$$Eo_b = \frac{g\Delta\rho d_b^2}{\sigma_l} \tag{2.14}$$

$$Mo_b = \frac{g\Delta\rho\mu_l^4}{\rho_l^2\sigma_l^3} \tag{2.15}$$

where Re_b is the Reynolds number of bubble,

Eo_b is the Eötvös number based on bubble diameter,

Mo_b is the Morton number based on liquid properties parameter in Fan-Tsuchiya equation reflecting system purity,

u_b is the bubble rise velocity,

d_b is the bubble diameter,

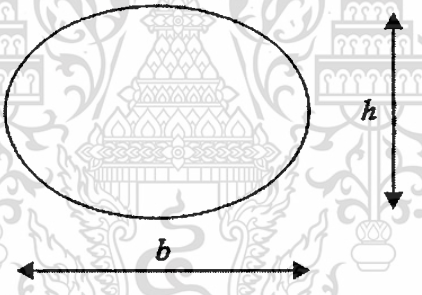

Figure 2.47 Shape of a bubble.

For bubbles in low *Mo* liquids ($Mo<10^{-3}$), below equations can be used to predict the bubble aspect ratio.

$$\frac{h}{b} = \begin{cases} 1, & Ta < 1, \\ \{0.81 + 0.206\ tanh[2(0.8 - log_{10}Ta)]\}^3, & 1 \le Ta \le 39.8, \\ 0.24, & 39.8 \le Ta \end{cases}$$

where the dimensions of the bubble, b and h, are given described in **Figure 2.47**, Ta is the Tadaki number, which is depend as

$$Ta = Re_b Mo_b{}^{0.23} \tag{2.16}$$

Drag coefficient, C_D, depends on bubble diameter and velocity that can be expressed as (Loubière and Hébrard, 2003)

$$C_D = \frac{24}{Re_b}(1 + 0.15Re_b^{0.687})\alpha_l^{-1.7};\ Re_b < 1000, \tag{2.17}$$

$$C_D = 0.44;\ Re_b > 1000 \tag{2.18}$$

where α_l is the liquid hold-up dimensionless.

Bubble formation at a single submerged orifice can occur in many types, i.e. chain bubbling, wobbling and jetting. The type of the formation depends on the orifice configuration, the gas velocity, gas-liquid system properties, and the magnitude of gravitational force acting on the system (Kulkarni and Joshi, 2005).

Parameters of bubble formation are always considered in terms of Weber number. The Weber number of a single bubble, We_b, (Zhang *et al.*, 2000; Pamperin, 1995; Tsuge *et al.*, 1997; Carrera *et al.*, 2006) can be written as

$$We_b = \frac{\rho_g u_o^2 d_o}{\sigma_l} \tag{2.19}$$

For $We_b < 4$, the proportion between bubble diameter and nozzle diameter is given by $d_b \sim d_o^{1/3}$, while for $4 < We_b < 30$, the formation of secondary bubbles occurs. When $We_b > 4$, relationship between bubble and nozzle diameter is $d_b \sim d_o^{1/2}$. For $We_b > 30$, the shape of gas bubbles are usually ellipse and expand always immediately at the nozzle or orifice tip. Bubble detachment also always occurs directly at the orifice (Pamperin, 1995).

Weber number is also commonly used in the studies of bubble coalescence and represents by the ratio of the inertial force to the surface tension force:

$$We_b = \frac{\rho_l u_o^2 r_b}{\sigma} \tag{2.20}$$

where We_b is the Weber number of bubble,

r_b is the bubble radius.

In pure water, Duineveld, 1998 observed three different bubble interaction behaviours: (1) when the We_b based on the relative approaching velocity is less than 0.18, bubbles coalesce; (2)

for We_b larger than 0.18, and for Weber number We_b based on the terminal velocity of a single bubble v_∞ less than 3.3, bubbles bounce at the first contact but eventually coalesce; (3) for We_b and $We_{b\infty}$ larger than 0.18 and 3.3, respectively, bubbles bounce at the first collision and separate (Pilon and Viskanta, 2004). For bubble formation without buoyancy at constant Weber and Reynolds number, the bubble diameter is directly proportional to the orifice diameter (Pamperin, 1995).

2.2.1.2 Multi-Bubble

Behaviour of multi-bubbles is complex. Skurtys *et al.* (2008) have studied the formation of bubbles and foams in a vertical tube, and described flow patterns that have two principal regimes: (1) bubbly regime and (2) foam regime, as shown in **Figure 2.48**. There are two patterns of bubbly regime including monodispersed (Ω < 10 %) bubbles and polydispersed bubbles (10%< Ω <50%), and four patterns of foam regime consisting of wet foam (50%< Ω <75%), critical wet foam (75%< Ω <90%), dry foam (90%< Ω <98%), and slug ($\Omega \geq$98%). Transitions between regimes depend on liquid and gas flow rates and can be differentiated using a fixed value of the homogeneous gas fraction, Ω, defined as

$$\Omega = \frac{Q_g}{Q_l + Q_g} \tag{2.21}$$

where Q_g is the gas flow rate,

Q_l is the liquid flow rate.

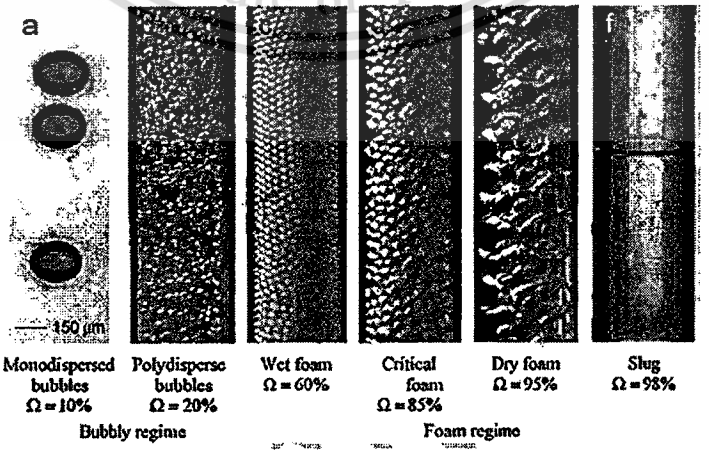

Figure 2.48 Flow patterns of air–gelatine solution (3% w/w) observed in a 2.75mm internal diameter tube for various gas fractions, Ω (Skurtys *et al.* 2008).

Apart from bubble generation from orifices or spargers, bubbles can be generated by an impeller in a stirred vessel. The diameter of bubbles generated by the rotation of an impeller in a stirred vessel can be calculated using equations summarised in **Table 2.5**.

Table 2.5 Equations for the calculation of bubble diameter generated using a rotating impeller.

Reference	Equation	Remark
Deqing *et al.*, 2006	$d_b = \frac{27.3V^{0.3}W^{0.4}}{R^{1/3}} \times \frac{p_o Q_o^{0.3} H^{0.5} d_o^{0.5}}{(1.56 \times 10^4 - 804\sigma) n_i^{0.3} \mu^{0.545} \rho_l^{0.33}}$	Bubbles generated by a rotating impeller with gas injection.
	$d_{Al} = \frac{p_0 \sqrt[3]{(T/T_0) \times (VW/R\rho_{Al})} \times \sqrt{Q_o d_o H / n_i \mu_{Al}}}{2.83 - 1.46\sigma_{Al}}$	
Martín *et al.*, 2009	$d_b = k_d \left(\frac{C'P \left(\frac{N^2 D_i^3 \rho_l}{\sigma} \right)^m \left(\frac{u_g \pi (D_c/2)^2}{N.T^3} \right)^\gamma \left(\frac{\rho_l}{\rho_D} \right)^n}{V} \right)^\delta$	For a stirred vessel with an turbine impeller in a Non-Newtonian fluid.
Patwardhan and Joshi, 1999	$d_b = J \left(\frac{\sigma^{0.6}}{\rho_l^{0.2} (P_g/V)^{0.4}} \right)$	Using an inducing impeller (no bubble coalescence)
	$d_b = J \left(\frac{\sigma^{0.6}}{\rho_l^{0.2} (P_g/v_i)^{0.4}} \right) \epsilon_g^\alpha$	
Sobrino *et al.*, 2009	$d_b = \left\{ \frac{[(U - U_{mf})A_o]^2}{32\pi^2 \sqrt{g^2 + \left(\frac{1}{2}\omega^2 r\right)^2}} \right\}^{1/5}$	
Warke *et al.*, 2005	$r_b = \frac{1}{2} D \left(\frac{Q_g}{Q_{go}} \right)^m \left(\frac{We_c \sigma}{\rho} \right)^{0.6} \frac{1}{\varepsilon^{0.4}}$	Rotary degasser with $We_c \approx 4$

Where d_b is the bubble diameter, N is the impeller rotation speed, D_i is the impeller diameter, ρ_l is the liquid density, ρ_D is the dispersed phase density, V is the vessel volume, D_c is the vessel diameter, δ is the empirical coefficient related to bubble diameter, γ is the empirical coefficient related to the aerated input power, m is the aeration coefficient, n is the power law exponent, u_g is the gas velocity, k_d is a constant, J is the specific absorption rate of solute gas, σ is the surface tension, v_i is the impeller tip velocity, P_g is the power drawn by a gassed impeller, ϵ_g is the fractional gas holdup, α is a constant, A_o is the distributor area per number of holes, U is the superficial gas velocity, U_{mf} is the minimum fluidization velocity, r is the radial coordinate, g is the gravitational acceleration, ω is the angular velocity of distributor, d_{Al} is the bubble diameter of aluminium, W is the position of propeller shaft along baffle width, R is the propeller speed, p_o

is the gas pressure at orifice, Q_0 is the air flow rate, H is the total height of liquid, σ_{Al} is the surface tension of molten aluminium, n_i is the orifice number, μ_{Al} is the viscosity of molten aluminium, ρ_{Al} is the density of aluminium, T is the foaming temperature of aluminium, T_0 is the experimental simulation temparature, We_c is the critical Weber number and ε is the energy dissipation rate.

2.2.2 Foam Stability

Foam stability depends on various factors. Nowadays, there is no general theory to explain the mechanism of formation and stabilisation of all kinds of foam systems (Malysa and Lunkenheimer, 2008). However, the foam stability can be described based on three phemomena: drainage, coalescence and collapse.

2.2.2.1 Drainage

Foam drainage is a complex hydrodynamic process involving liquid flow from the foam films into the Plateau borders, distribution of the liquid along the foam column and its drainage under the influence of capillary and gravitational forces (Khristove and Exerowa, 1995). Drainage occurs during formation and rising movement of foam. Foam drainage causes both the decrease of liquid volume fraction and increase of capillary pressure that are related with the size of bubble in a foam layer and the height of foam. The mechanism of the foam decay depends not only on liquid volume fraction but also on the type of surfactant and the foam films separation in the foam cell (Kruglyakov *et al.*, 2007; Khristove and Exerowa, 1995). Velocity of drainage of a microscopic horizontal liquid film can be calculated using the equation 2.22 (Simulescu *et al.*, 2008; Angarska *et al.*, 2007).

$$V_{Re} = -\frac{dh}{dt} = \frac{2h^3\Delta P}{3\mu r^2} \tag{2.22}$$

where V_{Re} is the rate of film thinning,

h is the film thickness,

r is the film radius,

$\Delta P = P_c - \Pi$ is the driving pressure of film thinning,

P_c is the capillary pressure,

Π is the disjoining pressure.

2.2.2.2 Coalescence

Coalescence results in a decrease of bubble number in foam layer and an increase in a bubble volume. It occurs because the faces of bubbles are not identical (Bhakta and Ruckenstein, 1997). There are three steps in the bubble coalescence process: (1) approach of two bubbles to form a thin liquid film between them, (2) thinning of the film by the drainage of the liquid under the influence of gravity and suction due to capillary forces and (3) rupture of the film at a critical thickness. The bubble coalescence rate can be approximated by the film-thinning rate (Yang *et al.*, 2006). The film thinning velocity can be expressed by the below equation.

$$-\frac{dl}{dt} = \frac{32l^3\sigma}{3\emptyset R_d^2 \mu_l d_b} \tag{2.23}$$

where $\emptyset$ is a measured value of surface drag or velocity gradient at surface due to the adsorbed layer of gas,

l is the thickness of the liquid film between two coalescing bubbles,

R_d is the radius of a contacting circle between two bubbles.

It is known that surface tension decreases and liquid viscosity increases with increasing pressure. In addition, $\emptyset$ increases with pressure. All of variations contribute to the reduction of the film thinning velocity, and hence the bubble coalescence rate, as pressure increases. The time required for two bubbles to coalesce is longer and the rate of overall bubble coalescence in the foam layer is reduced at high pressures. Moreover, the frequency of bubble collision decreases with increasing pressure. As the bubble size and the rise velocity reduce at high pressures, the likelihood of small bubbles being caught and trapped by the wakes of large bubbles decreases. Therefore, bubble coalescence is suppressed by the increase in pressure, due to the longer bubble coalescence time and the smaller bubble collision frequency (Yang *et al.*, 2006).

2.2.2.3 Collapse

Two basic phenomena cause foam collapse: coarsening (also called disproportionation) and film rupture. Coarsening is the process of gas transfer between bubbles which causes a progressive increase in mean bubble size, in poly-disperse foams. It is relatively rapid in fine-scale foams, but insoluble gas may be used to suppress the effect. When it is allowed to proceed

in crystalline foam, there is, to a first approximation, no gas transfer to be expected between bubbles in the interior, because they have equal gas pressures, or at defects. But at the surface, gas can escape to the outside (Vignes-Adler and Weaire, 2008). Foam coarsening in which smaller bubbles shrink and disappear because of gas diffusion between neighbouring bubbles can be hindered, either by using insoluble gas in the liquid to generate the foam, or by generating foams with equal-sized bubbles.

Film rupture occurs when waves generated on liquid surface due to growth of imposed mechanical and thermal perturbations (Bhakta and Ruckenstein, 1997; Barsimhan and Wang, 2006). The schematic of the film rupture is shown in **Figure 2.49**. Whether a surface wave is damped of undergoes catastrophic growth is determined mainly by the shape of a disjoining pressure isotherm. If a repulsive disjoining force increases in response to the local thinning due to a disturbance, the wave is damped and no rupture occurs. On the other hand, if the disjoining pressure decreases, the local thinning is accelerated and leads to rupture (Bhakta and Ruckenstein, 1997). The stability of the film rupture can be summarised as equations given below.

$$x_F > x_{Fm} \rightarrow \frac{d\Pi}{dx_F} < 0 \{Stable\} \tag{2.24}$$

$$x_F < x_{Fm} \rightarrow \frac{d\Pi}{dx_F} > 0 \{Unstable\} \tag{2.25}$$

$$x_F = x_{Fm} \rightarrow \frac{d\Pi}{dx_F} = 0 \{Metastable\} \tag{2.26}$$

where x_F is the film thickness,

x_{Fm} is the film thickness corresponding to the maximum disjoining pressure.

Film rupture can be avoided if they are prevented from becoming too thin. This can be achieved by hindering drainage as long as the foam is wet by the use of very viscous liquids and by using appropriate surfactants which stabilise the films when the foam is dry (Vignes-Adler and Weaire, 2008).

Collapse of foam film occurs at a critical film thickness can be calculated by

$$h_{cr} = 0.98 \frac{(kT)^{1/12} K_{VW}^{1/3}}{\mu^{1/6} \sigma^{1/4}} \left(\frac{1}{\alpha}\right)^{1/6} \tag{2.27}$$

provides limited information regarding bubble dynamics in 3D system. Various measurement techniques, including intrusive and non-intrusive methods, have been developed to investigate the bubble flow behaviour in the 3D system (Yang *et al.*, 2007).

2.2.3.1 Intrusive Techniques

Intrusive techniques using impedance, optical fiber, ultra sound and endoscopic probes and hot film anemometry, have been developed to study bubble behaviour in gas-liquid and gas-liquid-solid systems.

The impedance probe which uses the difference of conductivity between liquid and gas phase for measurement, can be applied to measure bubble volume fraction, bubble length and bubble rise velocity.

Based on the principle of light transitions in liquid media, the optical fiber probe is applied to measure bubble size, bubble rise velocity and bubble volume fraction. The optical probe is, however, not effective.

Volume fraction, frequency and bubble size distribution can be measured by ultrasonic technique. This technique is, however, not suitable for a high gas hold-up condition because of the significant acoustic attenuation due to the reflection on gas bubbles (Yang *et al.*, 2007).

2.2.3.2 Non- Intrusive Techniques

Non-intrusive techniques have the advantage of no measurement interference with the flow field. They are used to measure three phase fluidised bed properties including pressure transducer, visualisation technique, particle image velocimetry (PIV), X-ray, γ-ray, positron emission tomography (PET), radioactive particle tracking (RPT), ultrasonic tomography, nuclear magnetic resonance imaging (NMR), laser and electrical tomography (Yang *et al.*, 2007).

2.3 Impellers

2.3.1 Mixing

Generally, impeller is used for mixing or agitation of liquid-solid, liquid-gas, or liquid-solid-gas. High efficiency of mixing by an impeller depends on several factors such as impeller

type, baffle type and rotation speed. A basic stirred vessel design is shown as **Figure 2.50**. It consists of a vessel, baffles, a draft tube and an impeller. Baffles are used to prevent vortex occurred by the rotation of impeller. **Figure 2.51** shows agitation flow patterns of co-axis and off-axis rotation with and without baffle. The flow patterns under the rotation of an impeller depend on the impeller size, impeller type and operating conditions, and are described by the Reynolds, Froude, and Power numbers as given by equations 2.29, 2.30 and 2.31 respectively (Yapici *et al.*, 2008). The ratio of diameter of impeller and vessel equal 0.3-0.6 ($d/D_t = 0.3 - 0.6$) is commonly used (Walas, 1990) (Cheremisinoff, 2000).

$$Re = \frac{\rho N D^2}{\mu} \tag{2.29}$$

$$Fr = \frac{N^2 d}{g} \tag{2.30}$$

$$N_P = \frac{P}{\rho N^3 D^5} \tag{2.31}$$

where Re is the Reynolds number,

Fr is the Froude number,

N_P is the power number.

Impellers shown in **Figure 2.52** and **Figure 2.53** are generally used for mixing and agitation. However, special designed impellers are also, nowadays, used for stirring.

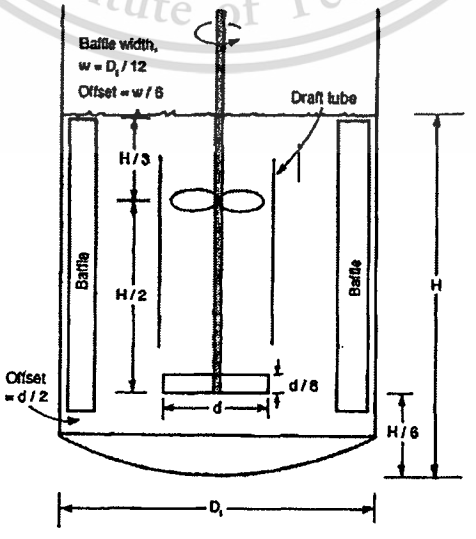

Figure 2.50 A basic stirred vessel design (Walas, 1990).

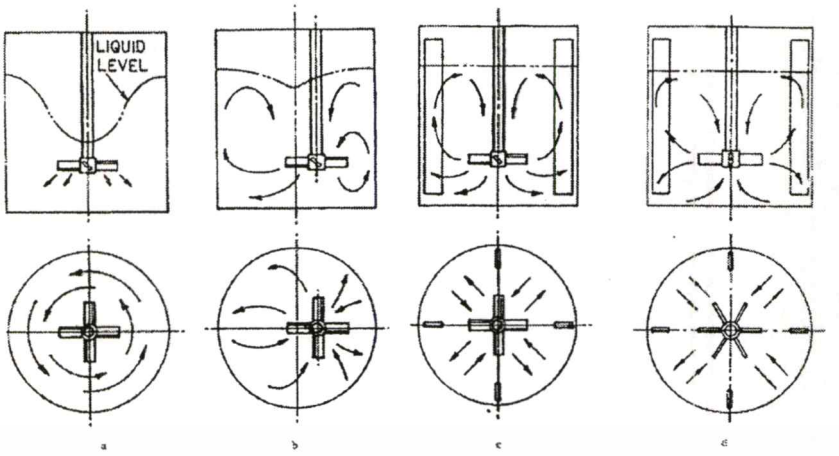

Figure 2.51 Agitation flow patterns (Walas, 1990).

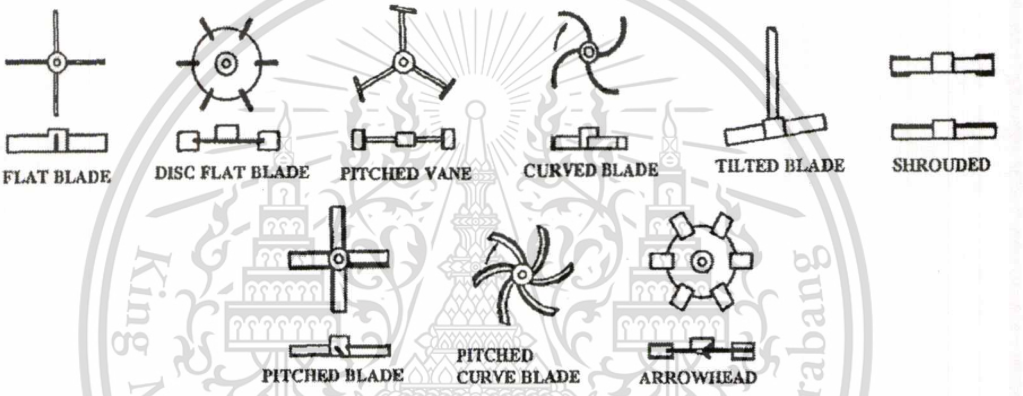

Figure 2.52 Turbine impellers (Cheremisinoff, 2000).

Scaba 3SHP1 (rotate counter-clockwise) | Lightnin' A315 (rotate counter-clockwise) | Hayward Tyler B2-45 (rotate clockwise) | Prochem Max Flow T (circa 1985) (rotate counter-clockwise) | Hayward Tyler LE20 (rotate counter-clockwise)

Figure 2.53 Hydrofoil impellers (Nienow and Bujalski, 2004).

2.3.2 Gas-Induction and Bubble Generation

Not only used in mixing applications, impellers are also used in gas induction (**Figure 2.54** and **Figure 2.55**) and bubble generation (**Figure 2.56** and **Figure 2.57**) in liquid. When the impeller speed increases, pressure at an orifice located on an impeller decreases, resulting in the

suction of gas into the liquid (Deshmuk *et al.*, 2006). In aluminium foam production, fine bubbles are required for high strength and stiffness, as well as structural uniformity of aluminium foams. Impellers have therefore been used in the gas injection process of aluminium foam production for refining and dispersing injected gas bubbles in molten aluminium. Impellers used for aluminium foam production are shown in **Figure 2.56** and **Figure 2.57**. **Figure 2.58** shows the foaming performance of the impellers shown in **Figure 2.57**.

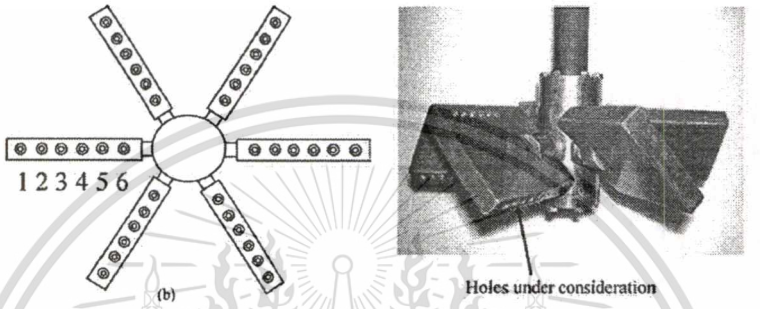

Figure 2.54 Gas induction impeller (Deshmukh *et al.*, 2006).

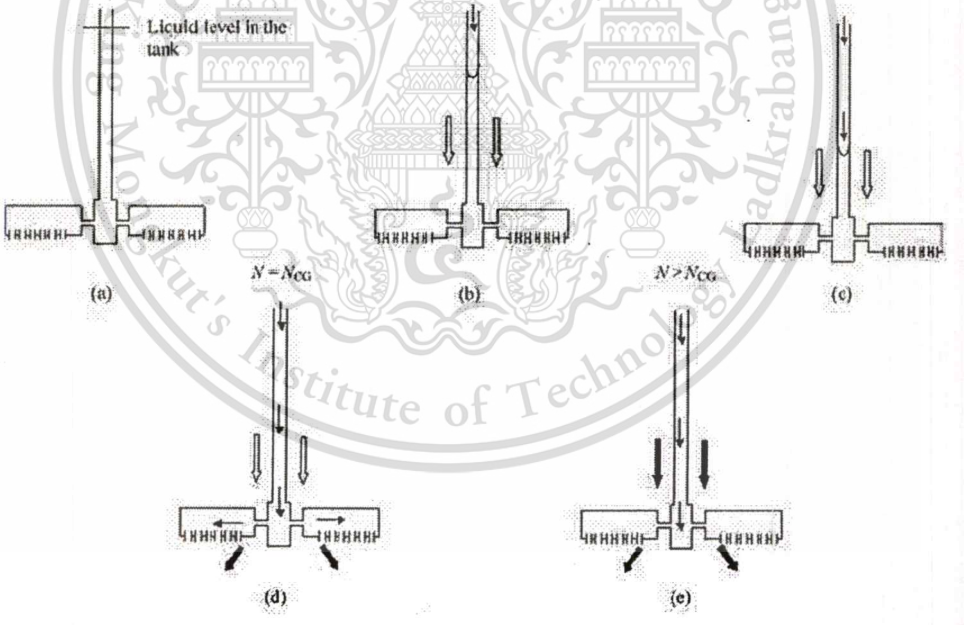

Figure 2.55 Mechanism of gas induction (Deshmuk *et al.*, 2006).

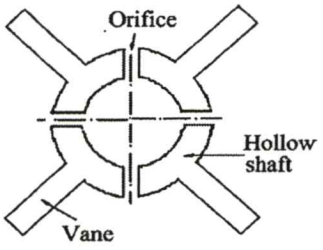

Figure 2.56 Impeller used for aluminium foam production (Deqiung *et al.*, 2006).

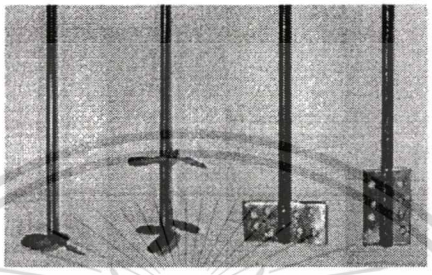

Figure 2.57 Impeller used for aluminium foam production (Oak *et al.*, 2002).

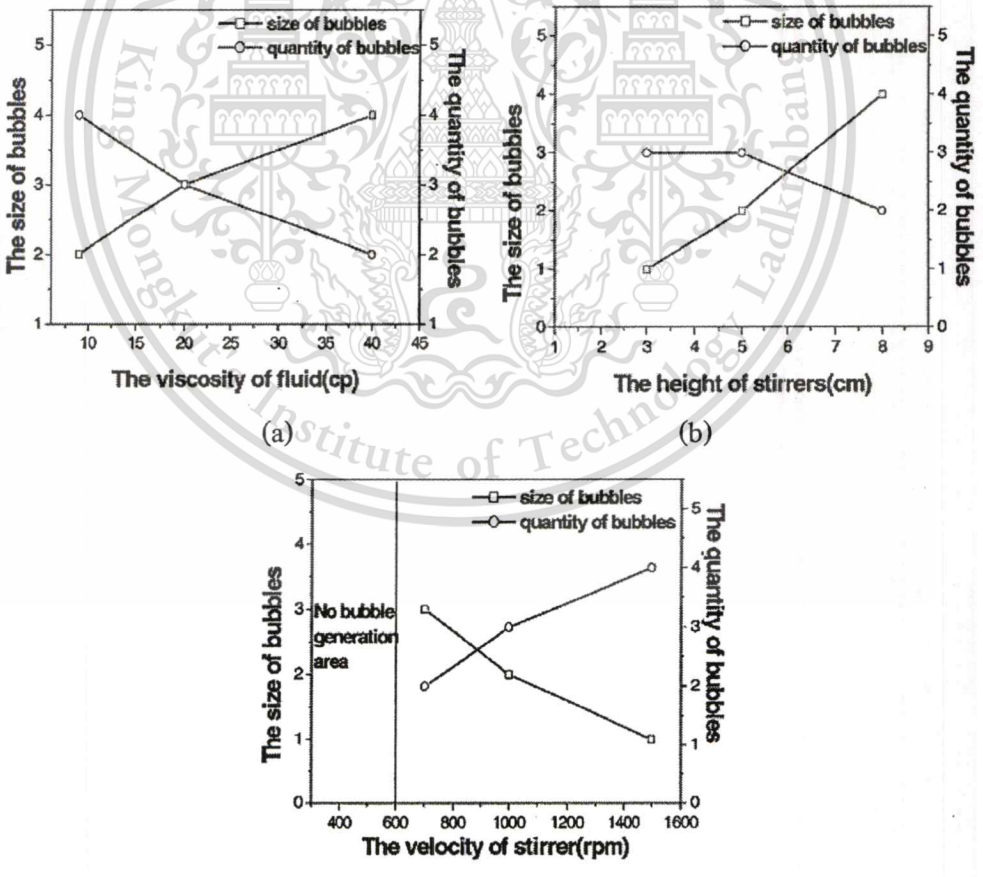

Figure 2.58 Foaming performance of the impellers shown in **Figure 2.57** (Oak *et al.*, 2002).

2.4 Summary

Aluminium foam is an interesting material for automotive applications because it combine various good properties such as high energy absorption, light weight and good thermal efficiency. For automotive applications, aluminium foam can be used for increasing strength of automotive part and improving crashworthiness.

There are two types of aluminium foam: closed-cell and open cell aluminium foam. Aluminium foam production can be classified into two groups: liquid and solid state. The cost of the liquid state method using a direct foaming based on a gas injection is lower than the solid state. Cymat is a company producing sheet aluminium foams with the minimum cell size of about 3 mm, using the liquid state method..

There are various factors effecting the foam formation in the direct gas injection method e.g. properties of liquid, flow rate of gas injection, foam stability and foaming apparatus. Impeller, which is the main component of the foaming apparatus, is used to generate bubbles in the foaming liquid. Suitable design and optimised operation of the impeller have a determinative influence on the final structure of the produced foam.

CHAPTER 3

EXPERIMENTAL PROCEDURES

This research aims to design and develop a gas injection device for aluminium foam production. The key processing steps of the research are shown in **Figure 3.1**. The physical model using water as a testing fluid was used to establish optimum designs and processing parameters for the gas injection device and the foam production respectively. The computational fluid dynamics (CFD) was carried out in parallel with foaming experiments in order to examine the physics of foaming. The obtained well-design foam generator and the optimal processing parameters were then used to produce actual aluminium foams. Details of the foam generator design, CFD and material characterisations are described below.

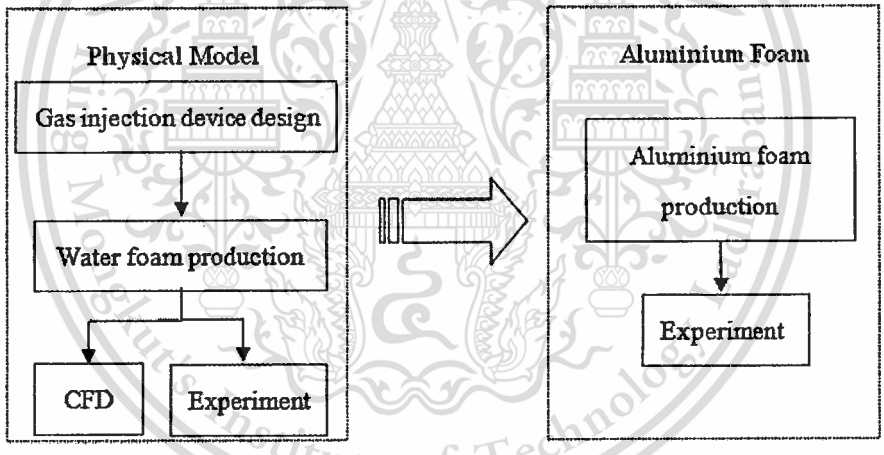

Figure 3.1 Key processing steps of the research.

3.1 Gas Injection Device Designs

Due to a high temperature and an opaque property of molten aluminium, it is difficult to observe the foaming behaviour of the aluminium. Therefore, physical model using water as a testing fluid and a transparent vessel as a fluid container was used for foaming experiments. Various impellers were made from acrylic for the reason of simple fabrication. For actual foaming using molten aluminium as a fluid, impellers were made of stainless steel coated with boron nitride (BN) and molten aluminium container was made of ceramic. Cooling system was

additionally used for aluminium foam production to protect device components from overheating and to solidify molten aluminium foam. The method of foaming used in this research is the gas injection. Experimental conditions are shown in **Table 3.1**. It is important to note that properties of fluids used in the experiments are different as shown in

Table 3.2.

Table 3.1 Experimental conditions.

Experiment	Air flow (l/min)	Temperature (°C)	Impeller Speed (rpm)
Water	1-40	23	0-1400
Molten Aluminium	1, 3, 5	700	600, 800, 1000

Table 3.2 Fluid properties.

Liquid	Density (kg/m^3)	Viscosity (mPa.s)	Surface Tension (N/m)
Water (23 °C)	997.44	941	0.07
Aluminium melt (700 °C)	2300	1.289	0.92
Air	1.15		

3.2 Computational Fluid Dynamics

Computational Fluid Dynamic based on COSMOSFloWork, a CFD software, was used to simulate the flow behaviour of the testing fluids in a cylindrical vessel under the rotation of various design impellers. In experiments, air was injected into water or aluminium, but the simulation was carried out without air injection. The simulation was used to determine the flow, velocity and pressure patterns of water under the rotation of impellers.

Schematic of the simulation methodology is shown in **Figure 3.2**. CAD model was first generated followed by specifying conditions and calculating to obtain simulation results.

Schematic diagrams of the vessel and the impeller set up for the simulation are shown in **Figure 3.3** and **Figure 4.3** respectively. The setup consists of a flat bottomed cylindrical vessel with the diameter of 92 mm and the height of 110 mm and an impeller positioned at the center of the vessel. The distance between the vessel bottom and the impeller bottom is 20 mm. The rotational speed of the impeller is 800 rpm. The testing fluid is water with the temperature of

23°C, the density, ρ, of 997.44 kg/m^3 and the viscosity, μ, of 941 mPa.s. The simulation conditions were set as a turbulent flow type under the gravitational acceleration, an adiabatic wall with the roughness of 0 μm and the environment pressure of 10^5 Pa.

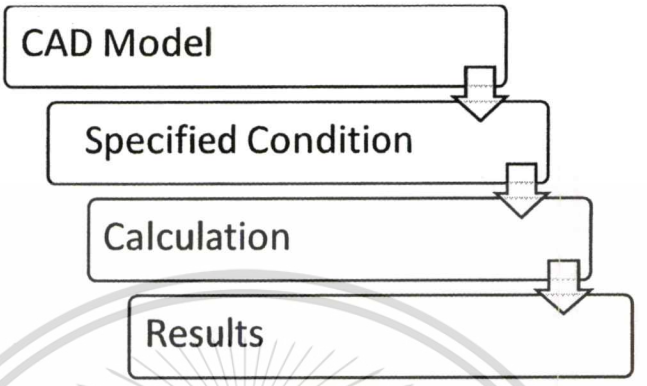

Figure 3.2 Simulation methodology of CFD using COSMOSFloWork.

Fluid flows of water in a cylindrical vessel under the rotation of impellers were simulated using properties of water at temperature of 23 °C taken from

Table 3.2. The initial conditions set for the simulation are shown in **Figure 3.3** and **Table 3.1**.

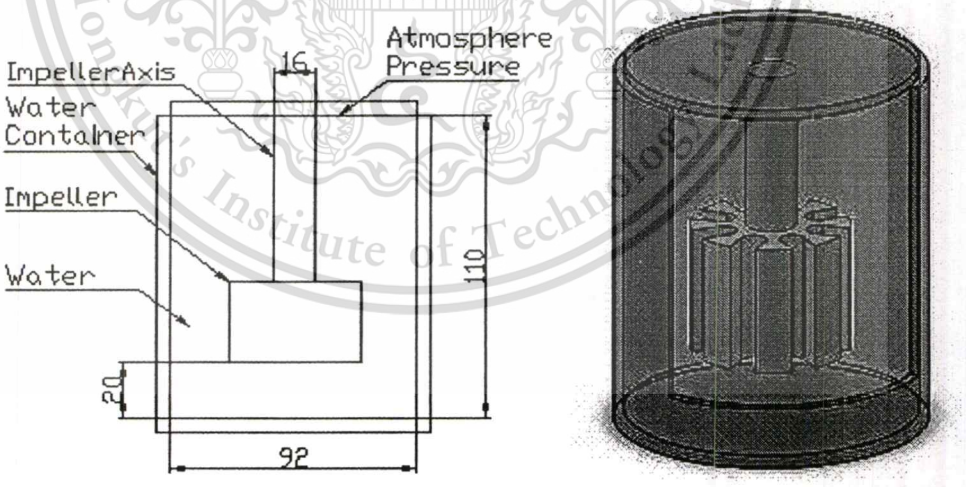

Figure 3.3 CAD Model with dimensions.

3.3 Characterisations

3.3.1 Cell Size

Cell size of foams was measured using two methods: an image analysis software and a

manual measurement. The Image-Pro 5.0 software was used to measure the cell size of bubble images taken from sections of aluminium foam samples. Some re-touching of the images was done manually to obtain accurate measurement of the cell size. The manual cell size measurement was used for water foams using images of water bubbles taken from a digital camera. Mean linear intercept method was used for the bubble size measurement. Bubbles were assumed to be spherical shape. Vertical lines paralling to the vessel body were drawn on the water foam image and intersections between bubbles and the lines were counted. The tangent intersection was counted as a half, while the others were counted as one, as shown for example in **Figure 3.4**. The mean bubble size can then be calculated using the below equation.

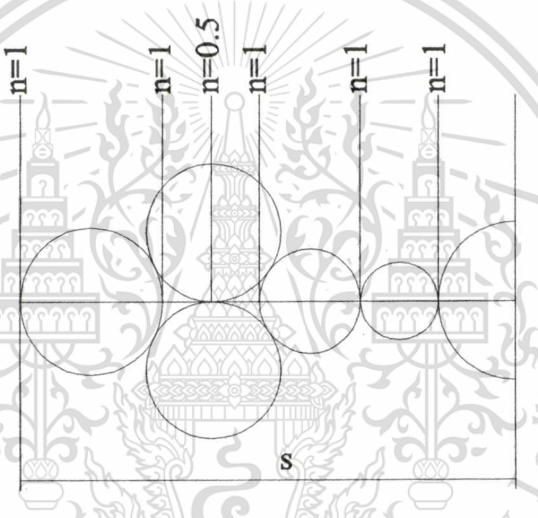

Figure 3.4 The count of bubbles using the mean linear intercept method.

$$d_{b,average} = \frac{S}{\sum n} \tag{3.1}$$

where, $d_{b,average}$ is the mean bubble size,

S is the length of intercept line,

n is the number of intercept.

It is important to note that when a cylindrical vessel was used, only lines in the vertical direction were used for the cell size measurement in order to avoid artefact occurred in the non-vertical directions, i.e. horizontal direction as shown in **Figure 3.5** (a). However, small artefact still exists in the measurement of cell size in the vertical intercept lines as shown in **Figure 3.5** (b). This artefact size measurement is estimated to be within ± 5 %.

3.3.2 Foam Extent

Foam extent or foam thickness is measured using the scale attached at the side of the vessel as shown in **Figure 3.5** (b).

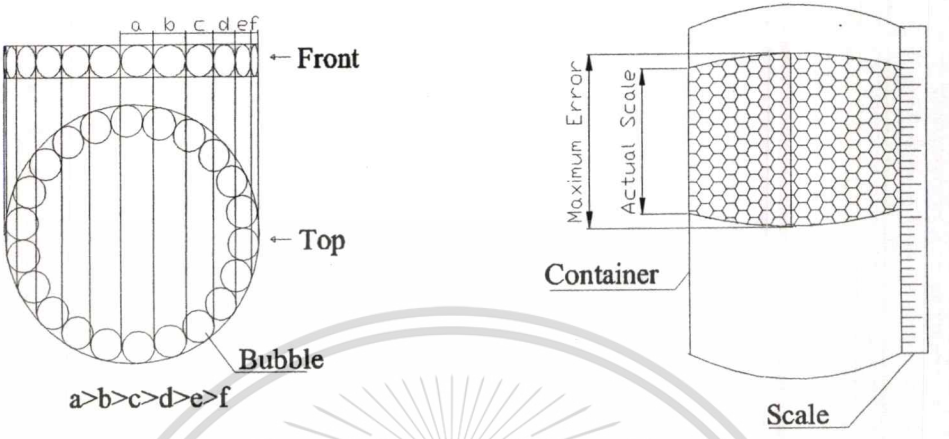

Figure 3.5 Artefact of cell size measurement by mean linear intercept method: (a) horizontal and (b) vertical lines.

3.3.3 Density

Basically, density of porous materials is measured using the Archimedes' method. However, the density of aluminium foams with large pore size and some open-cell obtained in this research cannot be measured by the Archimedes' method due to the unability of the foams to contain water without leakage. Therefore, a simple calculation, as given in below equation, was used for the estimation of aluminium foams density in this research

$$\rho_{foam} = \frac{m_{foam}}{V_{foam}} \tag{3.2}$$

where ρ_{foam} is the density of the foam.

m_{foam} is the mass of the foam.

V_{foam} is the volume of the foam.

CHAPTER 4

GAS INJECTION DEVICE DESIGN

The aim of this research is to obtain an optimal design of a gas injection device which is the main element of the direct gas injection process for low cost aluminium foam production. Small cell size and uniform foam structure are key features required for aluminium foams, therefore this chapter focuses on the investigation of the effects of design parameters of the gas injection device as well as processing conditions on the formation of foam. A small scale foaming apparatus was set up for producing a lab-scale aluminium foam. Experiments were divided into two sections: physical model and a lab-scale aluminium foam production.

4.1 Foaming using Physical Model

Simulation and physical model experiment, which is a method of carrying out experiment with conditions similar to those in a complex system, were performed using various gas injection device designs and a cylindrical foam vessel with the foam exit on the top. The obtained information of the effective gas injection design was then used to design a gas injection device for foaming in a foam vessel with side exit and a tri-cylindrical vessel with top exit. The influence of the device designs in parallel with operating conditions on foaming was examined using water as a testing fluid for the physical model experiment.

4.1.1 Foaming in a Cylindrical Foam Vessel with Top Exit

4.1.1.1 Apparatus

Figure 4.1 shows the schematic of the experimental apparatus for foaming experiments using a water model. The apparatus consists of three principal components: (1) a transparent vessel, (2) a gas injection device and (3) a photographic unit.

The transparent vessel used in this experiment is a transparent cylindrical vessel with a flat bottom and an open top, having an inner diameter of 92 mm and a height of 210 mm. The vessel was filled with water with 110 mm height. The gas injection device consists of a changeable impeller, an impeller shaft, a rotational system and a compressed air supply. Foaming

experiments were carried out using various design impellers. The photographic unit was used to take bubble photographs. Size and extent of bubbles were measured using the linear intercept method and the direct measurement on the taken photographs as describe in sections 3.3.1and 3.3.2. An impeller was dipped into the water with the distance of 20 mm above the vessel bottom. The actual apparatus is shown in **Figure 4.2**. The experimental conditions are given in **Table 4.1**.

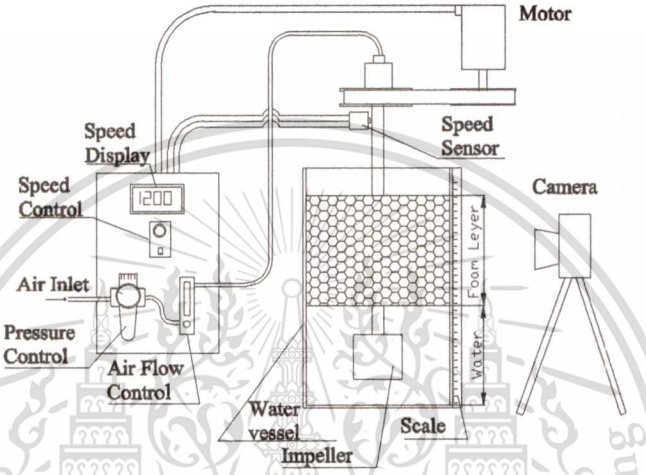

Figure 4.1 Schematic of experimental set up for physical water model foaming experiments in a cylindrical vessel.

Table 4.1 Experimental conditions for foaming experiments in a cylindrical vessel.

Air Pressure (MPa)	Air flow rate (l/min)	Temperature (°C)	Impeller rotation speed (rpm)
0.2	10, 20, 30, 40	23 ± 0.5	0-1200 ± 5

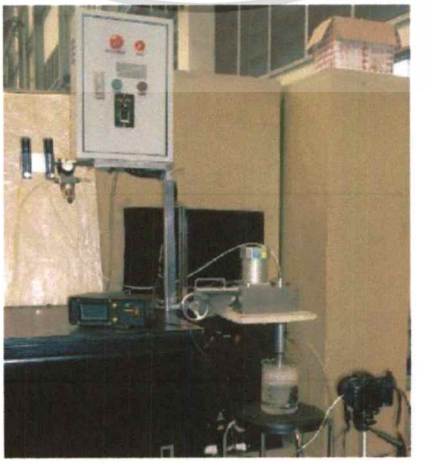

Figure 4.2 Apparatus for foaming experiments in a cylindrical vessel.

4.1.1.2 Impeller

For foaming experiments in the cylindrical vessel, five types of impellers (A-E) and a single type of stators having three different hole sizes (S1-S3) were used (**Figure 4.3** and **Figure 4.4**). Dimensions of impellers and stators are given in **Table 4.2**. Impeller A is a cylindrical nozzle without any blade. Impeller B is a turbine type impeller having blades and a gas injection hole. Impeller C is a combined design of impellers A and B. It has four blades and 20 orifice holes to obtain both high shear rotation and fine bubbles. Impeller C is also equipped with stators S1, S2 and S3, denoted as C-S1, C-S2 and C-S3. Similarly, impeller D and E, which are a tree-like blade impeller with orifice holes at the blade tails and sides respectively, are equipped with stator S2, denoted as D-S2 and E-S2. The aim of these combinations is to be able to inject more gas and higher impeller rotation speed without increasing disturbance in liquid media.

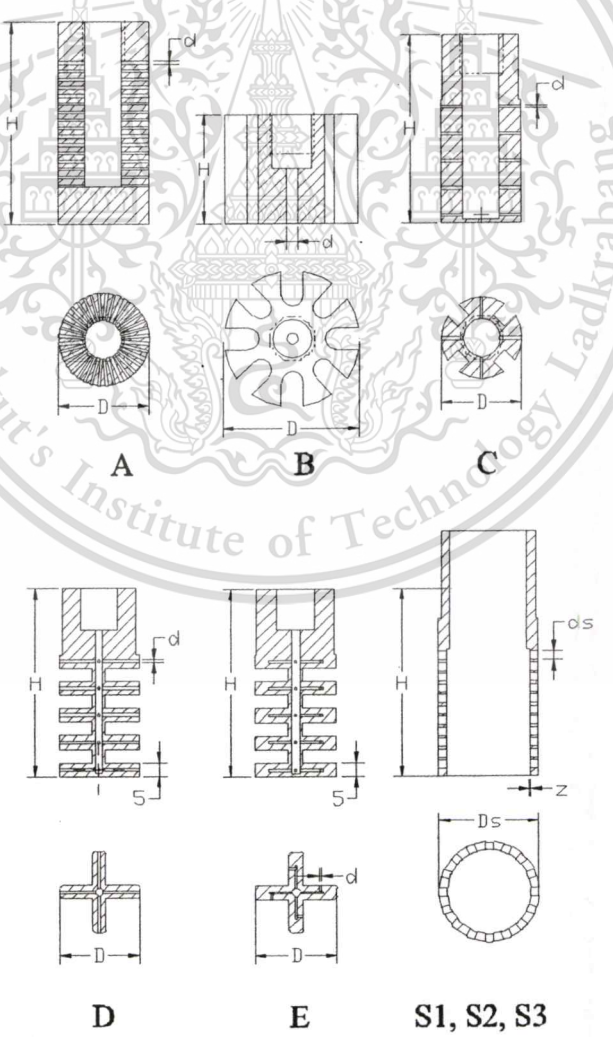

Figure 4.3 Geometry of impellers and stators.

Table 4.2 Dimensions of impellers and stators.

Dimension	Impeller and stator							
	A	**B**	**C**	**D**	**E**	**S1**	**S2**	**S3**
Diameter, D (mm)	30	50	30	30	30	37	37	37
Height, H (mm)	69	40	69	69	69	90	90	90
Orifice diameter, d (mm)	1	4	1	1	1	1	2	3
Orifice number	1	1152	20	20	20	1800	464	336
Gap between impeller C and stator, z (mm)	-	-	-	-	-	0.5	0.5	0.5

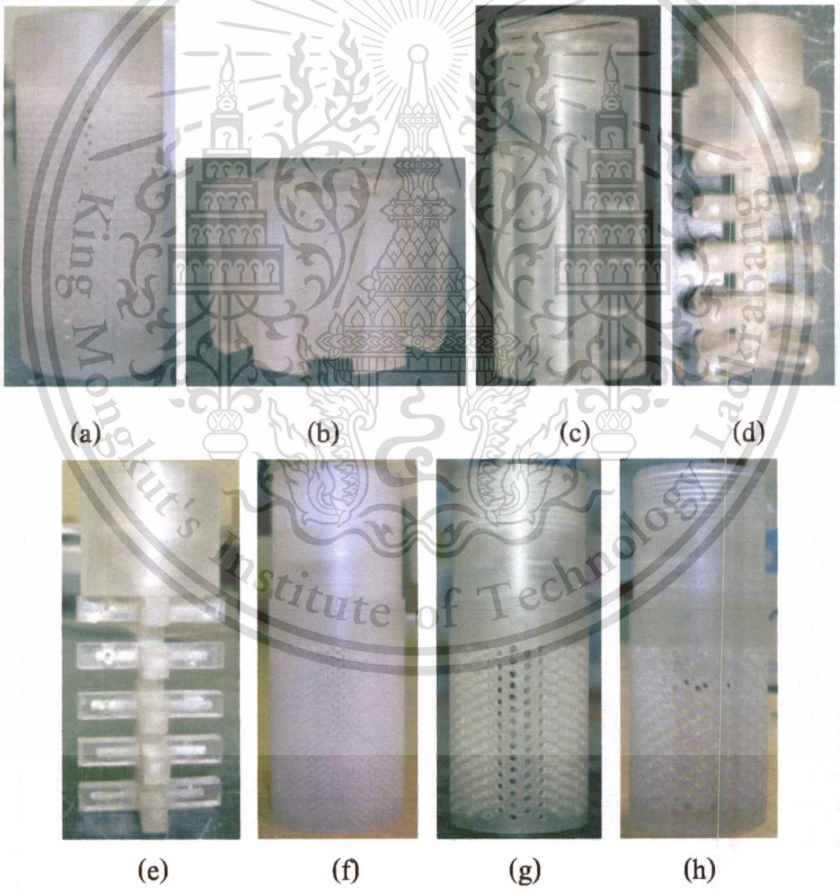

Figure 4.4 Actual impellers and stators: (a) impeller A, (b) impeller B, (c) impeller C, (d) impeller D, (e) impeller E, (f) stator S1, (g) stator S2, and (h) stator S3.

4.1.1.3 Results

4.1.1.3.1 Simulation

COSMOSFloWork software was used to determine the profile of velocity, pressure, motion vector, shear force and shear stress of water under the rotation of various design impellers and stators. **Figure 4.5-Figure 4.10** show the velocity profile, pressure profile and motion vector of water under the rotation at 800 rpm of impeller A, B, C, D, E, and impeller C, D and E equipped with stator S2. It can be seen that different design impellers generated different degrees of disturbance to the water. Severe disturbance was found under the rotation of impeller B and to the less extent by impellers C, D and A respectively. When impellers C, D and E were equipped with stator S2, the disturbance in water was removed. The degree of disturbance can be determined by considering the velocity of water under the rotation of impellers at locations shown in **Figure 4.11**, whose results under the impeller rotation speed of 800 rpm show in **Figure 4.12**. High velocity of water was found at locations closed to impeller blades particularly with the large diameter impeller, i.e. impeller B. Stator was effective in reducing fluid velocity in the locations outside the stator.

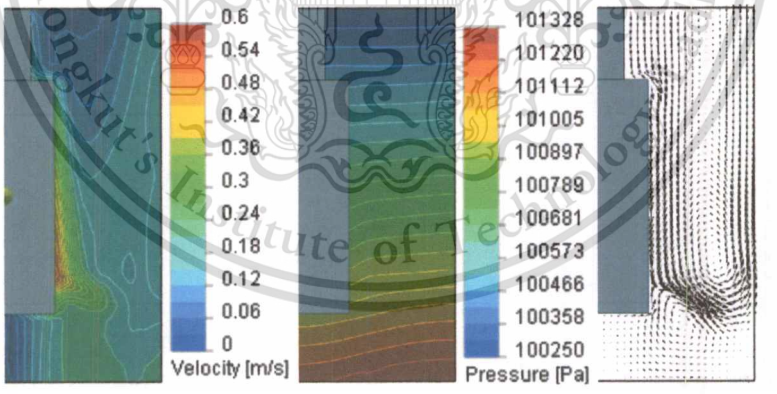

(a) (b) (c)

Figure 4.5 CFD results of water under the rotation at 800 rpm of impeller A: (a) velocity profile, (b) pressure profile and (c) velocity vector.

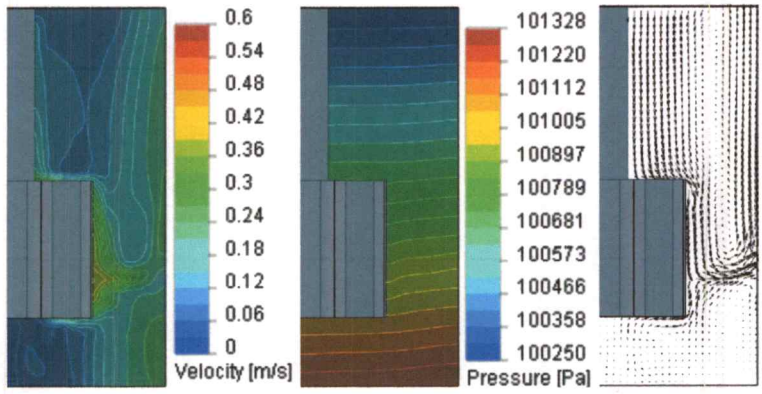

Figure 4.6 CFD results of water under the rotation at 800 rpm of impeller B: (a) velocity profile, (b) pressure profile and (c) velocity vector.

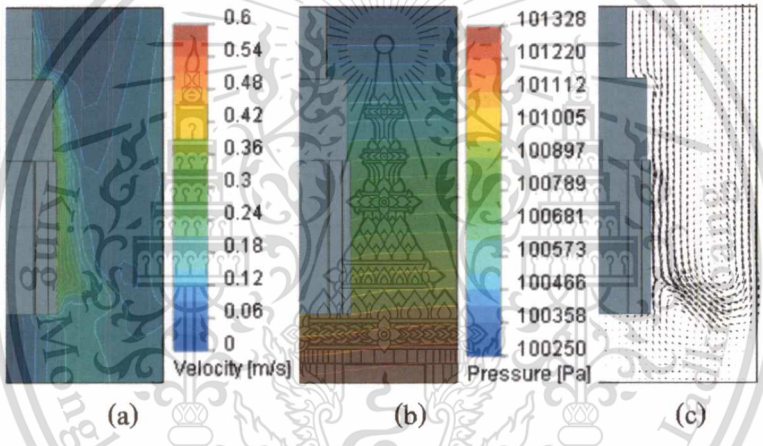

Figure 4.7 CFD results of water under the rotation at 800 rpm of impeller C: (a) velocity profile, (b) pressure profile and (c) velocity vector.

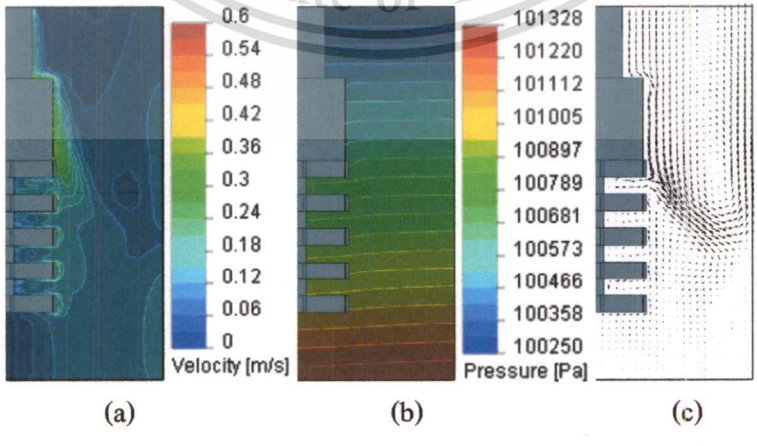

Figure 4.8 CFD results of water under the rotation at 800 rpm of impellers D and E: (a) velocity profile, (b) pressure profile and (c) velocity vector.

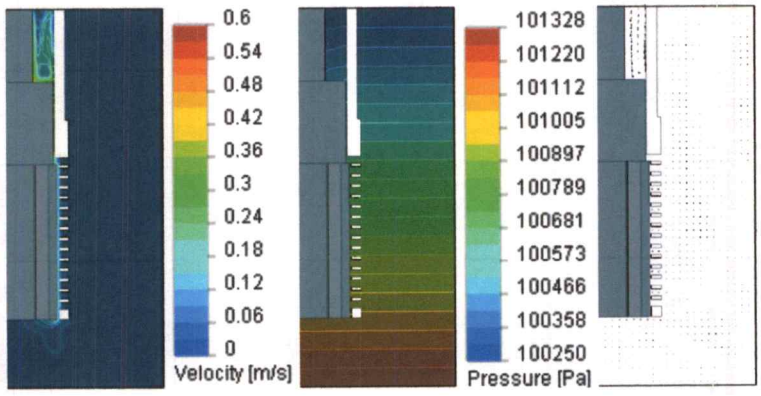

Figure 4.9 CFD results of water under the rotation at 800 rpm of impeller C-S2: (a) velocity profile, (b) pressure profile and (c) velocity vector.

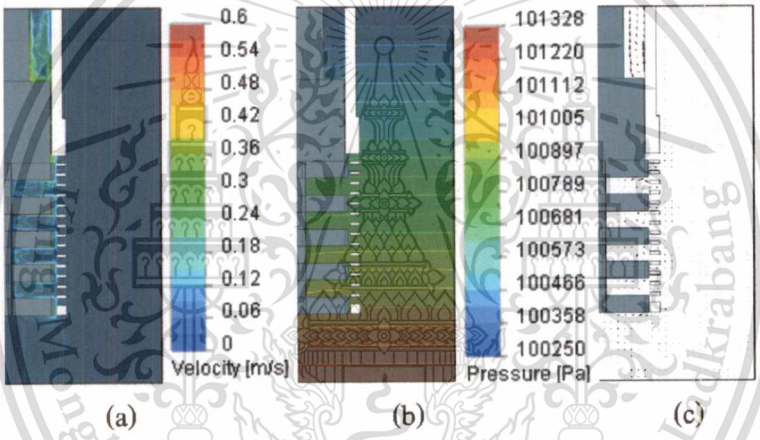

Figure 4.10 CFD results of water under the rotation at 800 rpm of impellers D-S2 and E-S2: (a) velocity profile, (b) pressure profile and (c) velocity vector.

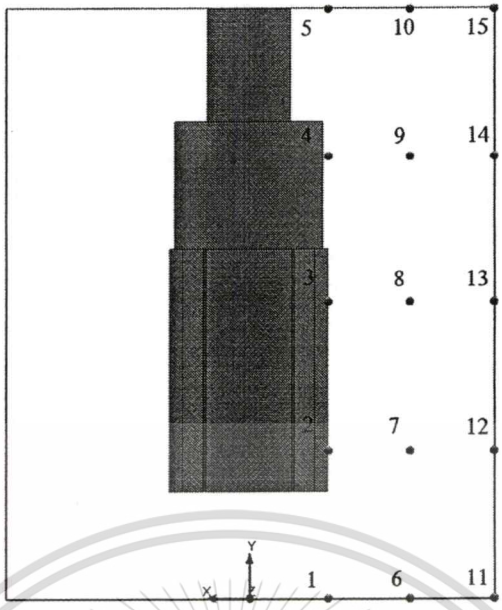

Figure 4.11 Locations for velocity measurement.

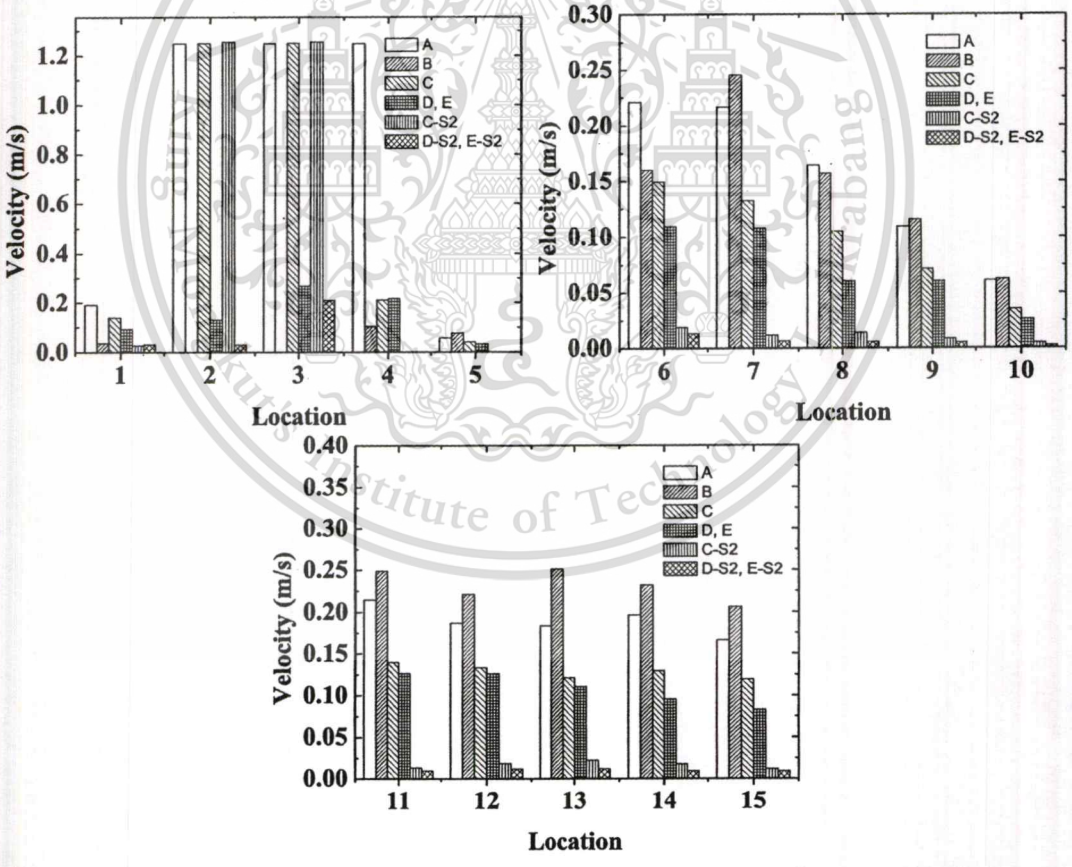

Figure 4.12 Velocity of water under the rotation of impeller at 800 rpm at location defined in Figure 4.11.

Figure 4.13 and **Figure 4.14** show shear stresses and shear forces in water occurred by the rotation of impellers at 800 rpm, respectively. **Figure 4.15** shows shear stresses in water at circumferential surface of impellers rotating at 800 rpm. Large impeller diameters tend to generate high shear stresses and shear forces. When impeller C equipped with stator S2, high shear stresses occurred in the region between the impeller and the stator, while small shear stresses occurred in the region outside the stator.

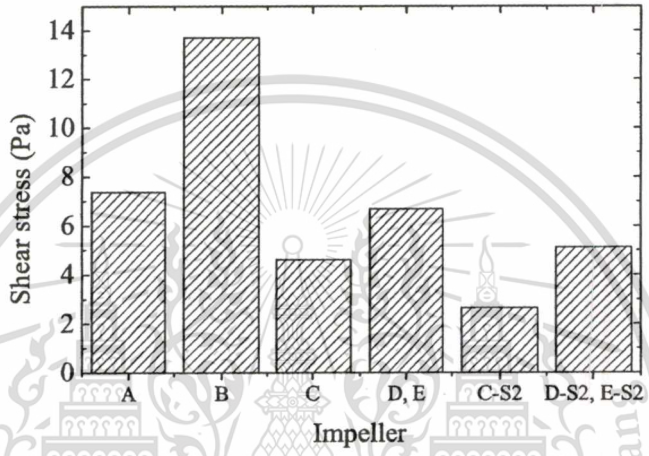

Figure 4.13 Shear stresses occurred by the rotation of impellers at 800 rpm.

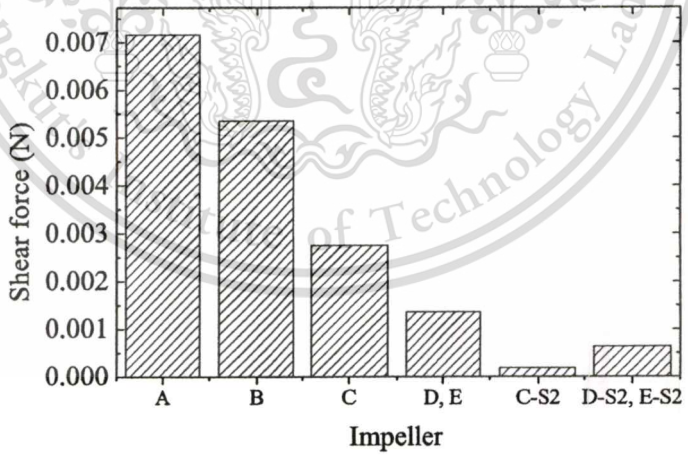

Figure 4.14 Shear forces in water occurred by the rotation of impellers at 800 rpm.

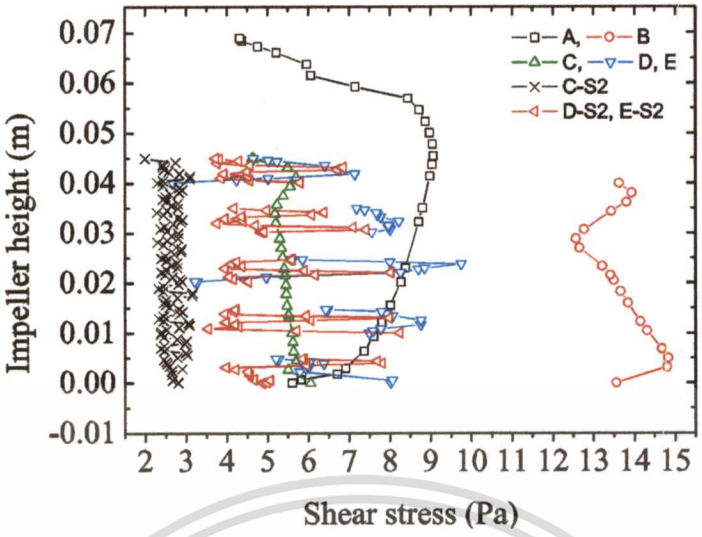

Figure 4.15 Shear stresses in water at circumferential surface of impellers rotating at 800 rpm.

4.1.1.3.2 Physical Model

The effects of impeller rotation speed and air flow rate on the formation of bubbles in water are shown in **Figure 4.16-Figure 4.17** for Impeller A, **Figure 4.18-Figure 4.19** for Impeller B, **Figure 4.20-Figure 4.21** for Impeller C, **Figure 4.22-Figure 4.23** for Impeller D, **Figure 4.24-Figure 4.25** for Impeller E, **Figure 4.26-Figure 4.27** for Impeller C-S1, **Figure 4.28-Figure 4.29** for Impeller C-S2, **Figure 4.30-Figure 4.31** for Impeller C-S3, **Figure 4.32-Figure 4.33** for Impeller D-S2, and **Figure 4.34-Figure 4.35** for Impeller E-S2.

Figure 4.16-Figure 4.17 show that during stirring and air injecting with impeller A, having a total of 1152 orifice holes surrounding the impeller, at a constant air injection rate the bubble size and the foam extent decreased with increasing impeller rotation speed, while at a constant impeller rotation speed the bubble size and the foam extent increased with increasing air injection rate. It is interesting to note that air can only emit at upper orifices. However, a larger number of orifices were active when more air was supplied. The smallest bubble size of 3.5 mm was reached at the impeller rotation speed of 1,200 rpm and the air injection rate of 40 l/min, while the highest foam extent of 92 mm was obtained with the air injection rate of 40 l/min and the stationary impeller. The tendency of the change of bubble size and foam extent with the variation of impeller rotation speed and air injection rate of the other impellers was similar to those observed in impeller A.

In impeller B, a turbine type impeller with eight blades and a gas injection hole, the addition of severe vortex was observed during stirring the impeller at the impeller rotation speed of even slow speeds. Another noticeable difference of foaming of this impeller is the absence of bubbles at impeller rotation speeds higher than 400 rpm. The smallest bubble size of 3.3 mm and the largest foam extent of 90 mm were observed at the air injection rate of 40 l/min with the impeller rotation speed of 200 rpm and 0 rpm respectively.

In impeller C, a four-blades impeller with 20 orifice holes, higher foam extents were obtained at all foaming conditions comparing with those of impellers A and B. The highest foam extent of about 150 mm was observed when the air injection rate of 40 l/min and the impeller rotation speed of 200 rpm were used. The size of bubbles was indifferent comparing with those of other impellers. The smallest bubble size of 3.0 mm was observed at the impeller speed rotation speed of 400 rpm and the air injection rate of 40 l/min.

Impeller D, a tree-like blade impeller with orifice holes at blade tails, and impeller E, a tree-like blade impeller with orifice hole sitting on the side of the blades, showed similar foaming behaviour. The highest foam extent of 105 mm was observed at the impeller rotation speed of 100 rpm and the air injection rate of 40 l/min in impeller D, while the highest foam extent of slightly under 100 mm was observed with the still impeller at the air injection rate of 40 l/min.

Stators, when equipped with impeller C, gave obviously higher foam extents, as shown in **Figure 4.26-Figure 4.31** in which the highest foam extents of 132, 160 and 135 mm were obtained with the impeller equipped with stators S1, S2 and S3 respectively. The best foaming performance obtained when the impeller was equipped with stator S2 and operated at the impeller rotation speeds beyond 200 rpm and at the air injection rate of 40 l/min. The narrow variation of bubble size, i.e. 2.9-5.2 mm, was received within the testing conditions for impeller C equipped with all stators.

The influence of stator on the improvement of foaming performance of impellers D and E, as shown in **Figure 4.32-Figure 4.35**, is similar to that of impeller C. However, the less foaming performance improvement were found in these two impeller comparing with that of impeller C.

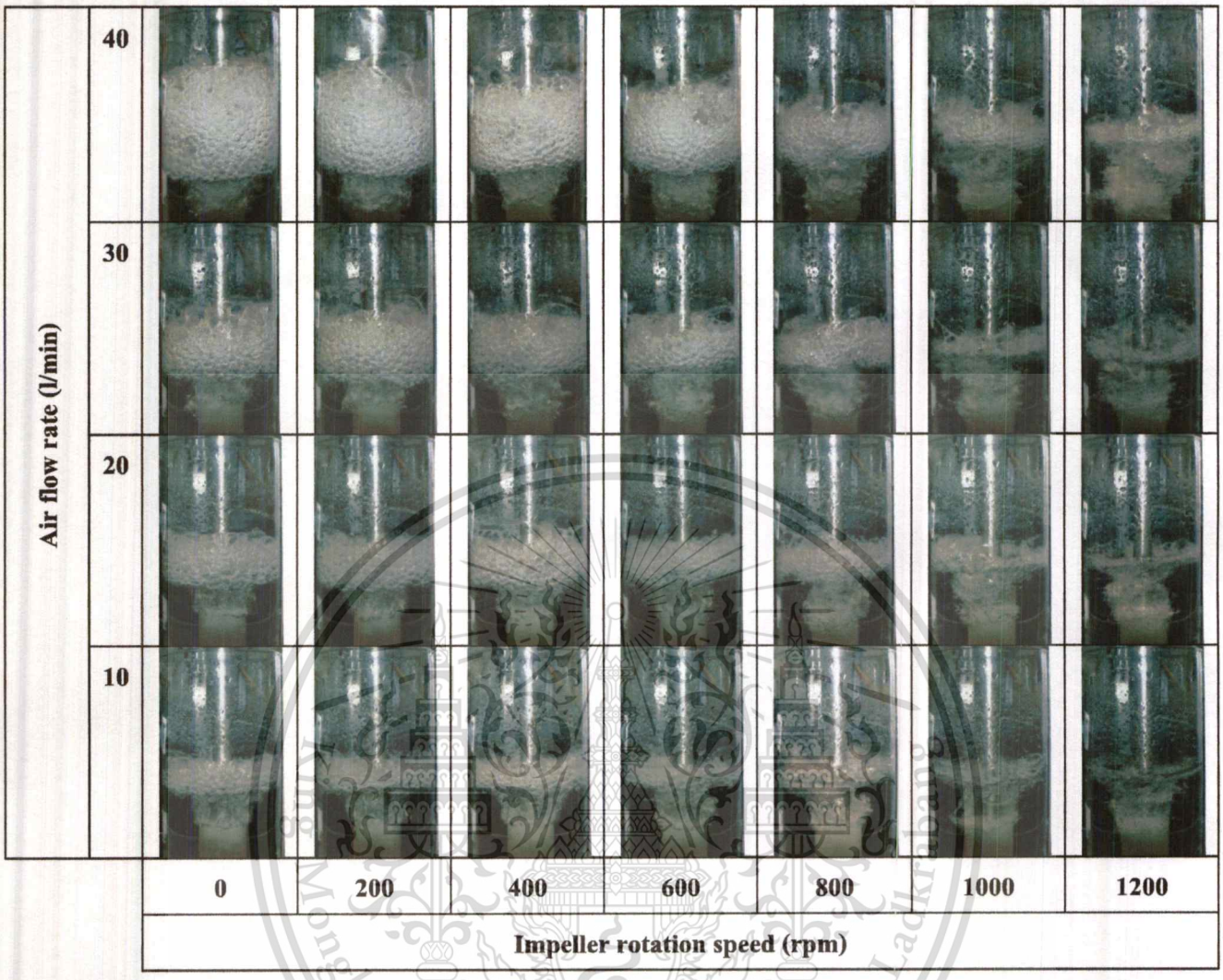

Figure 4.16 Photographs showing the effect of impeller rotation speed and air flow rate on the formation of bubbles in water with impeller A.

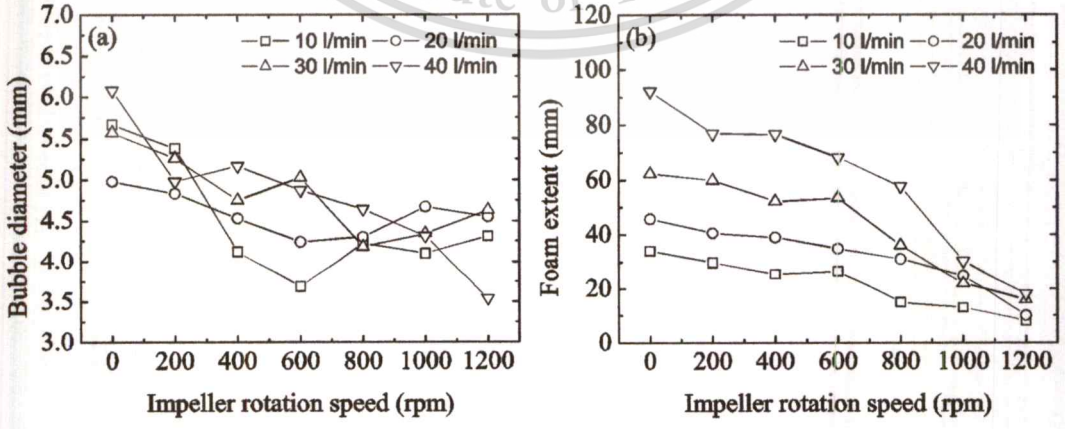

Figure 4.17 (a) Bubble diameter and (b) foam extent of impeller A.

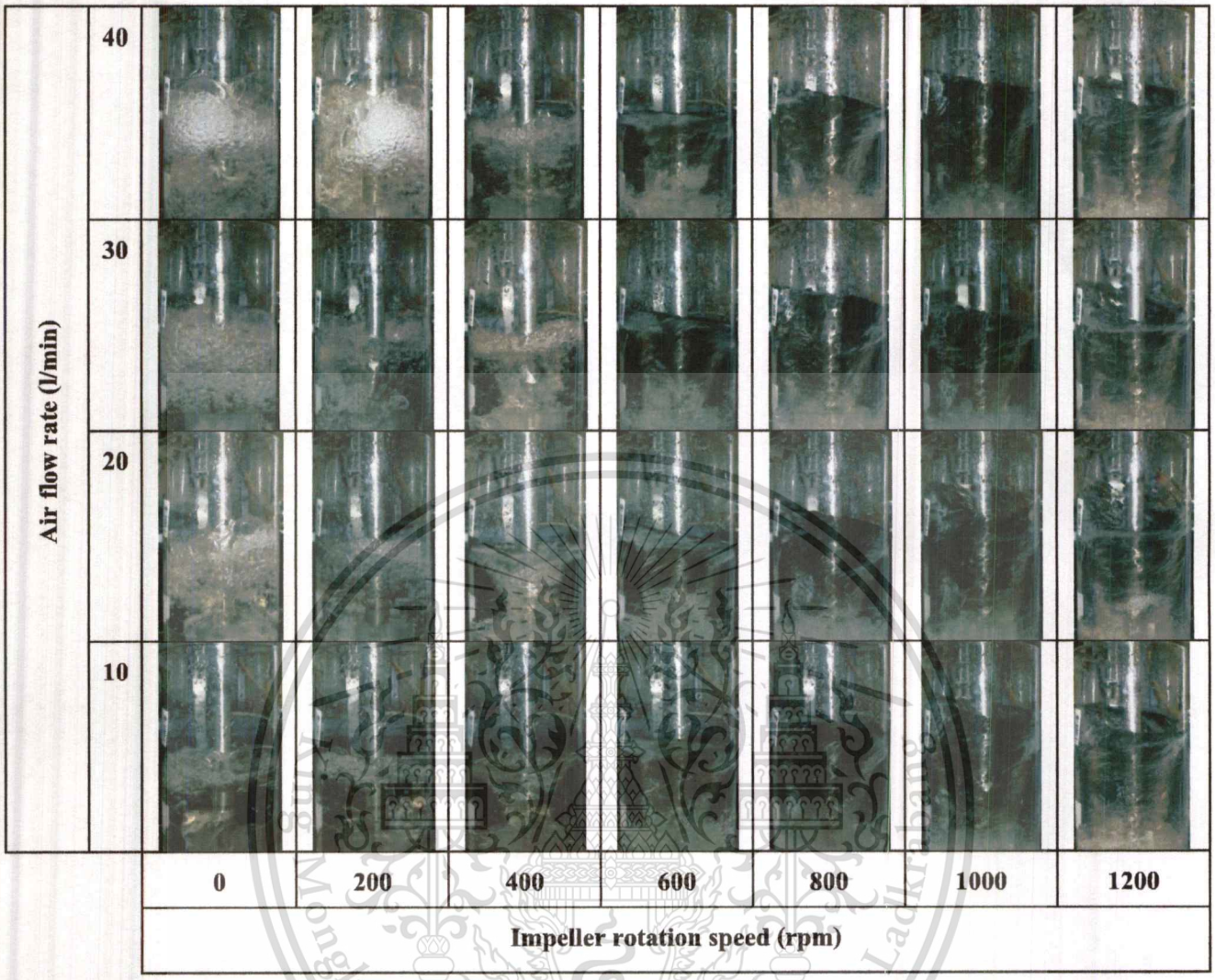

Figure 4.18 Photographs showing the effect of impeller rotation speed and air flow rate on the formation of bubbles in water with impeller B.

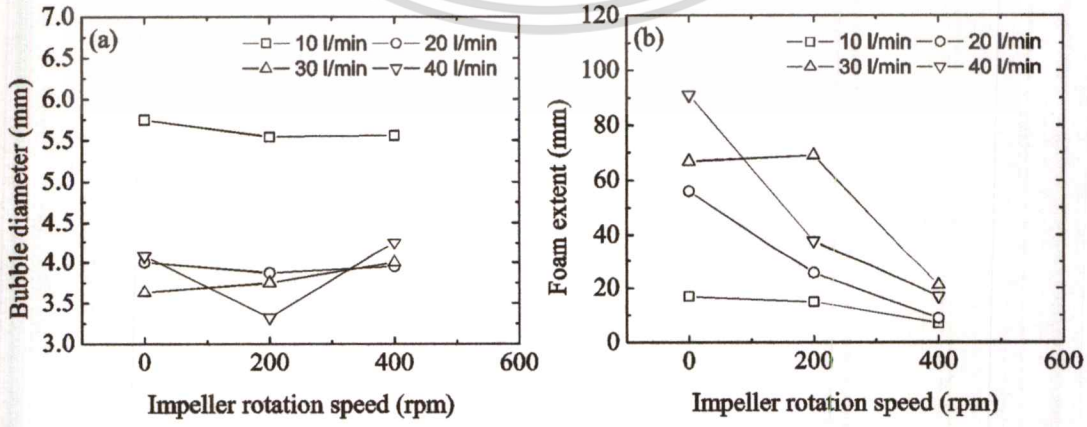

Figure 4.19 (a) Bubble diameter and (b) foam extent of impeller B.

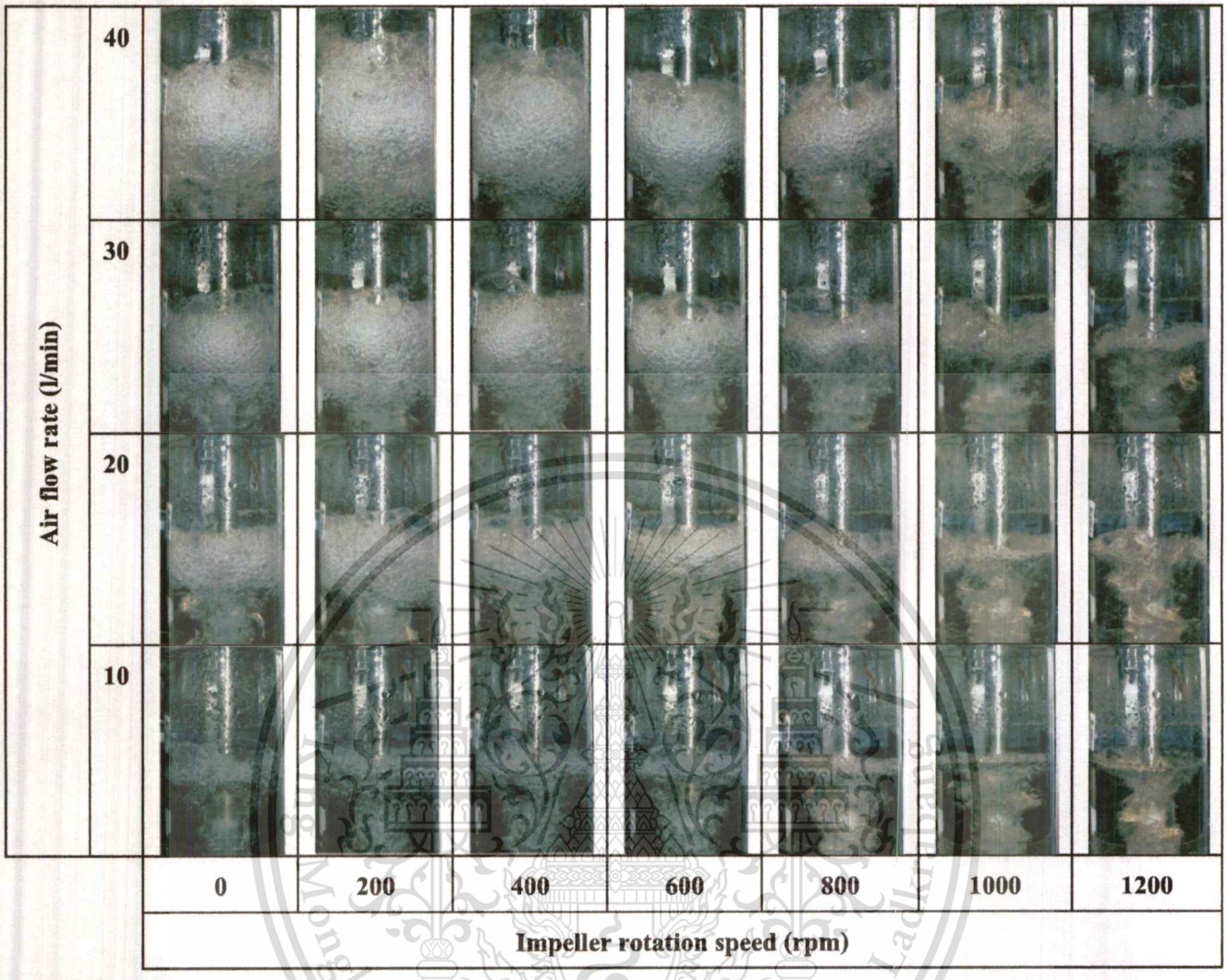

Figure 4.20 Photographs showing the effect of impeller rotation speed and air flow rate on the formation of bubbles in water with impeller C.

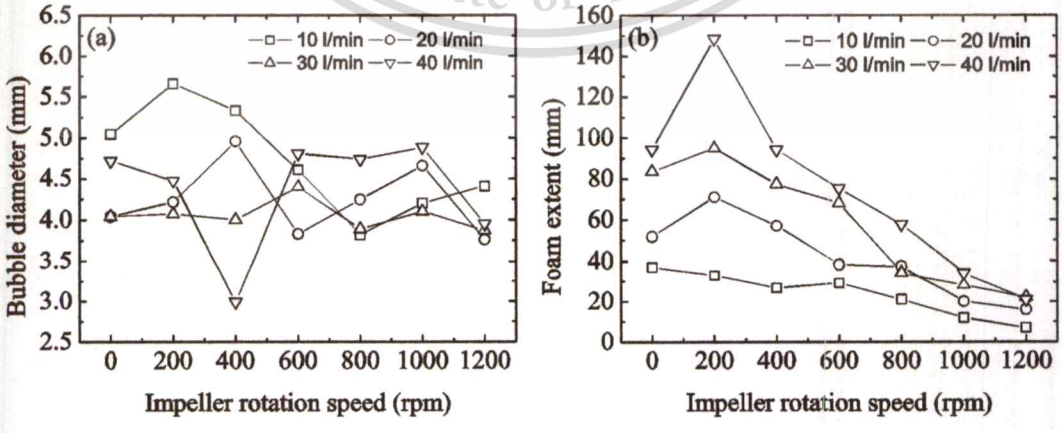

Figure 4.21 (a) Bubble diameter and (b) foam extent of impeller C.

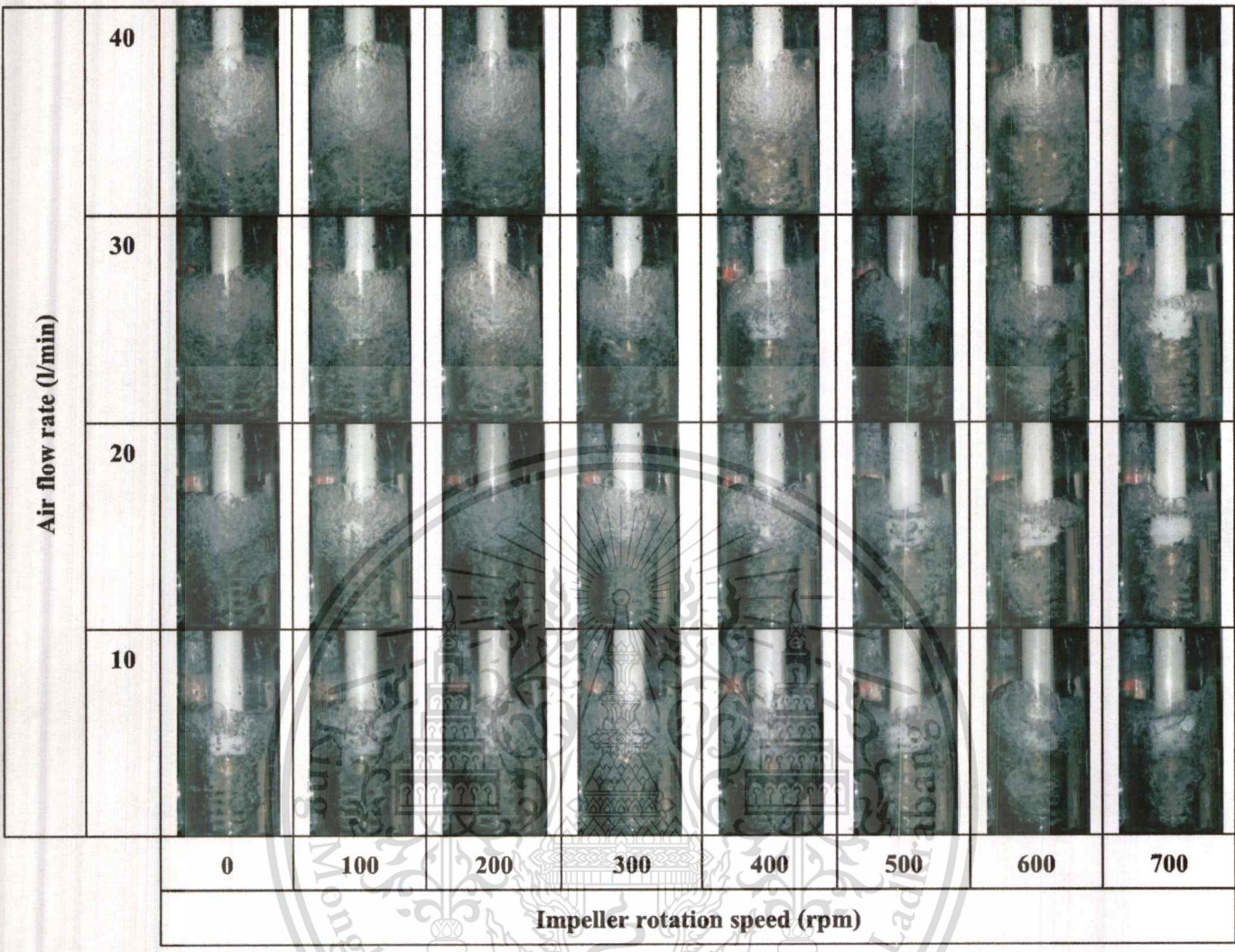

Figure 4.22 Photographs showing the effect of impeller rotation speed and air flow rate on the formation of bubbles in water with impeller D.

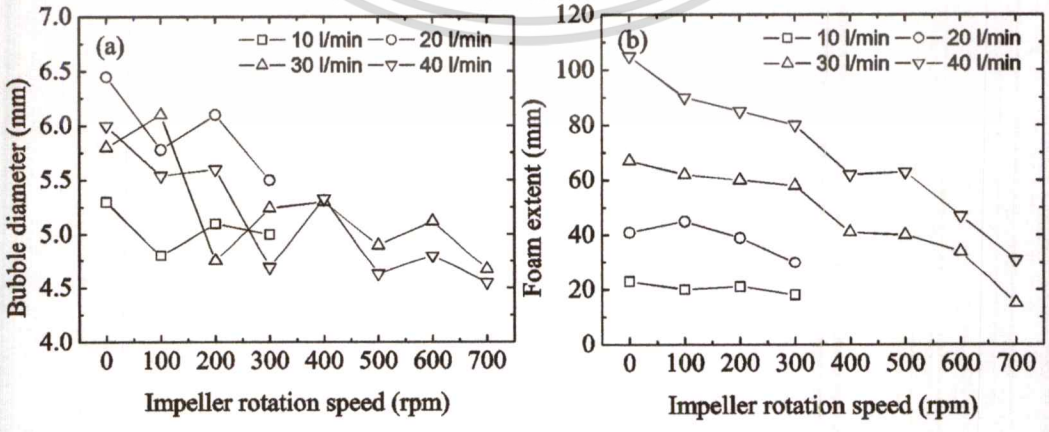

Figure 4.23 (a) Bubble diameter and (b) foam extent of impeller D.

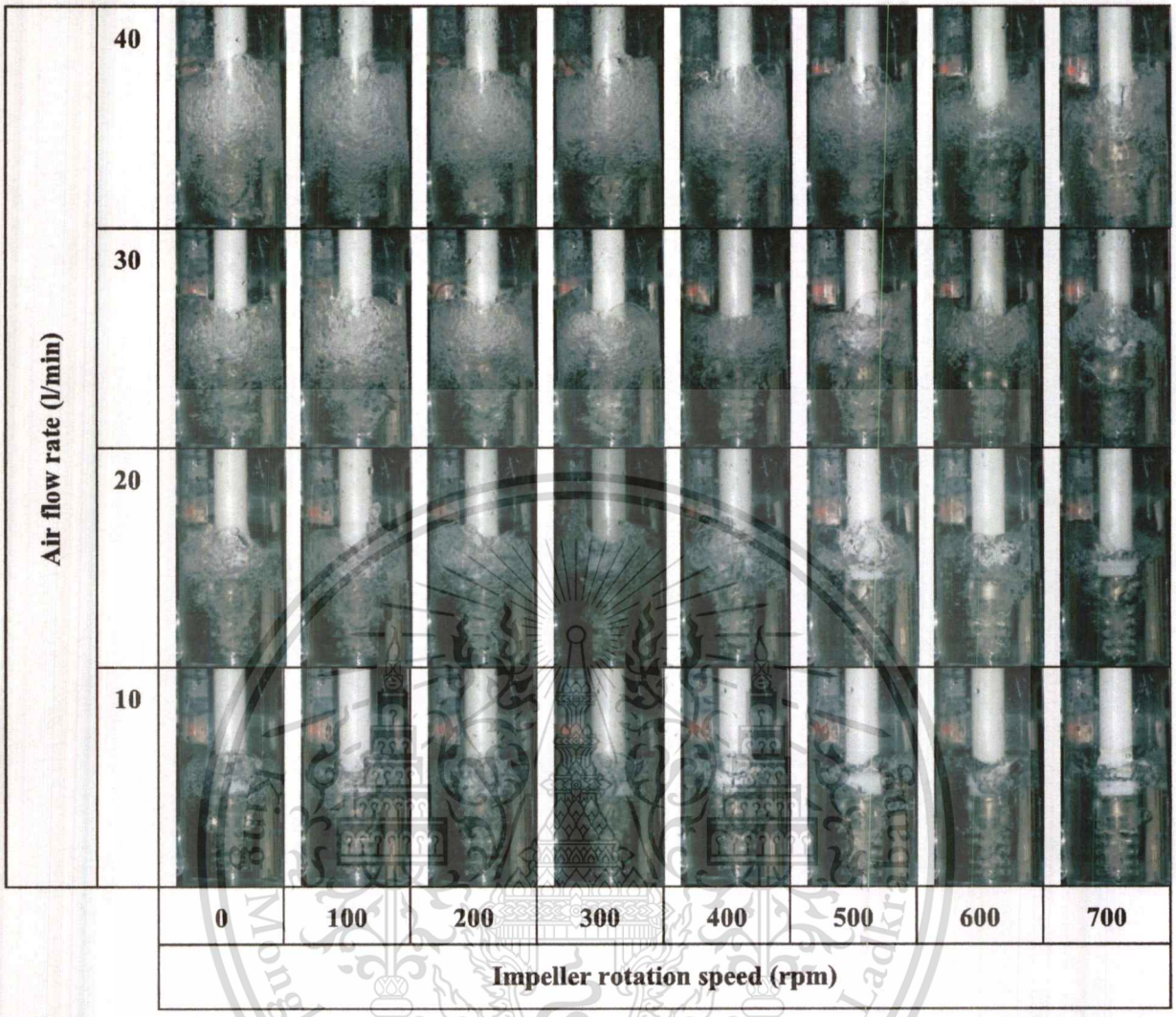

Figure 4.24 Photographs showing the effect of impeller rotation speed and air flow rate on the formation of bubbles in water with impeller E.

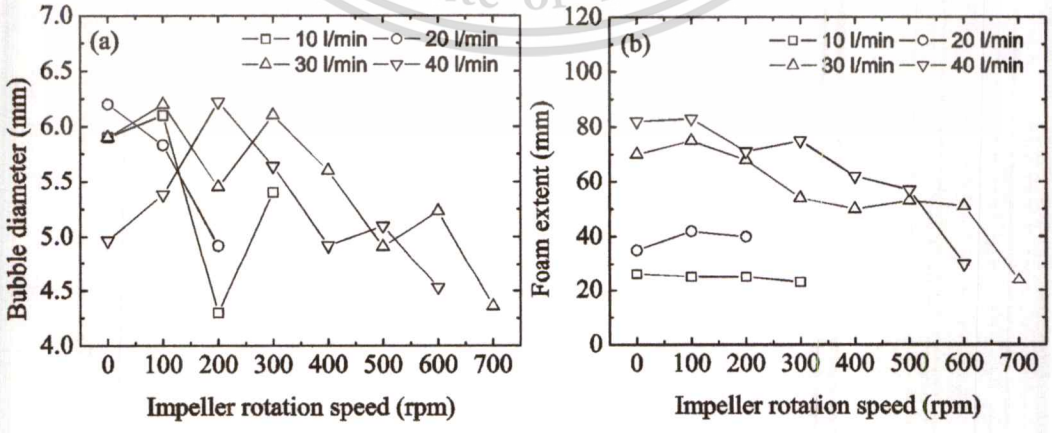

Figure 4.25 (a) Bubble diameter and (b) foam extent of impeller E.

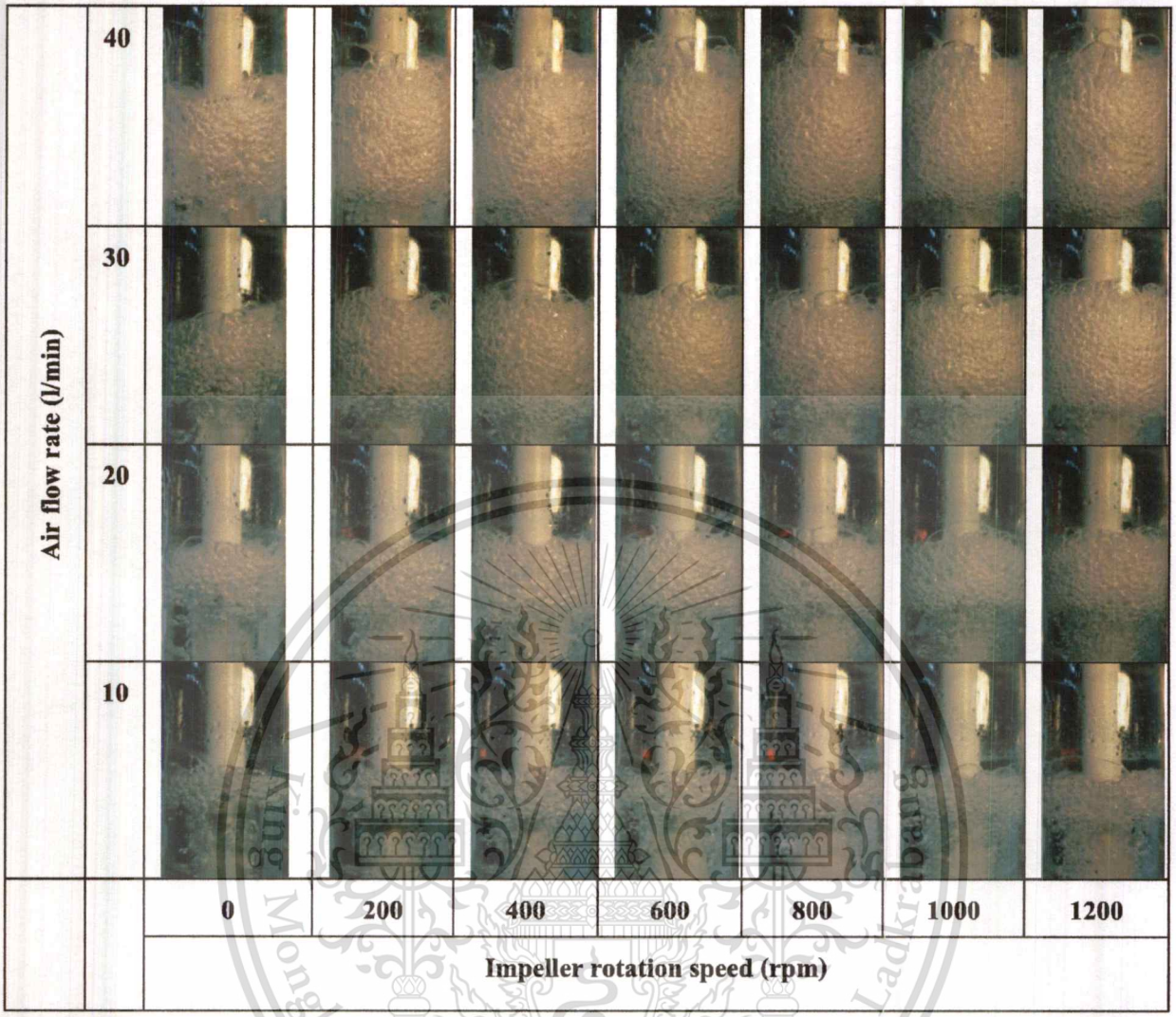

Figure 4.26 Photographs showing the effect of impeller rotation speed and air flow rate on the formation of bubbles in water with impeller C-S1.

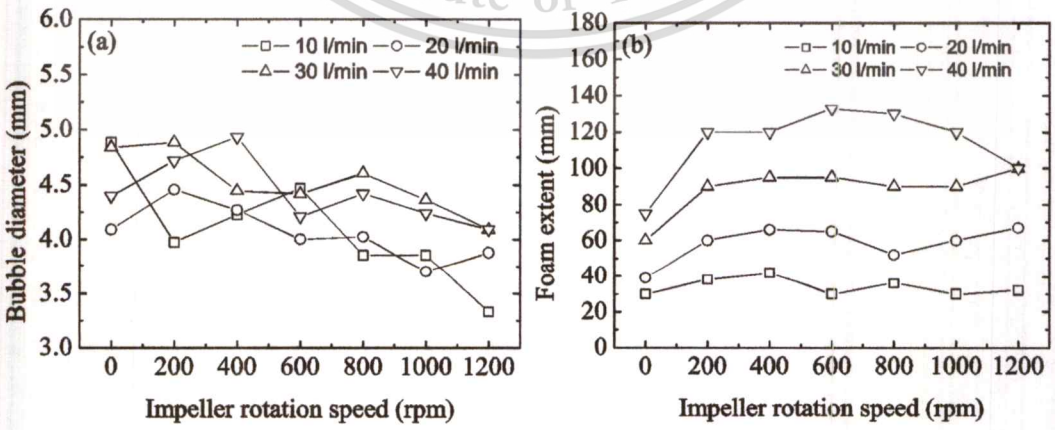

Figure 4.27 (a) Bubble diameter and (b) foam extent of impeller C-S1.

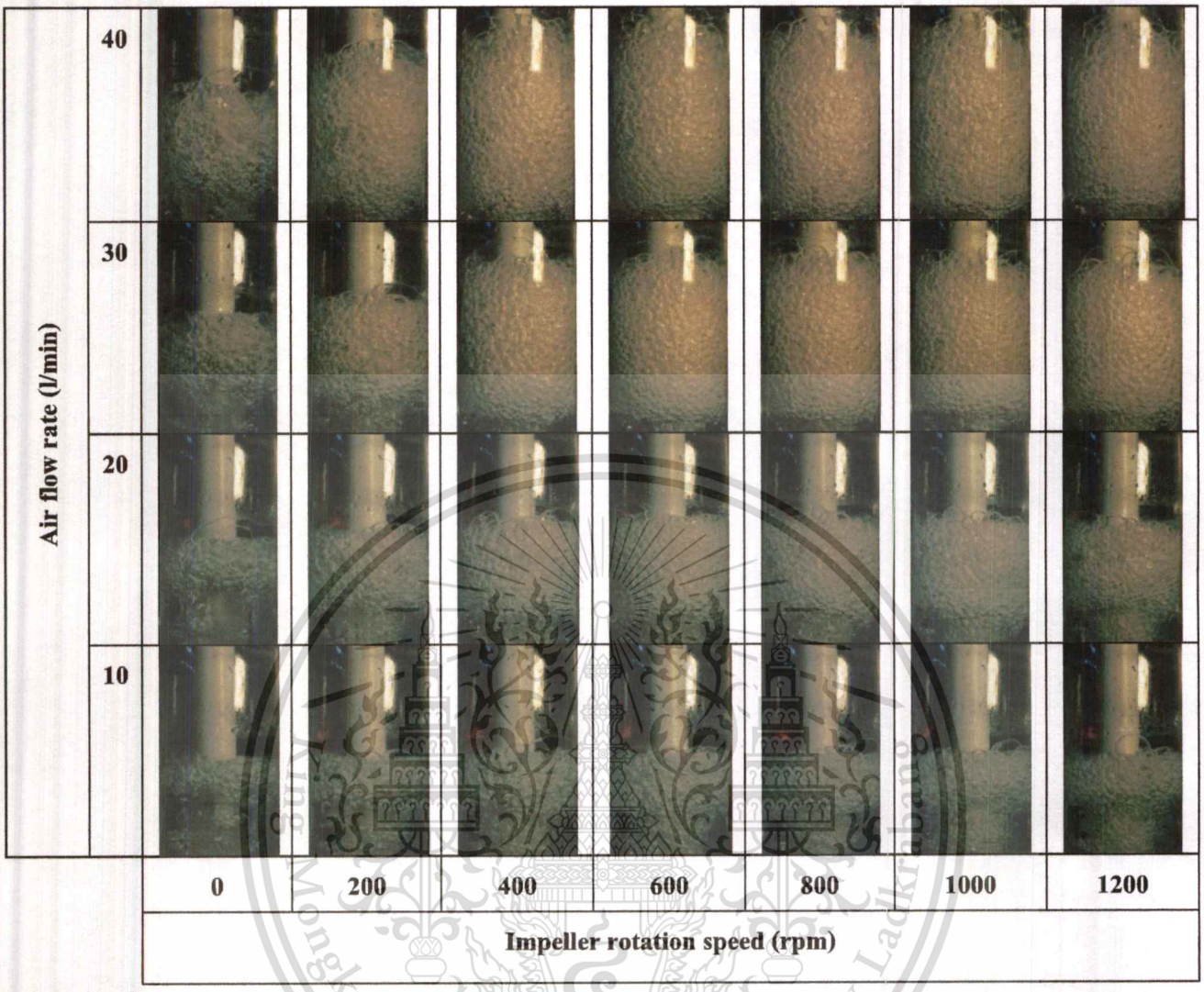

Figure 4.28 Photographs showing the effect of impeller rotation speed and air flow rate on the formation of bubbles in water with impeller C-S2.

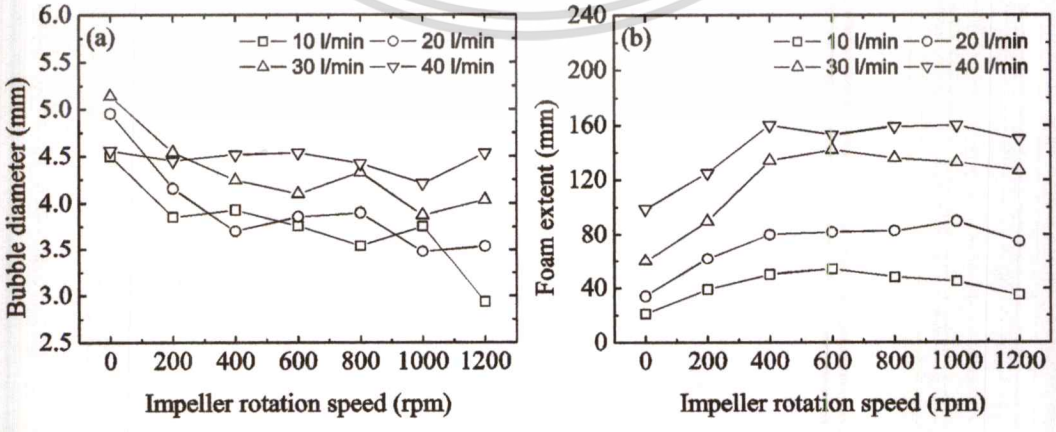

Figure 4.29 (a) Bubble diameter and (b) foam extent of impeller C-S2.

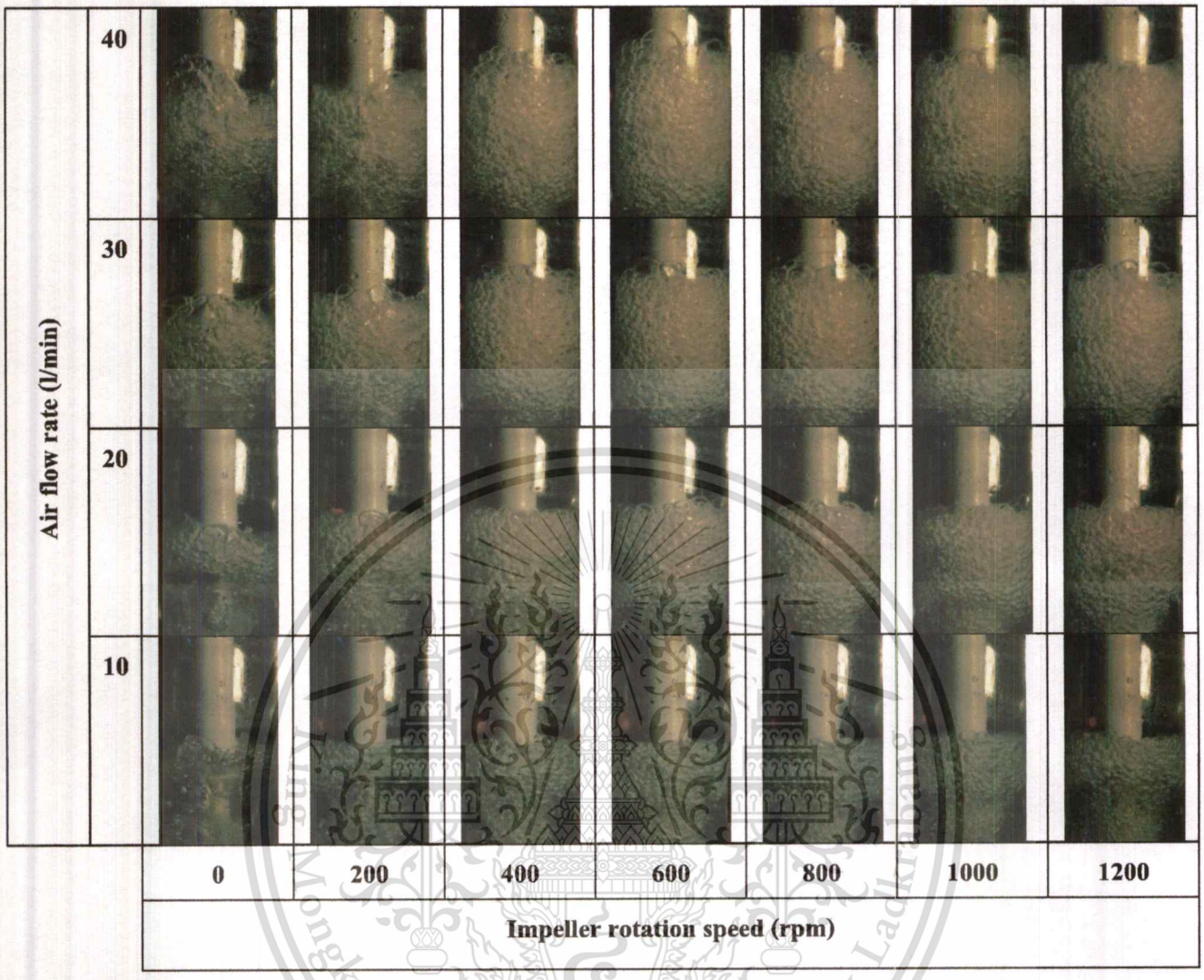

Figure 4.30 Photographs showing the effect of impeller rotation speed and air flow rate on the formation of bubbles in water with impeller C-S3.

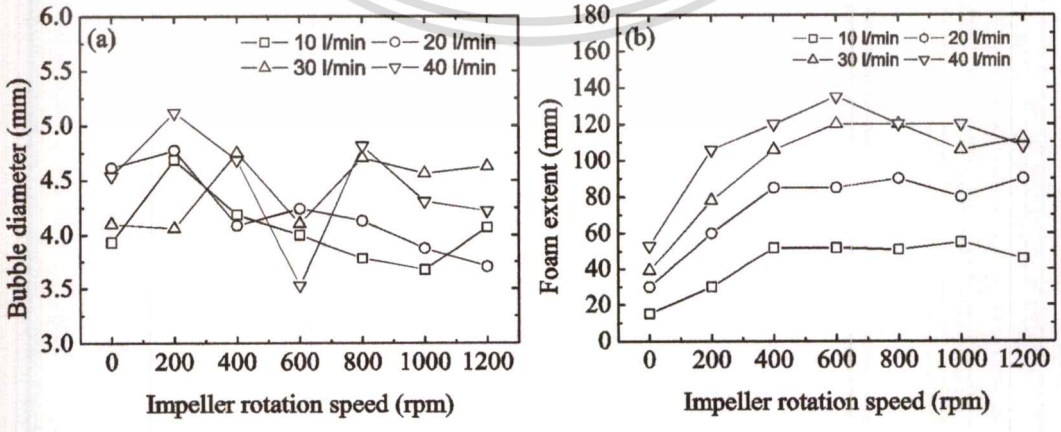

Figure 4.31 (a) Bubble diameter and (b) foam extent of impeller C-S3.

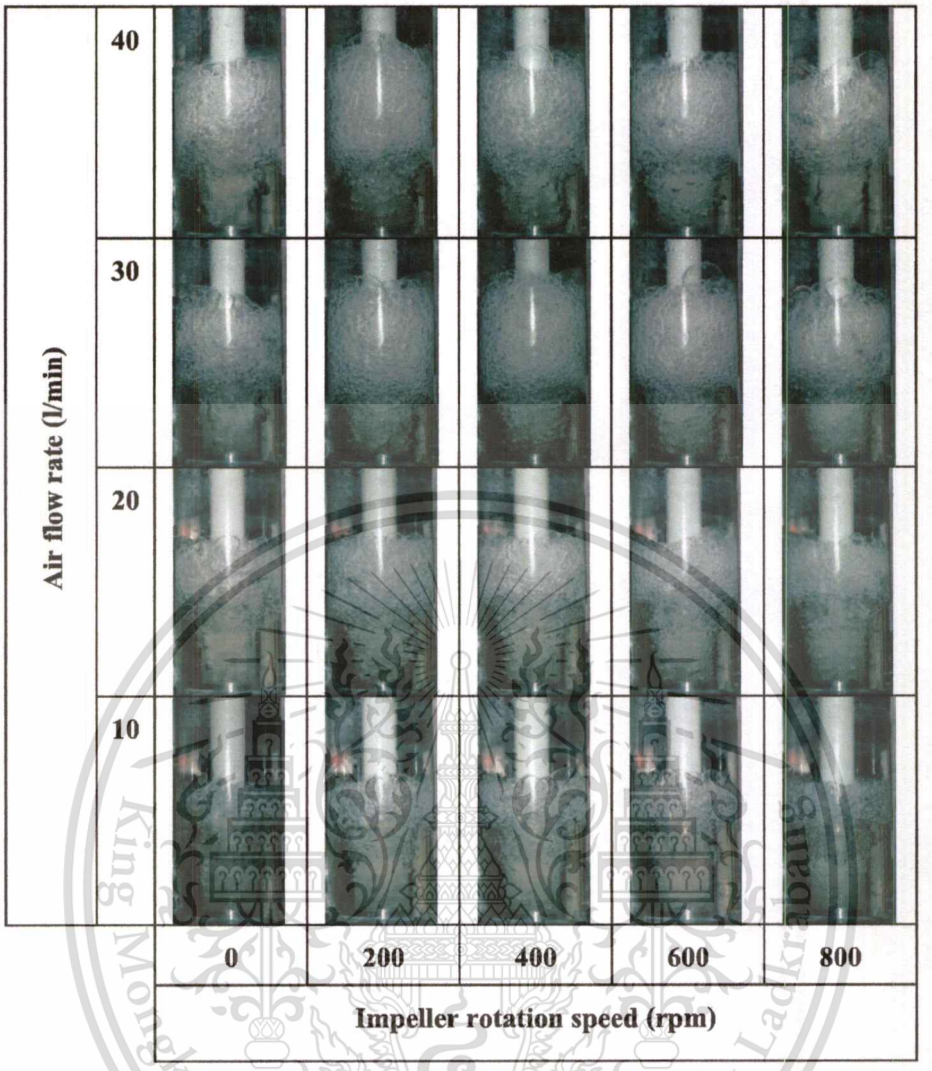

Figure 4.32 Photographs showing the effect of impeller rotation speed and air flow rate on the formation of bubbles in water with impeller D-S2.

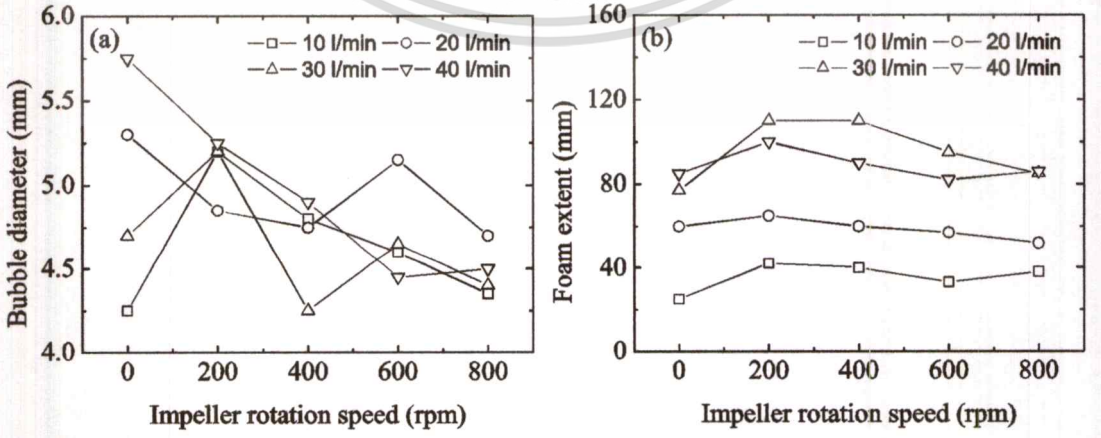

Figure 4.33 (a) Bubble diameter and (b) foam extent of impeller D-S2.

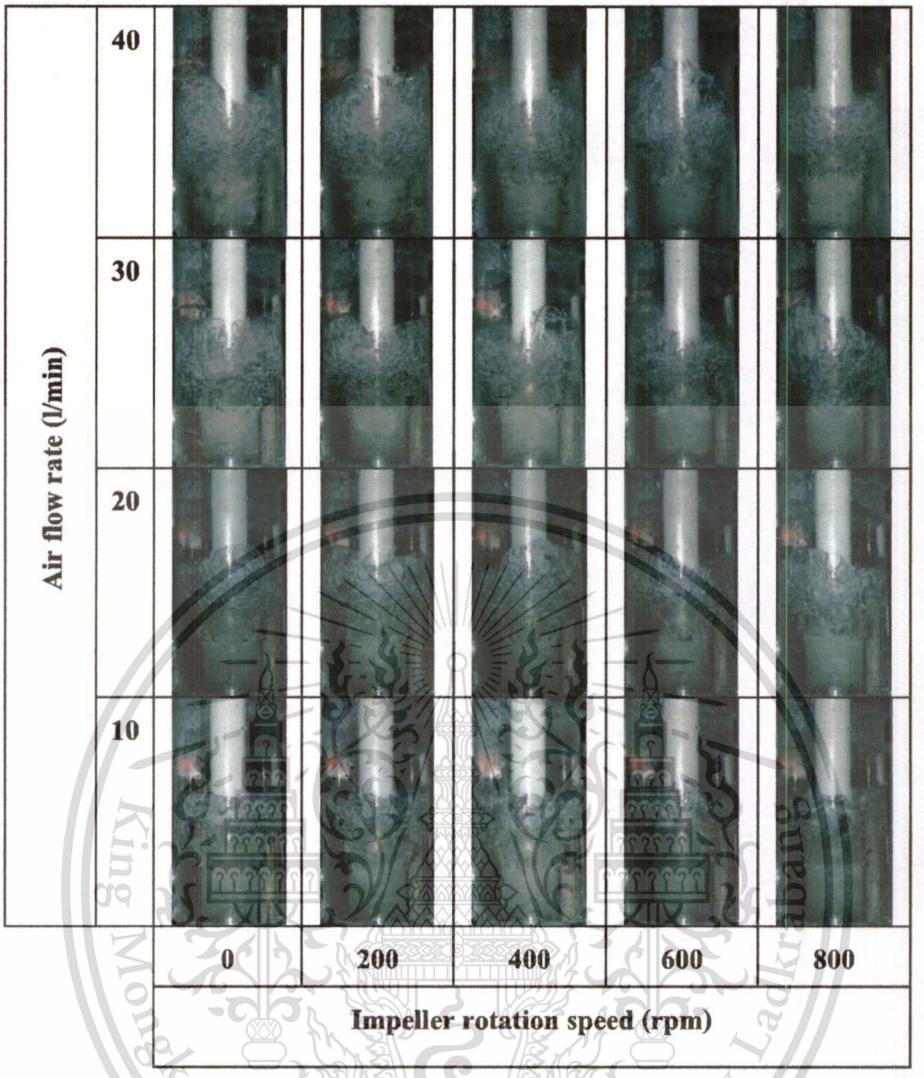

Figure 4.34 Photographs showing the effect of impeller rotation speed and air flow rate on the formation of bubbles in water with impeller E-S2.

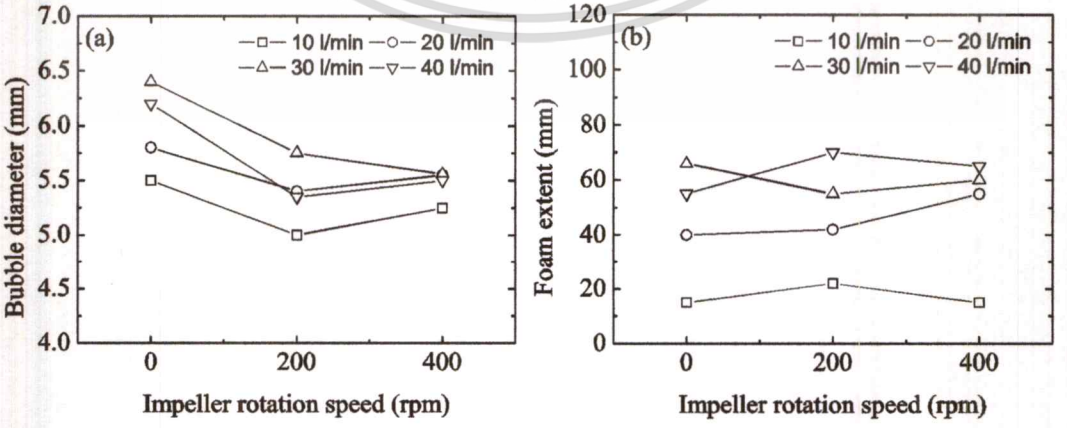

Figure 4.35 (a) Bubble diameter and (b) foam extent of impeller E-S2.

4.1.2 Foaming in a Foam Vessel with Side Exit

Figure 4.36 shows the schematic of the experimental apparatus for foaming experiments in a foam vessel with side exit using water as a testing fluid. Similar to the apparatus set up for the foaming experiments with a cylindrical foam vessel with top exit, this apparatus consists of a transparent vessel, a gas injection device and a photographic unit. The transparent vessel used in this experiment, as shown in **Figure 4.37**, is a transparent square vessel with a chimney located at the side of the vessel for releasing foam to a mould. An impeller equipped with a stator, having a number of orifice holes located at an area, was used as the gas injection device for this work. In principle, bubbles generated by the impeller, will pass through the orifice holes of the stator and form an extent of foam at the vessel chimney.

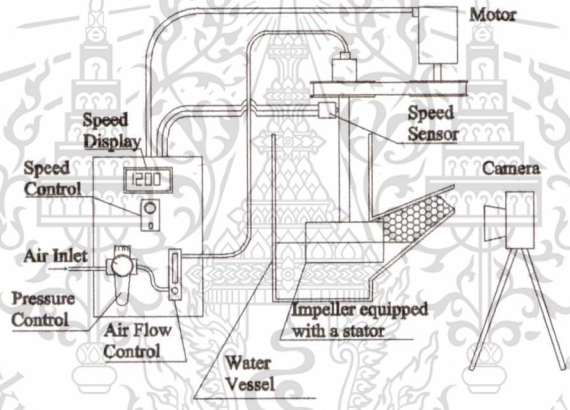

Figure 4.36 Schematic of the experimental set up for physical water model foaming experiments in a foam vessel with side exit.

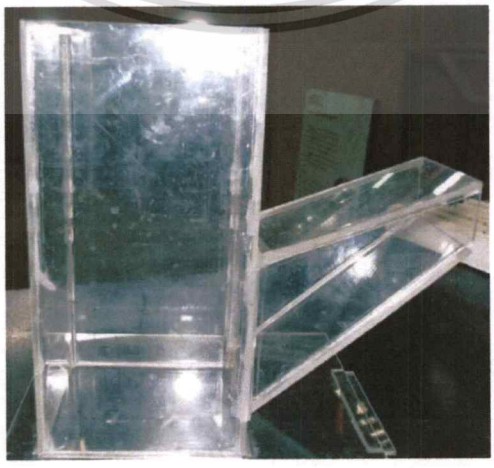

Figure 4.37 Foam vessel with side exit.

4.1.2.1 Gas Injection Device

The gas injection device used for this experiment consists of an impeller equipped with a stator. A turbine type impeller having two sets of blades separated by a disc was used. A cylindrical stator contains a number of orifice holes located at an area to direct bubbles to a particular direction. Turbine impellers with different blade angles were also tested to obtain the optimal impeller design for the best foaming performance. **Figure 4.38** shows the schematic of the gas injection device. **Figure 4.39** shows the actual gas injection device.

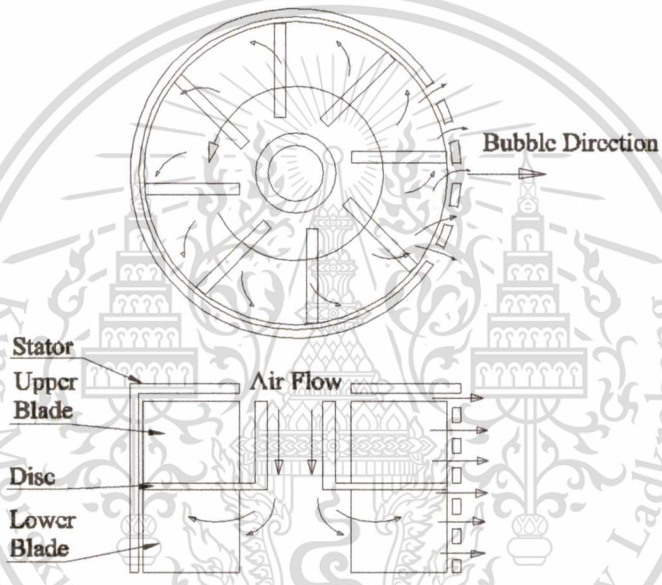

Figure 4.38 Schematic of gas injection device.

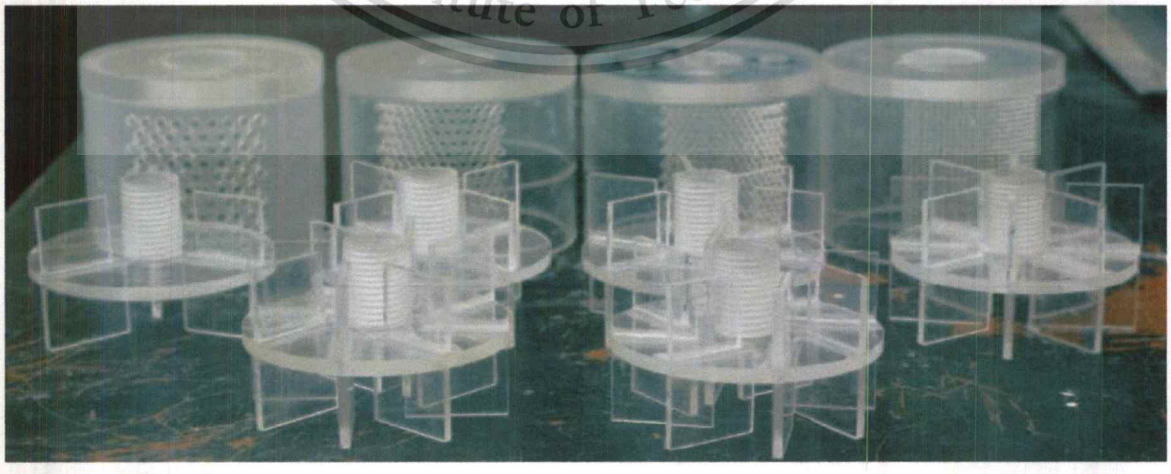

Figure 4.39 Actual impellers and stators used for physical water model foaming experiments in a foam vessel with side exit.

4.1.2.2 Results

The representative formation of bubbles foamed using the impeller with 30 degree of blade angle at the rotation speed of 800 rpm and the stator with the orifice hole size of 3 mm, at the air injection rate of 40 l/min in the chimney of the foam vessel with side exit is shown in **Figure 4.40**. Water filled in the vessel at half of the stator height was pumped and mixed with injected air to form bubbles. These bubbles were moved through the stator orifice holes and located at the chimney of the vessel.

Figure 4.40 Image of bubbles generated using the air injection rate of 40 l/min and the impeller rotation speed of 800 rpm in the chimney of the foam vessel with side exit.

Figure 4.41 shows results of bubbles generated in the chimney of the foam vessel using impellers with blade angles -60 to 60 degree and a stator with the orifice hole size of 3 mm under different air injection rates and at the impeller rotation speed of 800 rpm. Bubble diameter was found to increase with increasing impeller blade angle for all air injection rates and the difference of bubble diameter under different air injection rates was less than 1 mm as shown in **Figure 4.41** (a). Foam extent, on the other hand, increased with increasing air injection rate and was maximum when the impeller with 30 degree blade angle was used, as shown in **Figure 4.41** (b).

Figure 4.42 and **Figure 4.43** show the effects of impeller rotation speed, air injection rate and stator orifice hole size on the formation of water bubbles in the chimney of the foam vessel with side exit. Bubble diameter decreased with increasing impeller rotation speed, and decreasing air injection rate and stator orifice hole size. Foam extent, on the other hand, tended to increase with increasing all three investigated parameters.

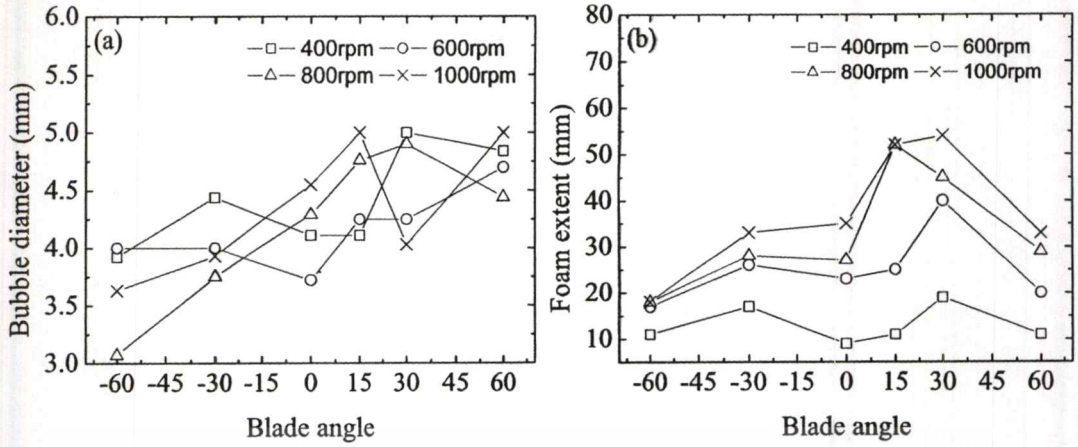

Figure 4.41 Effect of impeller blade angle and air flow rate on (a) the bubble diameter and (b) the foam extent of water in the chimney of the foam vessel with side exit under the impeller rotation speed of 800 rpm using a stator with the orifice hole of 3 mm.

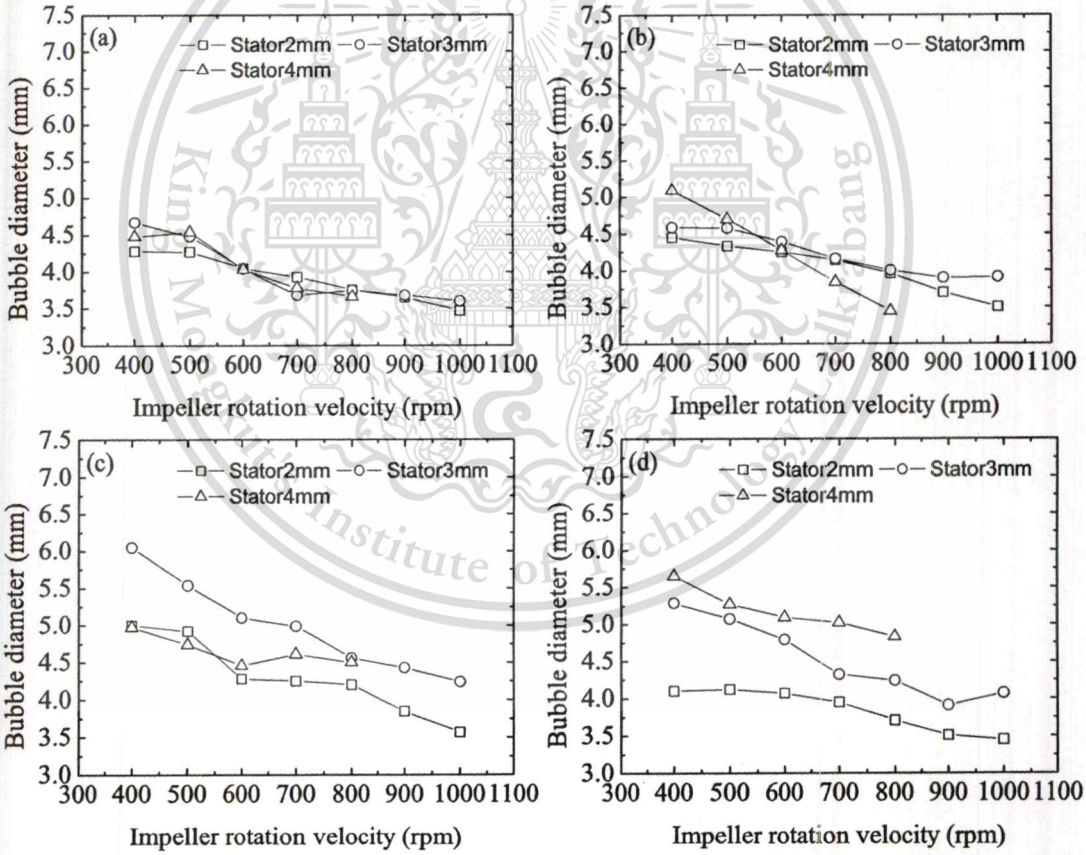

Figure 4.42 Effect of stator orifice hole and impeller rotation speed on the bubble diameter of water in the chimney of the foam vessel with side exit using the 30-blade angle impeller and air injection of (a) 10, (b) 20, 30 and 40 l/min.

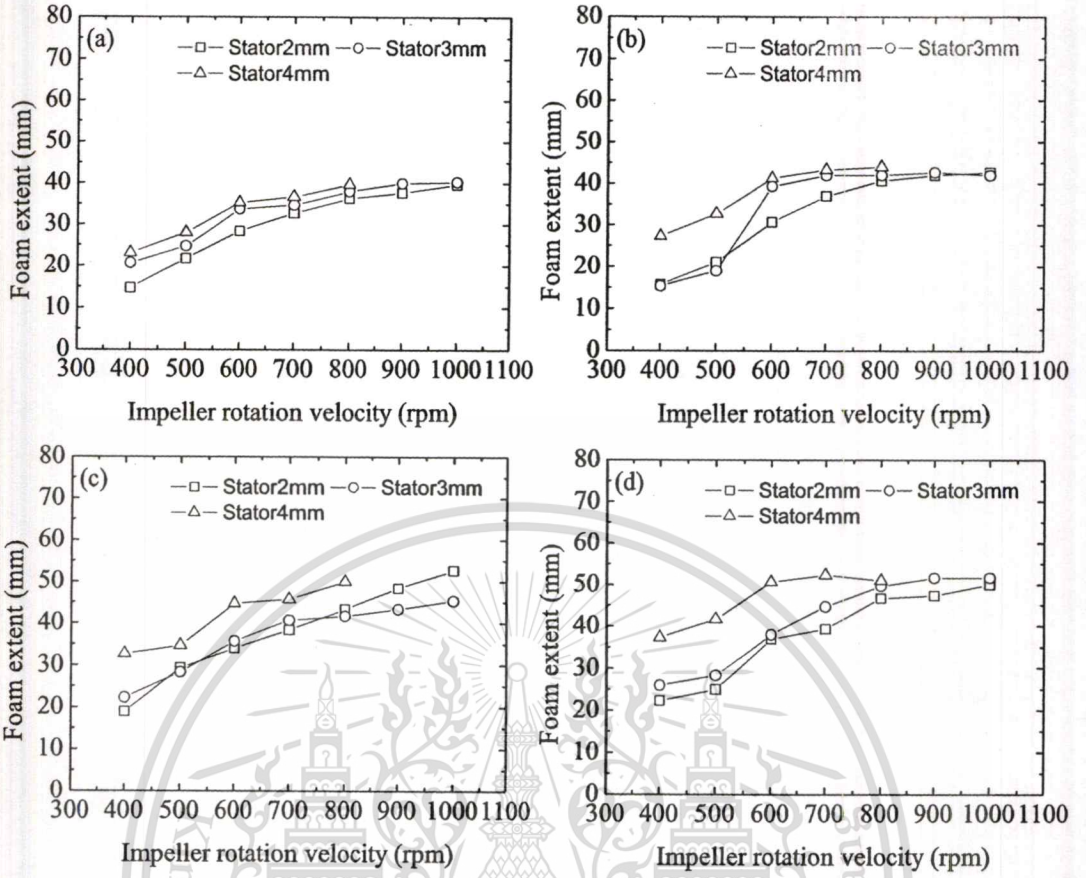

Figure 4.43 Effect of stator orifice hole and impeller rotation speed on the foam extent of water in the chimney of the foam vessel with side exit using the 30-blade angle impeller and air injection of (a) 10, (b) 20, 30 and 40 l/min.

4.1.3 Foaming in a Tri-Cylindrical Foam Vessel

4.1.3.1 Apparatus

Figure 4.44 shows the schematic of the experimental apparatus for foaming in a tri-cylindrical vessel using water as a testing fluid. The apparatus consists of three principal components: (1) a gas injection device, (2) a transparent foam vessel and (3) a photographic unit.

The gas injection device consists of a changeable impeller, a stator, a bubble cover, an impeller shaft, a rotational system and a compressed air supply. The transparent foam vessel used in this experiment contains three separated transparent cylindrical vessels, each having an inner diameter of 24 mm, whose bottoms connect to the top of the bubble and the cover of the gas injection device located in the water vessel. The vessel was filled with water with 110 mm height.

The impeller equipped with stator was dipped into the water and located at the position where the top of the stator is 20 mm below the water level. The photographic unit was used to take bubble photographs. Experiments were carried out using various design impellers. Bubble sizes were measured using the linear intercept method on the taken photographs as described in sections 3.3.1 and 3.3.2. The described apparatus is shown in **Figure 4.45** and **Figure 4.46**. The experimental conditions are summarised in **Table 4.3**.

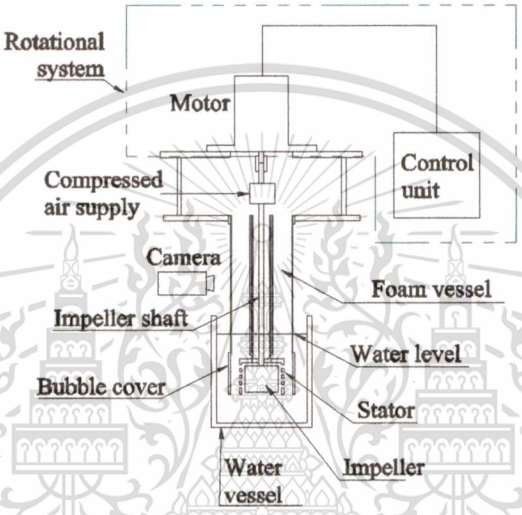

Figure 4.44 Schematic of the experimental apparatus for foaming in a tri-cylindrical vessel.

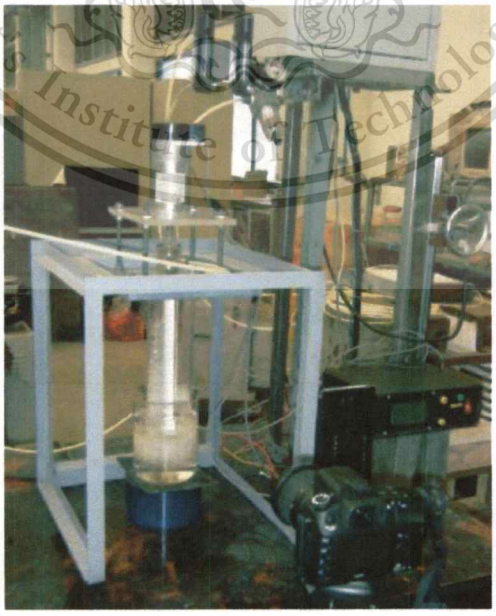

Figure 4.45 Apparatus for foaming in a tri-cylindrical vessel.

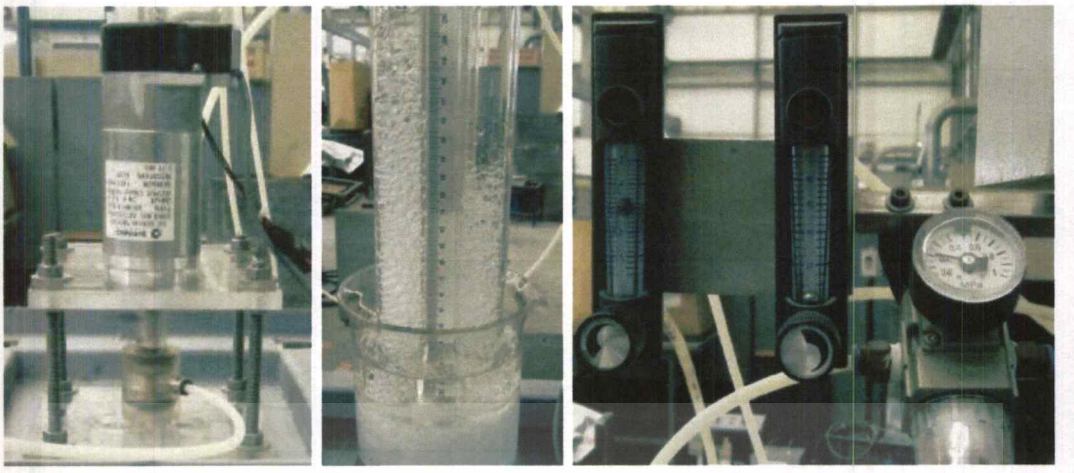

(a) (b) (c)

Figure 4.46 Details of the apparatus for foaming in a tri-cylindrical vessel: (a) a motor and a compressed air supply, (b) a water vessel and a tri-cylindrical vessel with a scale and (c) a pressure regulator and flow meters.

Table 4.3 Experimental conditions.

Compressed air pressure (MPa)	Air flow rate (l/min)	Temperature (°C)	Impeller rotation speed (rpm)
0.2	1, 2, 3, 4, 5	23 ± 0.5	600-1400 ± 5

4.1.3.2 Impellers

Four different design impellers, namely turbines A, B, C and D and a stator are shown schematically in **Figure 4.47**. Turbines A and B are 4-blade turbine type impellers having injection orifices on the side and at the bottom of the impeller axis, respectively. Turbines C and D are disc-turbine type impellers having 6 blades. Turbine C contains an injection orifice at the bottom of the impeller axis, while turbine D contains an additional nozzle head, having 16 injection orifices, connected to the bottom of the impeller axis. Dimensions of the impellers are given in **Table 4.4**. Photographs of example impellers are shown in **Figure 4.48**.

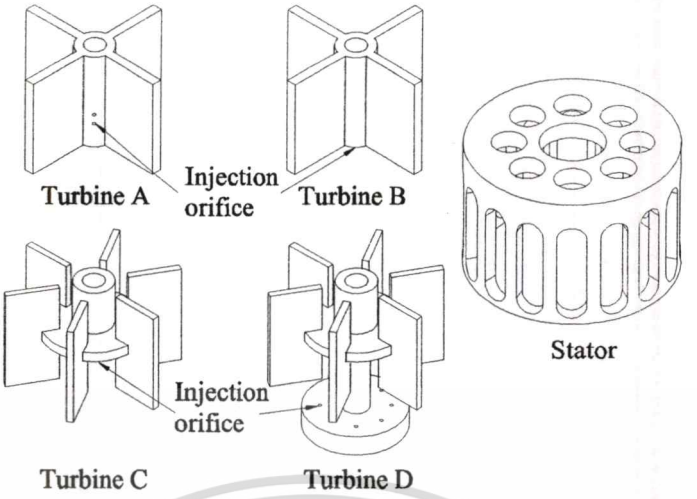

Figure 4.47 Geometry of impellers and a stator.

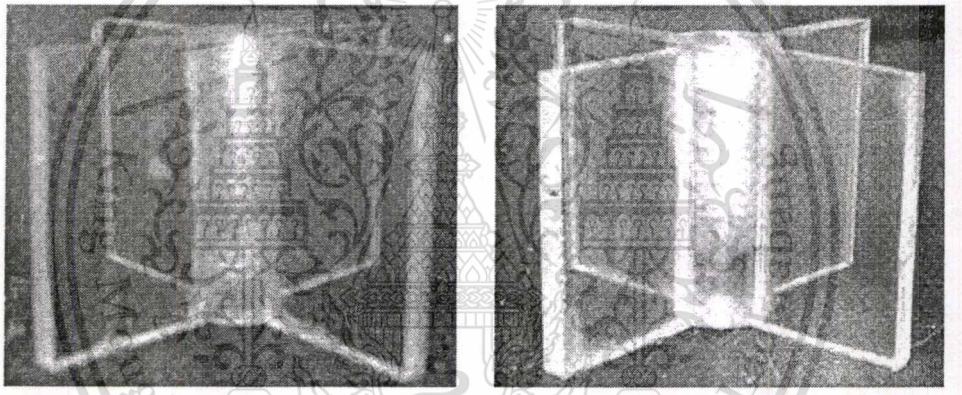

Figure 4.48 (a) Turbine A and (b) Turbine B.

Table 4.4 Dimensions of impellers

Impeller	No. of blade (mm)	Blade diameter (mm)	Blade length (mm)	No. of injection orifice	Orifice diameter (mm)
Turbine A	4	50	30	8	1
Turbine B	4	50	30	1	6.5
Turbine C	6	50	30	1	6.5
Turbine D	6	50	30	16	1

4.1.3.3 Results

Effects of impeller rotation speed of different impellers, as show in Figure 4.47, on bubble diameter and foam extent are shown in **Figure 4.49** and **Figure 4.50,** respectively. The representative of bubble generated by turbine D impeller is shown in **Figure 4.51**. Sizes of bubbles generated by all impeller are relatively close and they are within 3.5 to 6.5 mm. The smallest bubble of 3.5 mm was generated by turbine A impeller at the impeller rotation speed of 1,400 rpm and the air flow rate of 1 l/min. Turbine D impeller generated the highest foam extent, which is 127 mm at the impeller rotation speed of 1,000 rpm and air flow rate of 5 l/min.

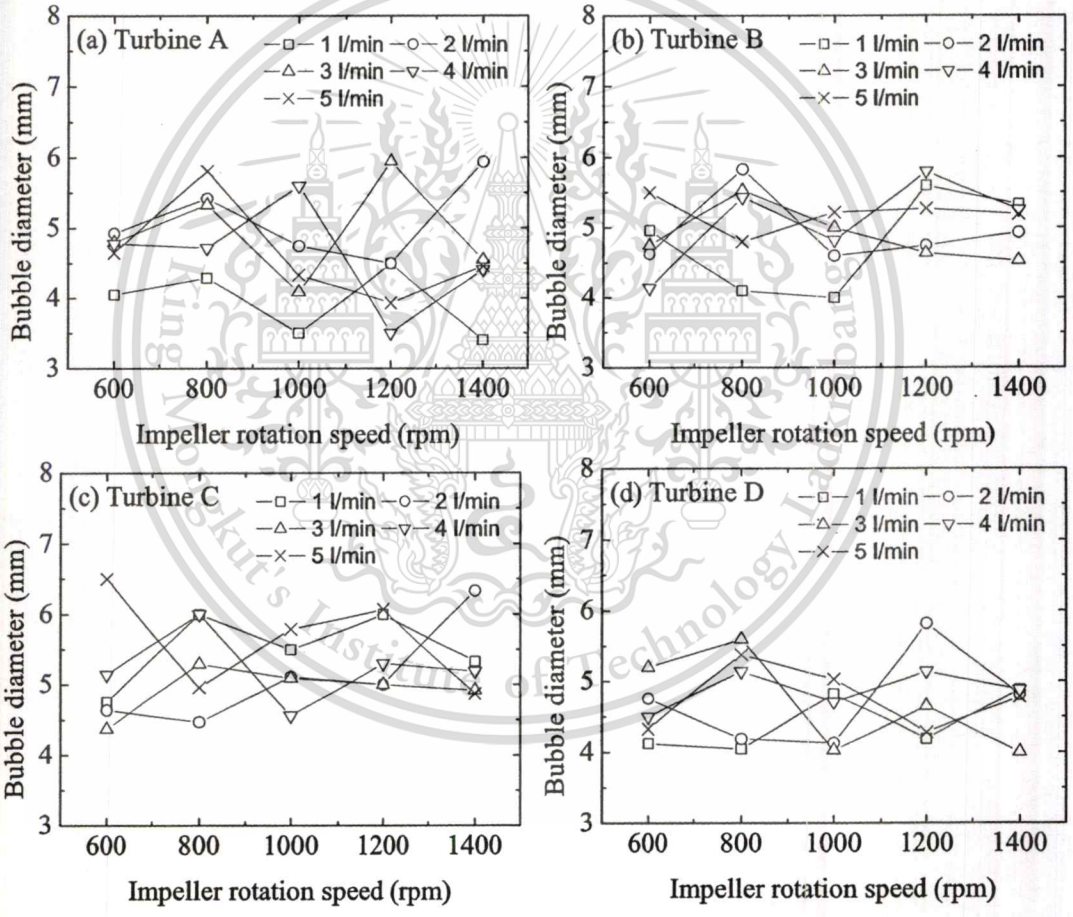

Figure 4.49 Effect of impeller rotation speed on bubble diameter of turbine: (a) A, (b) B, (c) and (d) D impellers.

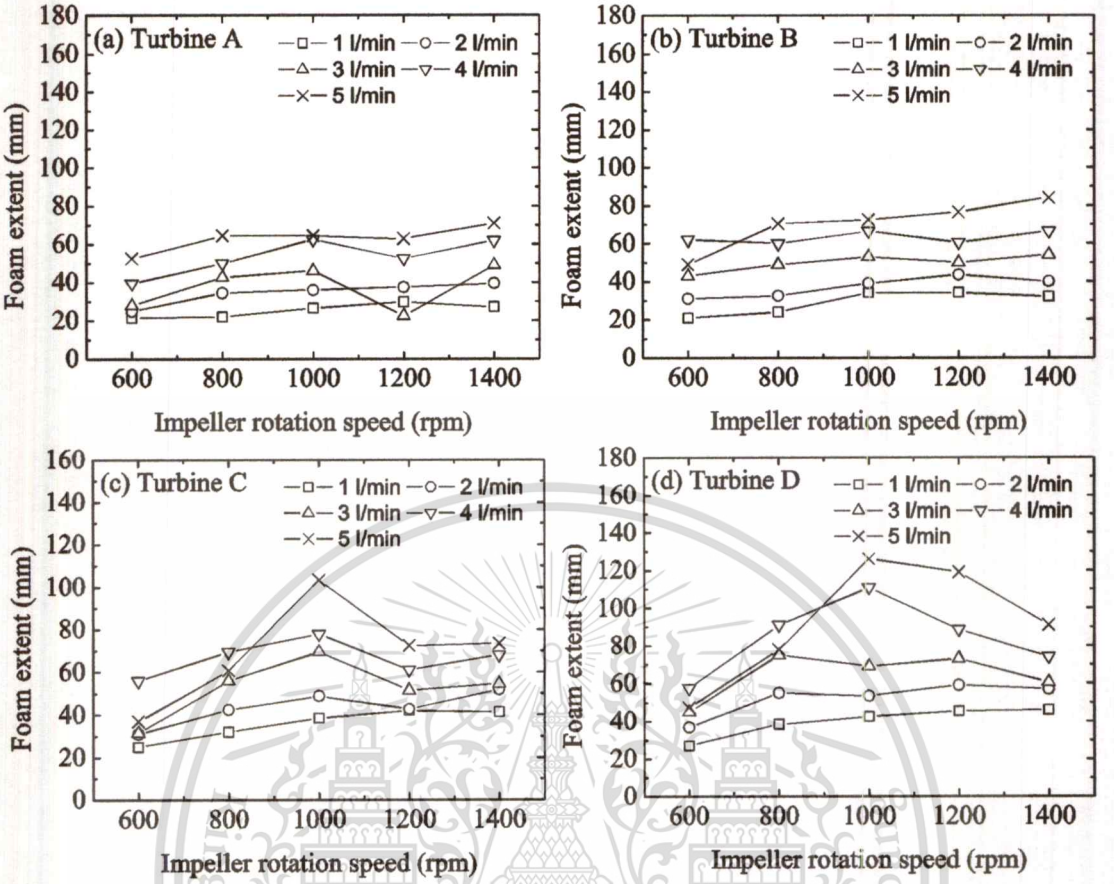

Figure 4.50 Effect of impeller rotation speed on foam extent of turbine: (a) A, (b) B, (c) and (d) D impellers.

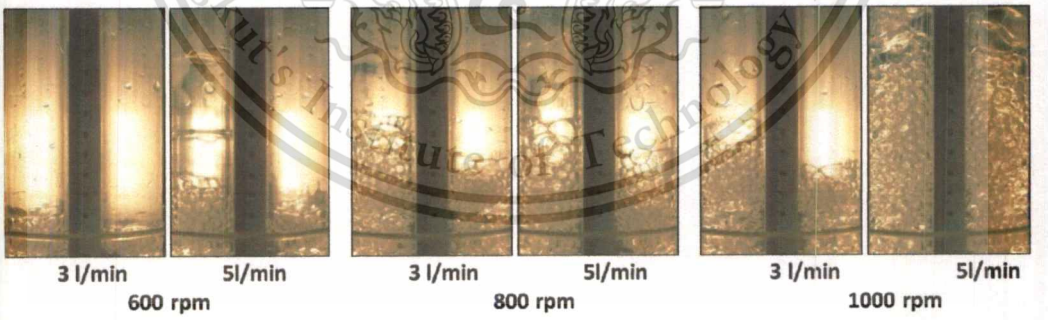

Figure 4.51 Example of bubble generated by turbine D impeller.

4.2 Aluminium Foaming Generators

The final work of this research is to produce an actual aluminium foam. Equipment design and processing parameters obtained from previous experiments including simulation and physical water model where used to develop apparatus for foaming aluminium. Two types of aluminium foaming generators were developed, a side exit and a tri-cylindrical foam vessel, to produce sheet

and cast foams. The main components of both foam generators are a furnace, a crucible, a gas injection device and a foam cooling system. The last component was used to prevent the foam generators from over heat and solidify molten aluminium foams.

4.2.1 Foaming in a Foam Vessel with Side Exit

Technical knowledge obtained in section 4.1.2 for foaming in a foam vessel with side exit was used to design a foam generator for aluminium sheet foam production. Dimensions of the foam vessel used for foaming aluminium are exactly identical to those used for foaming water (**Figure 4.37**). However, the foam vessel for foaming aluminium was made of ceramic, instead of acrylic. A twin roll caster with a circulating water cooling system was used to solidify molten aluminium foam and constrain the foam into a sheet form. In experiments, about 3 kg pure aluminium ingot was melted at 700 °C in a crucible sitting in a heat resistant furnace. The melt was then poured into a holding crucible placed on the top of the foam vessel in another heat resistant furnace prior to injecting air and rotating an impeller to foaming aluminium as shown schematically in **Figure 4.52**. **Figure 4.53** shows the foam generator and its components and **Figure 4.54** shows an aluminium foam obtained by the first try.

At present, aluminium sheet foam has not yet been successfully produced using this foam generator because of various factors as will be described in chapter 5.

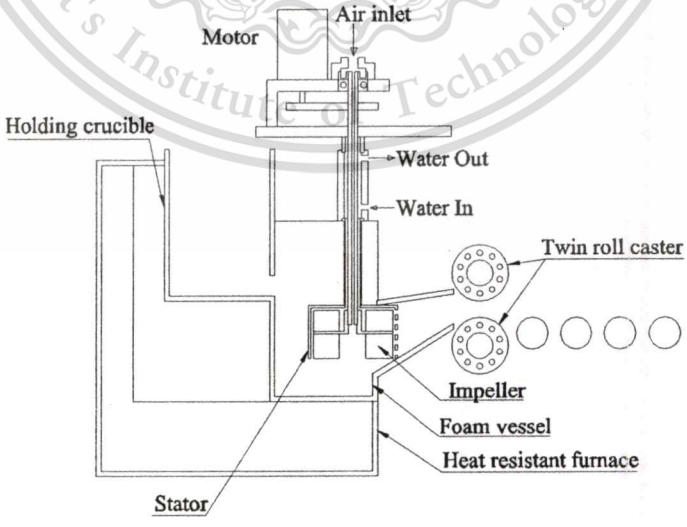

Figure 4.52 Schematic of aluminium foam generator for aluminium foam sheet production.

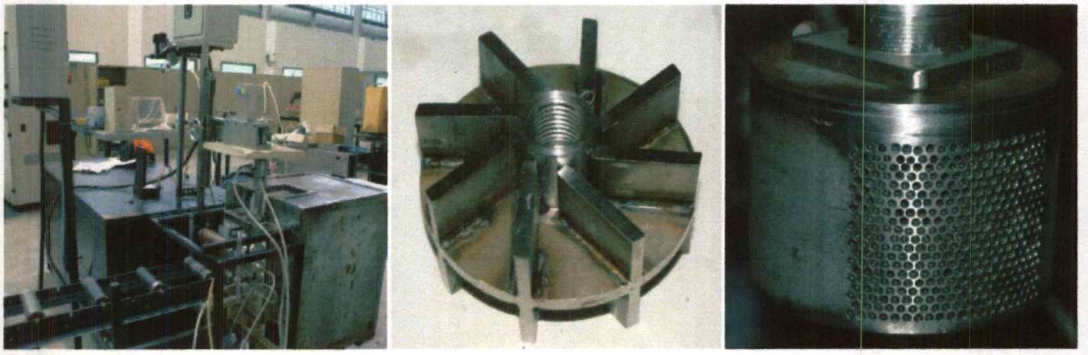

(a) (b) (c)

Figure 4.53 Aluminium foam sheet production generator: (a) the whole equipment, (b) an impeller and (c) a stator.

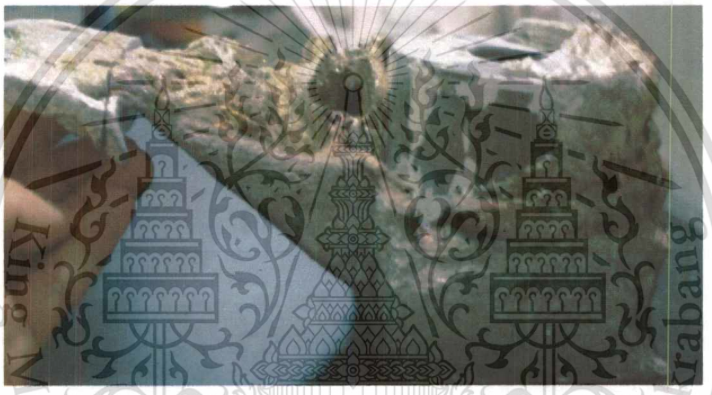

Figure 4.54 An aluminium foam obtained by the first try using the aluminium foam sheet production generator.

4.2.2 Foaming in a Tri-Cylindrical Foam Vessel

Foaming of aluminium in a cast foam was carried out using a tri-cylindrical foam vessel developed in section 4.1.3. The principal components of the foam generator for foaming aluminium, as shown schematically in **Figure 4.55**, are identical to those of the one used for foaming water, as shown schematically in **Figure 4.44**. Due to the difference in physical properties of the two materials, some foam generator components are different. The different components of the aluminium foaming foam generator are: (1) a foam vessel, an impeller and a stator made from stainless steel, (2) an inner diameter of the foam vessel of 27 mm (available tube in the market) and (3) additional water cooling system to solidify molten aluminium foam. The foam generator is shown in **Figure 4.56**. Turbine D (**Figure 4.47**), which is the best impeller for foaming water, was used. Experiments were carried out using pure aluiminium heated to 900 ° C, air pressure of 0.2 MPa, air flow rate of 1-5 l/min and impeller rotation speed of 600-1000 rpm.

Figure 4.57 shows steps for removing aluminium foams from the foam generator. A digital camera was used to record bubble images of the inner structure of aluminium foam vertical section samples and Image-Pro 5.0 software was used to measure bubble sizes of samples images.

Figure 4.58 shows aluminium foam samples produced by the foam generator. It was found that both pore size and foam extent decreased with increasing impeller rotation speed, and increased with increasing air flow rate, as shown in **Figure 4.59**. Aluminium foams with pore size of 10-24 mm and foam extent of 35.68 mm were produced using this foam generator.

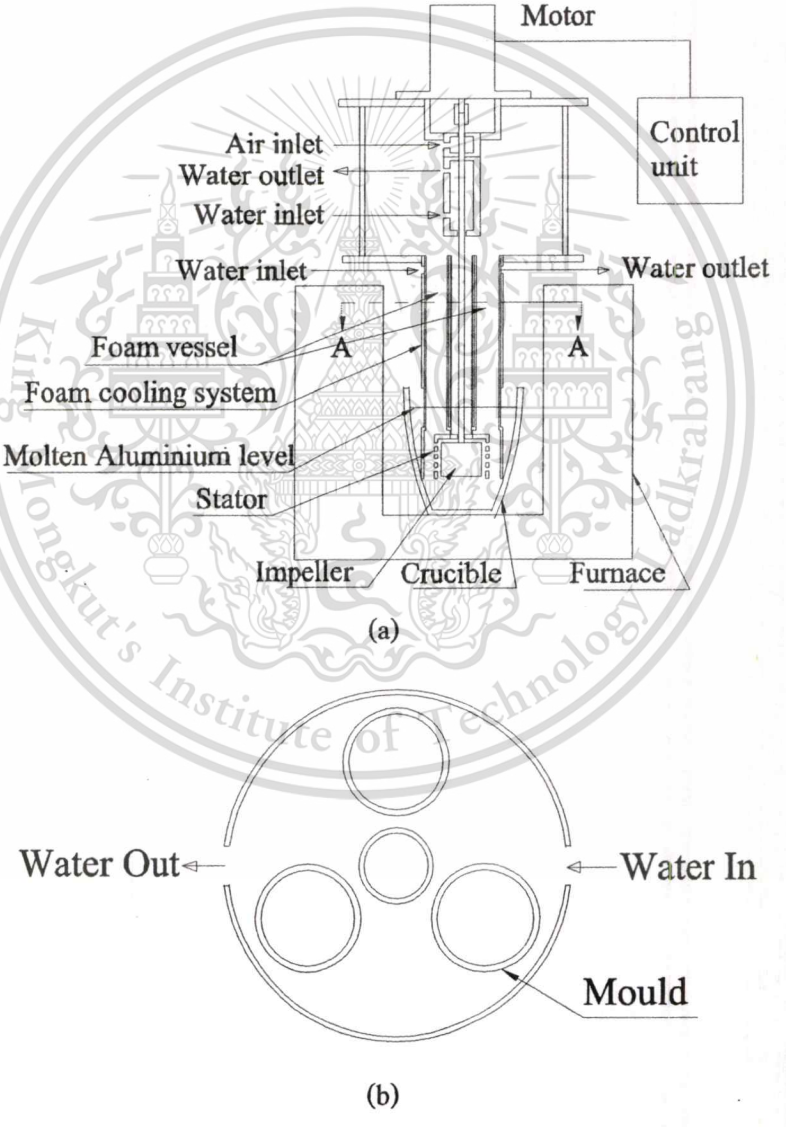

Figure 4.55 (a) Schematic of aluminium foam generator and (b) detail of water cooling system (section A-A).

Figure 4.56 Aluminium foam generator using a tri-cylindrical foam vessel.

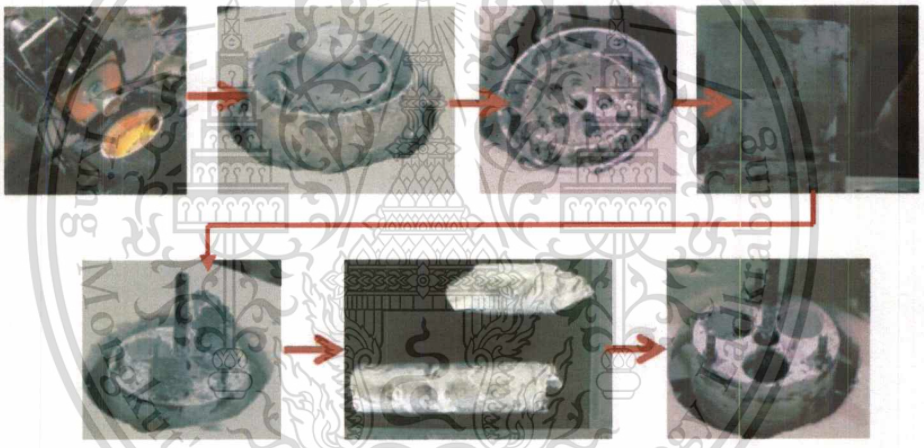

Figure 4.57 Steps for removing aluminium foam from the foam generator.

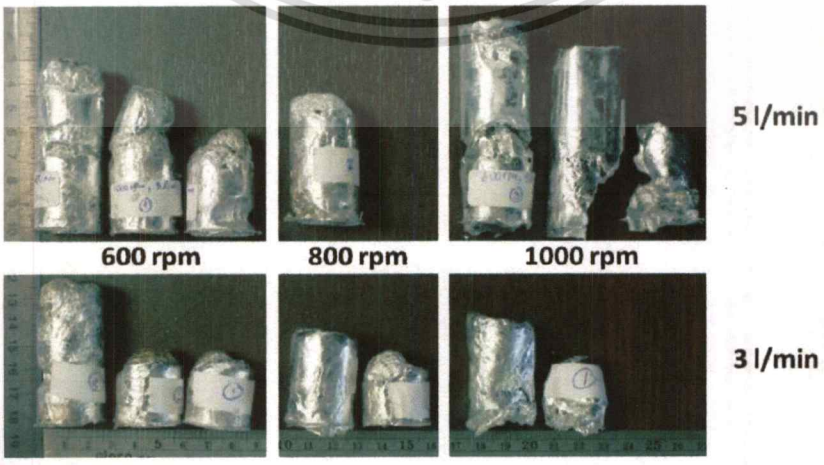

Figure 4.58 Aluminium foam samples.

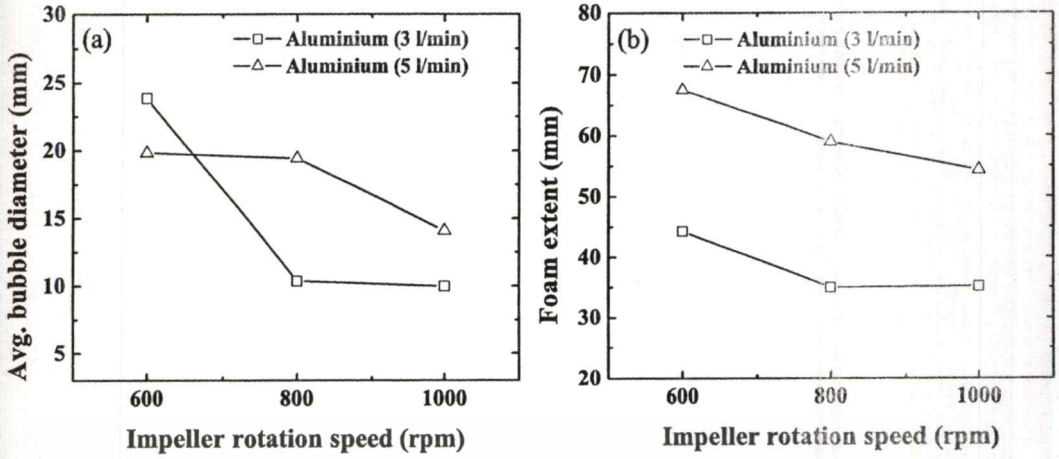

Figure 4.59 Effect of impeller rotation speed and air flow rate on: (a) pore diameter and (b) foam extent of aluminium foam produced by the foam generator with the tri-cylindrical foam vessel.

4.3 Summary

4.3.1 Physical Model

4.3.1.1 Foaming in a Cylindrical Foam Vessel with Top Exit

The minimum bubble diameter of 2.9 mm and the maximum foam extent of 160 mm were generated by impeller C-S2. Bubble diameter decreased with increasing impeller rotation velocity. For impellers without stator (A, B, C, D, E), the foam extent decreased with increasing impeller rotation speed. However, for impellers is equipped with a stator (C-S1, C-S2, C-S3), the reduction of foam extent were not found when the impeller rotation speed increased.

4.3.1.2 Foaming in a Foam Vessel with Side Exit

Performance of foam formation varied with the degree of impeller blade angle, impeller rotation speed, air flow rate, stator orifice size and impeller velocity. The smallest bubble of 3.2 mm was obtained by the impeller with impeller blade angle of -60 degree using the stator with 3 mm orifice size at 800 rpm impeller rotation speed and 30 l/min air flow rate. The highest foam extent of 53 mm was obtained by the impeller with impeller blade angle of 30 degree using the stator with 3 mm orifice size at 1000 rpm impeller rotation speed and 30 l/min air flow rate.

4.3.1.3 Foaming in a Tri-Cylindrical Foam Vessel

Turbine D impeller gave the best performance for generating foam in this experiment. The size of bubble was only slightly different. However, it gave the highest foam extent of about 130 mm.

4.3.2 Aluminium Foam Production

At present, aluminium foam cannot be produced using the foam vessel with side exit as a foam generator because molten aluminium was pre-maturely solidified in the foam vessel during foaming.

Although, the above foam generator has not yet been able for producing aluminium foam, aluminium foam in this research can be produced using the tri-cylindrical foam vessel as a foam generator. Bubble diameter of 10-25 mm and foam extent of 35-68 mm were obtained in this production. However, results between physical model and aluminium foam production is rather different.

CHAPTER 5

DISCUSSION

5.1 Foam Formation

5.1.1 Foam Extent

Liquid foam occurs by the accumulation of bubbles generated in liquid and floated to liquid surface. The extent of bubbles locating above the liquid surface, which is called "foam", depends on the rates of generation and rupture of the bubbles. High bubble extent occurs when bubbles contain a high generation rate and a low rupture rate, and vice versa. The stability of bubbles in the foam depends on three physical mechanisms: drainage, coalescence and rupture.

Figure 5.1 Images of bubbles foamed using different impellers and stators at the impeller rotation speed of 800 rpm and air flow rate of 40 l/min.

Vortex, which is a rotating liquid having a lower surface at the center of rotation, occurs by the rotation of impeller during gas injection. Foam cannot be formed in conditions of high vortex and turbulent flow because bubbles rupture quickly. As shown in **Figure 5.1**, foaming in a cylindrical foam vessel with top exit using impellers and stators shown in **Figure 4.3**, impeller B which is the largest diameter impeller generated the highest vortex and hence produced no foam. For impeller C equipped with stators S1, S2 and S3, on the other hand, produced relatively high foam extent even at high impeller rotation speeds. As the CFD results shown in **Figure 5.9**, when an impeller rotates, velocity of the liquid in a vessel is occurred. This velocity results in the reduction of foam extent. However, the liquid velocity in the vessel is extremely low when the impeller is equipped with a stator. The stator can therefore improve foaming at high impeller

rotation speeds. In experiments, stators were found to keep the liquid undisturbed outside the stators and hence give rise of the foam extent.

5.1.2 Bubble Size

Considering the formation of bubbles at a stationary and a rotational orifice as shown in **Figure 5.2**, large and small bubbles are generated by the former and the latter orifice respectively. When the orifice rotates, bubbles are acted by a shear force generated by the rotation. This force makes the bubbles to premature detachment and hence to become smaller. The higher the orifice rotation speed, the higher the shear force, and hence the smaller the bubble size.

Although small bubbles can be generated using a high impeller rotation speed, foam extent becomes lower due to the occurrence of vortex and turbulence in the liquid. However, this foaming problem can be solved using a stator to equip with the impeller to obtain a high shear force between the impeller and the stator while obtain the liquid undisturbed outside the stator.

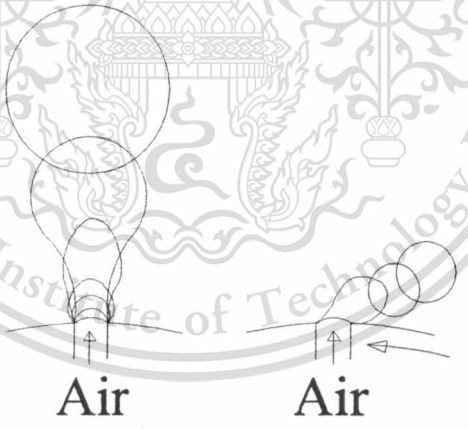

Figure 5.2 Bubble formation at (a) a stationary and (b) a rotational orifice.

5.2 Gas Injection Device Design

5.2.1 Foaming in a Cylindrical Foam Vessel with Top Exit

For foaming in a cylindrical foam vessel with top exit, different impeller design shows

different foaming performance as illustrated in **Figure 5.3** and **Figure** 5.4. Bubble diameter trends to decrease with increasing impeller rotation speed due the increase of shear rate in water. The smallest bubble size of about 3 mm, was generated using impeller C-S2 at the impeller speed of 1200 rpm and the air flow rate of 10 l/min. For impellers without stator, i.e. impellers A, B, C, D and E, foam extent decreased with increasing impeller rotation speed, while this tendency is not found with foaming using impellers equipped with stators, i.e. impellers C-S1, C-S2, C-S3, D-S2 and E-S2. Stators also help to increase the foam extent when the impeller rotation speed increases. For the impellers equipped with stators, foam extent increased until the impeller rotation speed of 400 rpm beyond which the foam extent remained relatively constant.

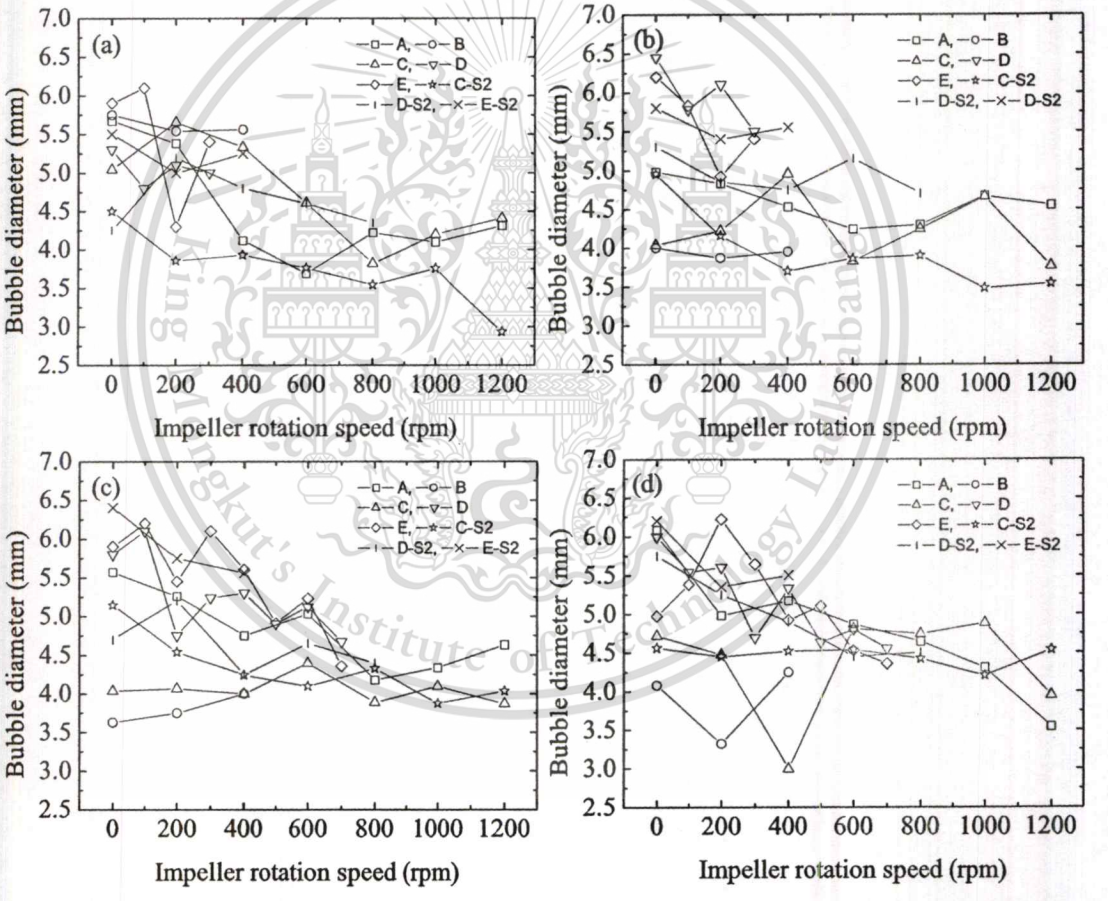

Figure 5.3 Comparison of bubble diameter generated using different impellers with air flow rate of: (a) 10, (b) 20, (c) 30 and (d) 40l/min.

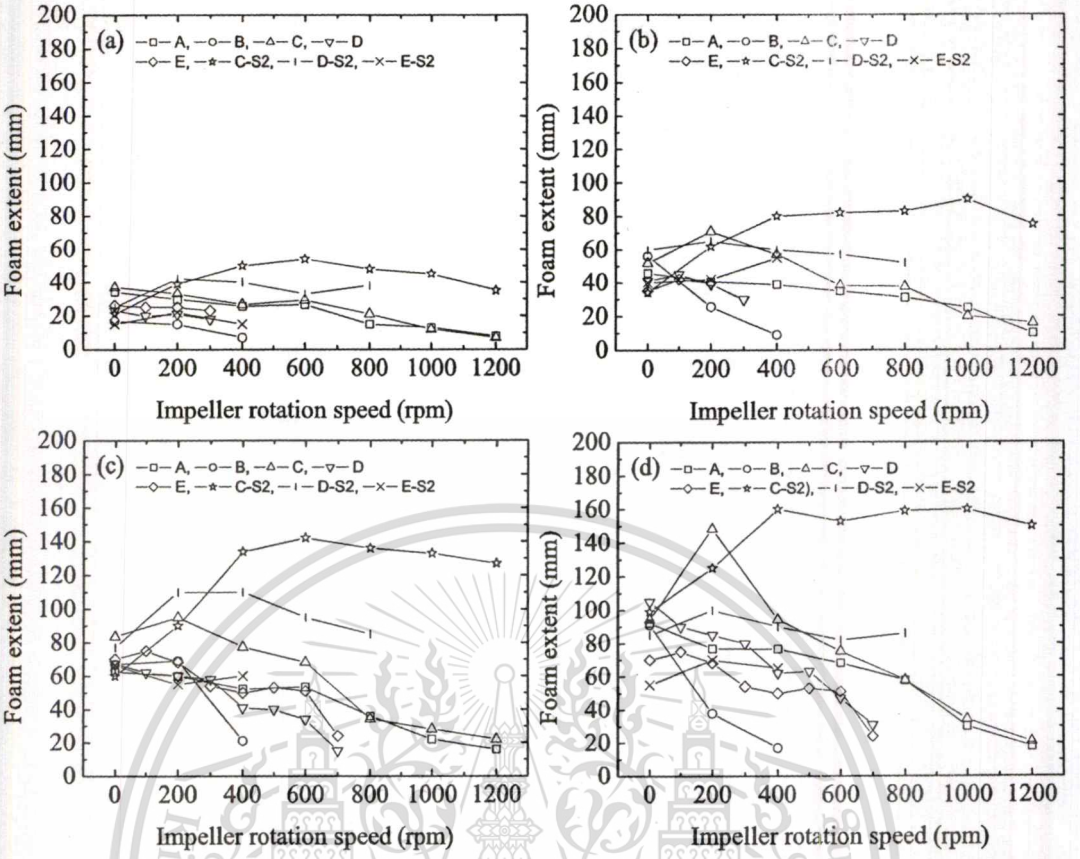

Figure 5.4 Comparison of foam extent generated using different impellers with air flow rate of: (a) 10, (b) 20, (c) 30 and (d) 40 l/min.

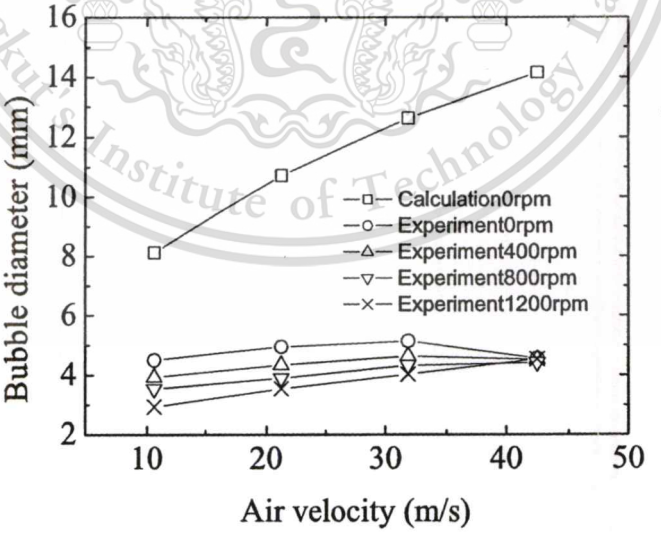

Figure 5.5 Comparison of bubble diameter generated by impeller C-S2 between the produced water foam and the calculation using the Valencia *et al.*'s equation (Valencia *et al.*, 2002) given in Table 2.4.

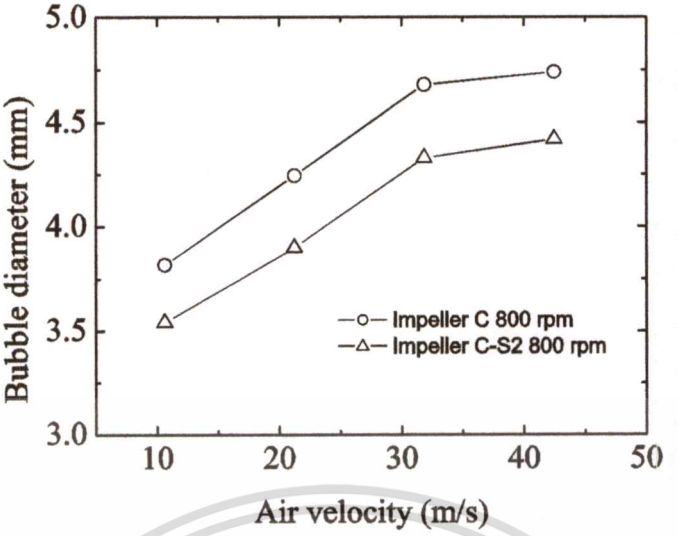

Figure 5.6 Comparison of bubble diameter generated by impellers C and C-S2 in the cylindrical foam vessel at the impeller rotation speed of 800 rpm and various air velocities.

Figure 5.7 Comparison of foam appearance between (a) the water foam produced in this work and (b) the typical foam pattern called "critical foam" (Skurtys *et al.* 2008).

Based on the mathematical model of bubble diameter given by Valencia *et al.* (2002), the bubble diameter of water generated by impeller C with and without stator can be estimated. Comparisons between predicted and experimental bubble diameter generated by impeller C at various impeller rotation speeds and air velocities, at the impeller rotation speed of 800 rpm and various air velocities are shown in **Figure 5.5** and **Figure 5.6**, respectively. Both the predicted and experimental results of bubble diameter show the same trend of the increase of bubble diameter with increasing air velocity. However, the bubble diameters obtained from the experiments are smaller than those of the calculation. The use of the impeller containing multi-

orifices with rotation, which is beyond the limit of the mathematical model constraints would be responsible for the difference of the results. The bubble diameter reduced about 8.5% when the impeller was equipped with stator S-2. Based on the appearance of the foam, the foam generated in this cylindrical foam vessel with top exit can be classified as the critical foam, which is supposed to have the mean gas fraction, Ω, of around 85%, as shown in **Figure 5.7**.

There are several phenomena occurring in liquid in the vessel during the rotation of impeller such as liquid flow and pressure variation. These phenomena can be investigated using CFD. **Figure 5.8** and **Figure 5.9** show the prediction of flow and velocity of water under the rotation of different impellers using COSMOSFloWork software. Water around the impellers flows in same direction under the rotation of the impellers. From both experiment and CFD results, a larger impeller generates a higher liquid velocity than a smaller one, so produces a larger vortex.

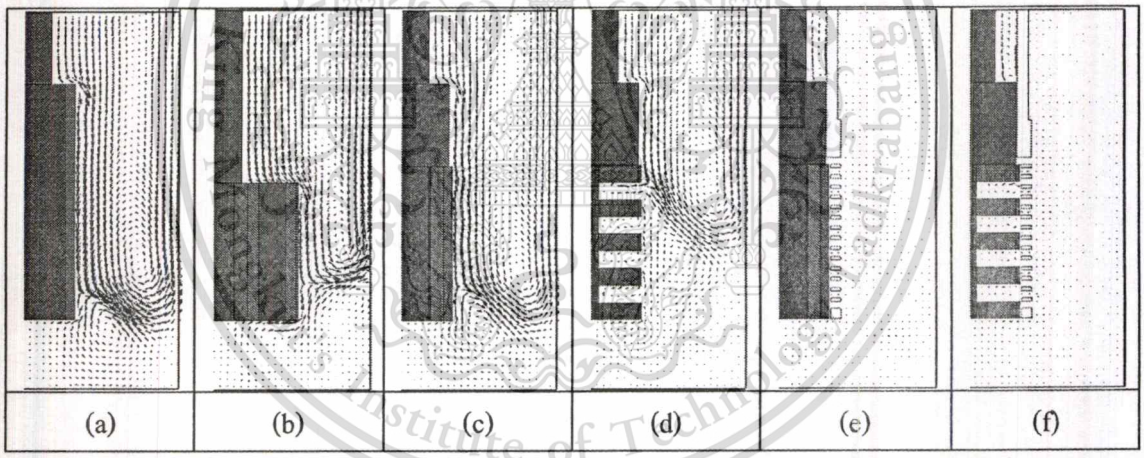

Figure 5.8 Flow patterns of water in a cylindrical vessel at impeller rotation speed of 800 rpm without air injection: (a) impeller A, (b) impeller B, (c) impeller C, (d) impellers D and E, (e) iC-S2, and (f) impellers D-S2 and E-S2.

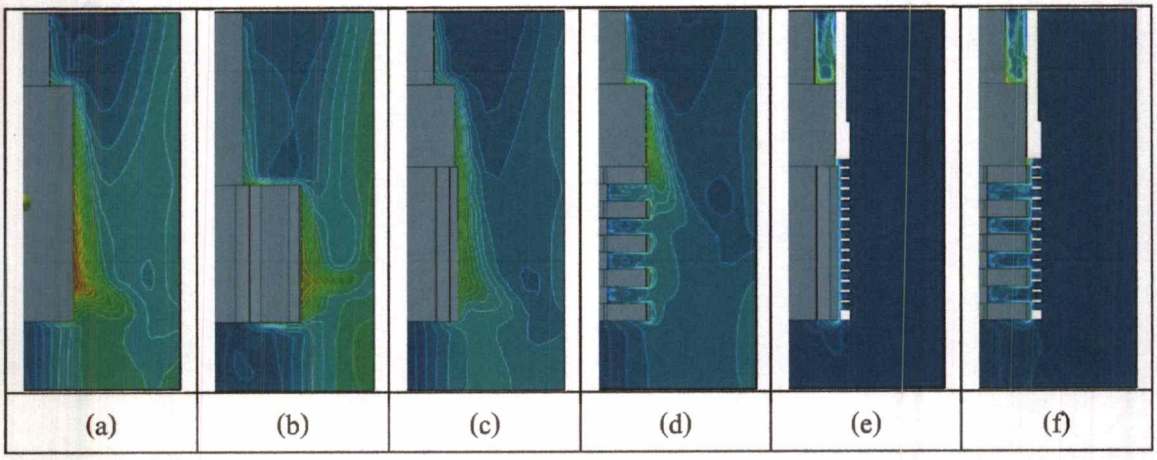

Figure 5.9 Velocity patterns of water in a cylindrical vessel at impeller rotation speed of 800 rpm without air injection: (a) impeller A, (b) impeller B, (c) impeller C, (d) impellers D and E, (e) impeller C-S2, and (f) impellers D-S2 and E-S2.

5.2.2 Foaming in a Foam Vessel with Side Exit

According to results in the previous chapter, the angle of impeller blade affected the formation of bubbles. Impeller with 30 degree blade angle generated the highest foam extent. Bubbles were generated by the gas injected through the impeller orifices and were forced to move out the foam vessel at a particular direction depending on the direction of the open area of the stator.

5.2.3 Foaming in a Tri-Cylindrical Vessel

Figure 5.10 shows the foaming performance of various impellers in a tri-cylindrical foam vessel, as shown in **Figure 4.47**, at the impeller rotation speed of 600-1400 rpm and the air flow rate of 5 l/min. Based on the results of bubble diameter, two groups of impellers can be classified: the impellers with small orifice size, but large orifice number (turbine A and D impellers) and the impellers with large orifice size but small orifice number (turbine B and C impellers). The former group of impellers seems to produce smaller bubble size. Based on the results of foam extent, two groups of impellers can be classified: the vertical flat blade impeller type (turbine A and B impeller) and the disc flat blade impeller type (turbine C and D impeller). The latter type of impellers trends to generate higher foam extent. These results suggest that a disc flat blade impeller with small size and large number of orifices is preferable for foaming.

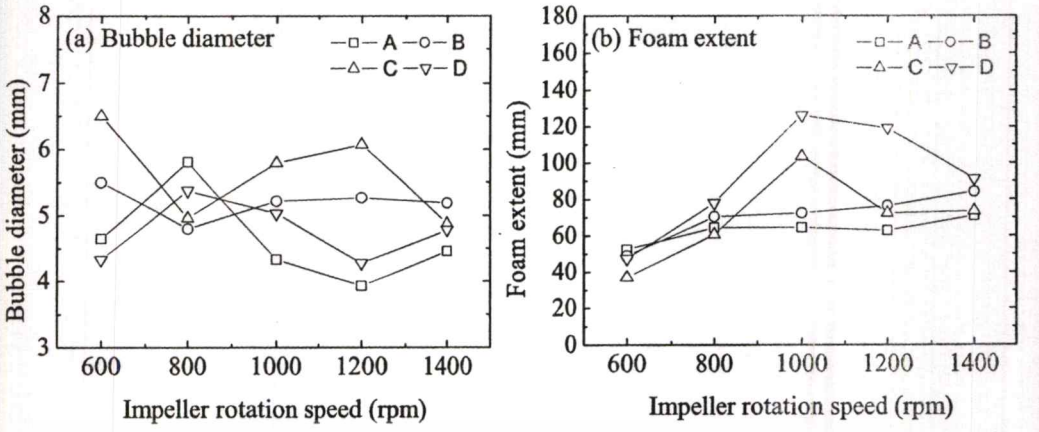

Figure 5.10 Comparison of foaming performance of impellers at the impeller rotation speed of 600-1400 rpm and the air flow rate of 5 l/min: (a) bubble diameter and (b) foam extent.

Apart from impeller design, stator also plays an important role on foaming. Two types of stators, with and without holes on the top of the stator, were used to equip with an impeller, and their foaming characteristics are shown schematically in **Figure 5.11**.

Figure 5.11 (a) shows that it is hardly to foam using the impeller equipped with the stator without any hole on the top since there is no significant pressure difference in the region above the stator and at the stator orifice. Unlike the stator with holes on the top, the floatation of bubbles is in the same direction of liquid flow and hence the mould located on the top of the stator was filled with the bubbles.

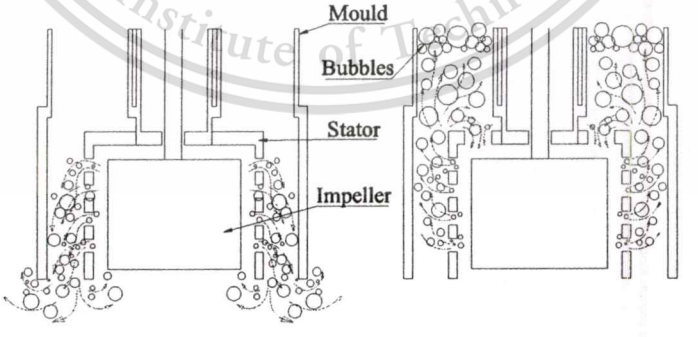

Figure 5.11 Schematic of bubble generation in a tri-cylindrical foam vessel by an impeller equipped with: (a) a stator without holes on the top and (b) a stator with holes on the top.

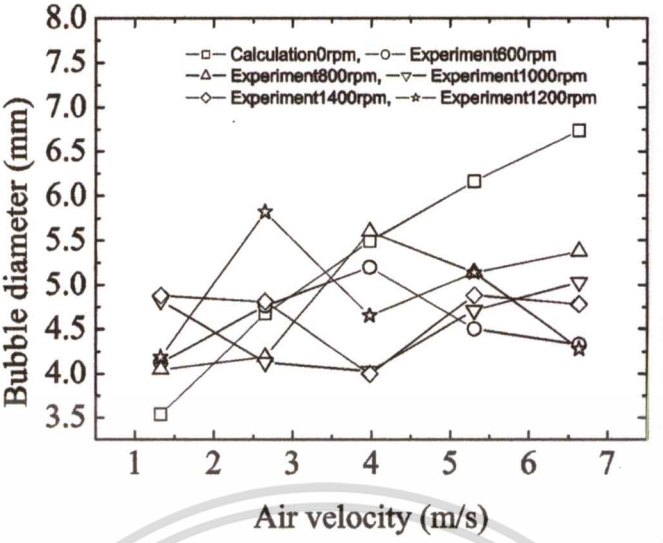

Figure 5.12 Comparison of bubble diameter generated by turbine D impeller between the produced water foam and the predicted water foam using the Valencia *et al.*'s equation (Valencia *et al.*, 2002) given in Table 2.4.

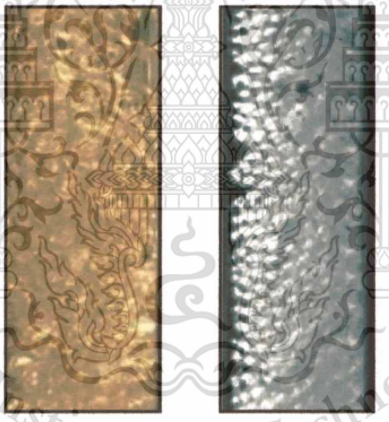

Figure 5.13 Comparison of foam appearance between (a) the water foam produced in this work and (b) the typical foam pattern called "critical foam" (Skurtys *et al.* 2008).

Based on the production calculation of bubble diameter using Valencia *et al.*'s mathematical model (Valencia *et al.*, 2002), the comparison of bubble diameter generated by turbine D impeller between the experiment and prediction is shown in **Figure 5.12**. The bubble diameter obtained from the experiment is similar to that of the prediction. The foam obtained in this experiment is classified as the critical foam type, as shown in **Figure 5.13**, similar to the foam occurred in the cylindrical foam vessel with top exit.

5.3 Difference of Foaming in Water and Molten Aluminium

The representative samples of water and aluminium foams produced using turbine D impeller are shown in **Figure 4.58**. It can be seen that aluminium foam samples contained smooth surface with some discontinuous portion. The effect of impeller rotation speed and air injection rate on the size of water and aluminium bubbles is plotted in **Figure 5.14**. It is noted that no experimental data at the air injection rate of 1 l/min presented since this air injection rate was found to be too low to generate bubbles in aluminium. At high impeller rotation speeds, the size of generated bubbles had a tendency to become significantly smaller for aluminium and relatively invariable for water, while the foam extent had a tendency to become slightly smaller for aluminium and significantly larger for water. At high air injection rates, both the bubble size and the foam extent trended to increase for aluminium, while the bubble size was invariable and the foam extent was larger at the impeller rotation speed beyond 800 rpm for water. In comparison of foam characteristics with water, the bubble size of aluminium was 2-4 times larger and foam extent of aluminium was approximately up to 2.5 times smaller. The difference observed might be attributed to the variation in physical properties between the two liquids, as shown in **Table 5.1**. Based on the parameters in **Table 4.4** and **Table 5.1**, and value of ρ_g at 900 °C, d_c of aluminium was predicted, using equation 5.1, to be 3.0 mm, which is approximately two times larger than the predicted value of water bubble diameter and 3-8 times smaller than experimental data of the aluminium foam samples in this work.

$$d_c = \left(\frac{3r_c\sigma}{2(\rho_l-\rho_g)g}\right) \tag{5.1}$$

where r_c is the orifice radius, σ is the surface tension, ρ_l is the liquid density, ρ_g is the injected gas density, g is the gravitational acceleration.

The larger size of aluminium bubbles comparing with that of water bubbles has also been found by other investigators. The difference between the predicted and experimental data in this work would be the tendency to form an oxide layer on aluminium bubbles and molten aluminium surface, and the different foaming mechanisms caused by different physical parameters.

In order to describe the foaming characteristics of the liquids having different physical and

geometric parameters, dynamic similarity criteria based on Weber, We, and Reynolds, Re, number are used. The former number, given in equation 5.2 and 5.3, represents the relative effect of inertial forces versus viscous force.

$$We = \frac{\rho_l N^2 D^3}{\sigma} \tag{5.2}$$

$$Re = \frac{\rho_l N D^3}{\mu} \tag{5.3}$$

Where N is the impeller rotation speed, D is the impeller diameter and μ is the liquid viscosity.

A bubble size in a stirring liquid is generally described by We, which combines the respective influence on bubble size of operating conditions, impeller geometry, rheological properties phase and surface tension of the continuous phase. The plot of bubble diameter of water and aluminium versus We, as shown in **Figure 5.15** (a), suggests that, at low We numbers, the size of bubbles trends to decrease with increasing We, while at high We numbers, the bubble size becomes independent of operating conditions. It seems to be a limit that increasing impeller rotation speed does not induce an increase in viscous forces. Consequently, no more bubble break-up occurs.

The plot of foam extent of water and aluminium versus Re, as shown in **Figure 5.15** (b), suggests that, at low Re numbers, the foam extent continuously increases with increasing Re. Further increasing Re numbers, the foam extent decreases and becomes nearly invariable at higher Re numbers. The results of these dimensionless parameter plots imply that in order to receive a smaller bubble size and a high foam extent, We number beyond 170 and Re number around 44000 are required. Higher impeller diameter and lower impeller rotation speed are therefore recommended in favour of aluminium foam production.

Table 5.1 Physical properties of water and aluminium.

Parameter	Water @23°C	Aluminium @900°C
Surface tension, σ (mN/m)	72.29	830.11
Density, ρ (kg/ m^3)	997.44	2301.11
Viscosity, μ (N.s/ m^2)	9.41×10^{-4}	8.11×10^{-4}

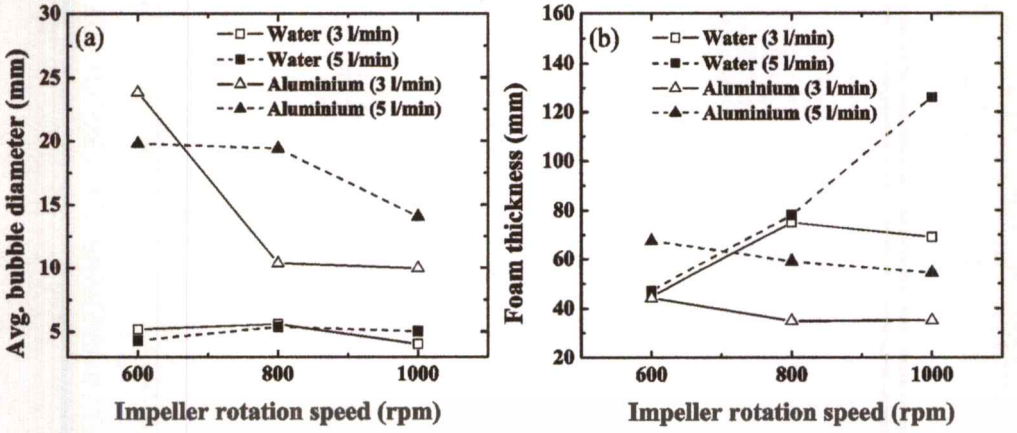

Figure 5.14 Comparisons of bubble in water and aluminium: (a) bubble size and (b) foam extent.

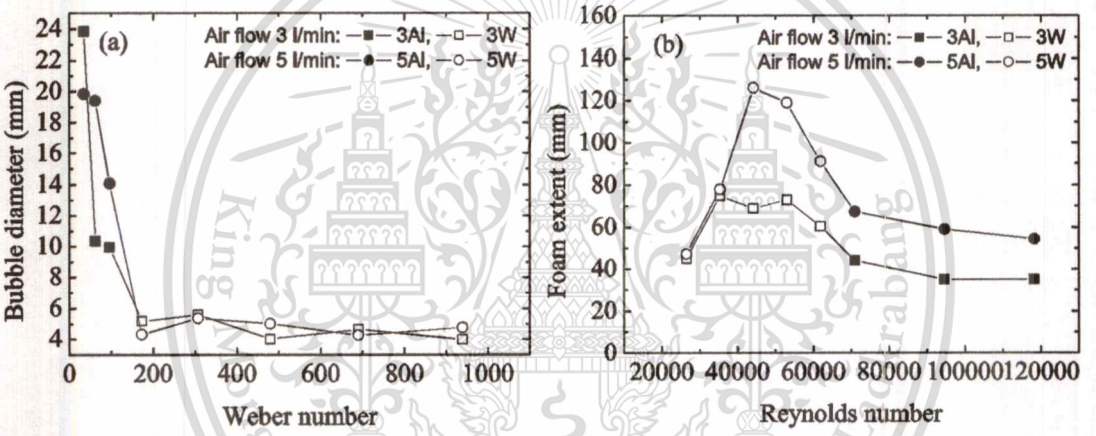

Figure 5.15 Characteristics of bubbles as a function of (a) Weber and (b) Reynolds number.

Figure 5.16 The appearance of (a) water foam and (b) aluminium foam produced in this work compared with (c) the typical foam pattern called "slug foam" (Skurtys *et al.*, 2008).

The type of foam generated in different fluid is different. **Figure 5.16** shows the foams produced in water and aluminium at the same foaming conditions comparing with the typical foam pattern called "slug foam" (Skurtys *et al.*, 2008). The alumionium foam obviously appeared to be the slug foam type while the water foam is the critical foam type. For the slug foam type, gas bubbles formed as gas pockets were deformed into "bullet" shape due to the tube wall effect (Skurtys *et al.* 2008). The average bubble size was larger than the size of tube. Different supply air temperature seem to cause the different appearance between the water and aluminium foams. For aluminium foam, the supply air was supposed to be heated from room temperature to the temperature of foam production, i.e. 700°C. As a result, air would be substantially expanded at the higher temperatures. Based on the relation among pressure, volume and temperature of a given ideal gas shown in equation 5.4, the volume of injected air at the tested condition in aluminium is estimated to be approximately 30 times higher than that of water.

$$\frac{P_1V_1}{T_1} = \frac{P_2V_2}{T_2} \tag{5.4}$$

where P is the pressure,

V is the volume,

T is the temperature.

5.4 Prototypes of Aluminium Foaming Generator

Based on the CFD simulation and physical water model experiments, two types of foam generator for aluminium foam production were developed: (1) a foaming generator in a foam vessel with side exit and (2) a foam generator in a tri-cylindrical foam vessel with top exit as shown in **Figure 4.53** and **Figure 4.56** respectively.

5.4.1 Foaming in a Foam Vessel with Side Exit

This foam generator can be used to produce aluminium foam in the form of sheet because bubbles can be forced out from the foam vessel directly to a sheet casting machine. The advantage of this generator is the capability of continuous foam production. There are two furnaces used with this generator: furnace for melting aluminium and a furnace for controlling temperature of the foam vessel. Therefore temperature drop during foaming in this foam generator occurred during the transfer of molten aluminium from the former to the latter furnace.

5.4.2 Foaming in a Tri-Cylindrical Foam Vessel

This foam generator can be used to produce a near net shape aluminium foam product provided that a mould is placed on the foam vessel. For example, a tri-cylindrical mould was used in this work to produce three identical cylindrical aluminium foams.

CHAPTER 6

CONCLUSIONS AND SUGGESTIONS

6.1 Conclusions

Gas injection is the cheapest method for mass production of aluminium foam, however it is difficult to produce aluminium foam with a controllable cell size and uniform structure. Therefore, effects of various parameters on foam formation such as impeller design, air flow rate, impeller rotation speed were investigated in this work. In this research, foaming apparatuses were set up to investigate foaming behaviour using water as a physical model and pure aluminium as an actual foam. In the physical water model, the smallest bubbles of about 3 mm in diameter were produced, which is about 2-4 times smaller than those of aluminium.

6.1.1 Foaming Mechanisms

Foam production using gas injection method is occurred from the accumulation of bubbles. In principle, bubbles generated in liquid rise to and sustain at liquid surface. The extent of foam depends on the rate of generation and rupture of the bubbles. A high generation rate and a low rupture rate of bubbles are required to receive the possibly highest foam extent. Stators were found in this work to effectively reduce the rupture rate of bubbles by minimising liquid disturbance. It is noted that during rising, bubbles size increases due to the decrease of liquid pressure. There are three phenomena occurring at the foam extent: drainage, coalescence and film rupture. Stability of foam depends on these phenomena which are based on surface tension, viscosity, surfactant and type of flow in the foam vessel.

6.1.2 Development of Impellers and Foam Generators

Impeller is the main component for aluminium foam production using a gas injection method to produce fine bubbles. However, the rotation of the impeller gives a negative effect of vortex and turbulent flow generation. The higher the impeller diameter, the larger the liquid disturbance. This problem can be solved by using a stator to equip with the impeller to reduce the liquid disturbance in the foam vessel as described in chapter 5. Stator can also be used to reduce

the size of bubbles generated by the impeller. Two types of foaming generator for aluminium foam production were developed in this research. The one was used with a foam vessel with side exit and the other was used with a tri-cylindrical foam vessel. They were used for producing aluminium foam in the foam of sheet and near net shape respectively.

6.2 Suggestions

Although this work has finished, it was only the first step of the development of foam generators for aluminium foam production. There are some suggestions to improve aluminium foam production process as described below.

1. Results of simulations of single phase fluid flow used in this research are expected to significantly differ from experiments which are multi-phase system. A multi-phase flow simulation software would be an alternative way to accurately predict the foaming behaviour of a liquid-gas system in the foam vessel.

2. Properties of water such as surface tension and viscosity should be adjusted to nearly equal to those of aluminium melt because foam formation depends largely on liquid properties.

3. For producing an aluminium foam sheet using the foam vessel with side exit as a foam generator, the temperature of molten aluminium should be substantially higher than the melting temperature of aluminium to compensate the temperature drop during melt transfer, which causes the premature solidification in the foam vessel.

4. For producing an aluminium foam product using the tri-cylindrical foam vessel as a foam generator, more experiments are required to improve aluminium foam production. Foam stability enhancement and mechanical property tests are important parameters for aluminium foams to be further investigated.

REFERENCES

Andreussi, P., Paglianti, A. and Silva, F.S. 1999. "Dispersed Bubble Flow in Horizontal Pipes" **Chemical Engineering Science**. 54: 1101-1107.

Andrews, E., Sanders, W., and Gibson, L.J. 1999. "Compressive and Tensile Behaviour of Aluminum Foams" **Materials Science and Engineering A**.270: 113–124.

Aly, M.S. 2007. "Behavior of Closed Cell Aluminium Foams upon Compressive Testing at Elevated Temperatures: Experimental Results" **Materials letters**. 61: 3138-3141.

Angarska, J. Stubenrauch, C. and Manev, E. 2007. "Drainage of Foam Films Stabilized with Mixtures of Non-Ionic Surfactants" **Colloids and Surfaces A**. 309: 189-197.

Babcsan, N., Banhart, J., and Leitlmeier, D. n.d. "Metal Foams-Manufacture and Physics of Foaming"

Bhakta, A. and Ruckenstein, E. 1997. "Decay of Standing Foam: Drainage, Coalescence and Collapse" **Advances in Colloid and Interface Science**. 70: 1-124.

Banhart, J. and Brinker, W. 1999. "Fatigue Behavior of Aluminum Foams" **Journal of Materials Science Letters**. 18: 617-619.

Banhart, J. 2000. "Manufacturing Routes for Metallic Foams" **Solidification** Science.

Banhart, J. 2001. "Manufacture, Characterisation and Application of Cellular Metals and Metal Foams" **Progress in Materials Science**. 46: 559–632.

Bennett, M.A., West, R.M., Luke, S.P. and Williams, R.A. 2002. "The Investigation of Bubble Column and Foam Processes using Electrical Capacitance Tomography" **Minerals Engineering**. 15: 225-234.

Banhart, J. 2005. "Aluminium Foams for Lighter Vehicles" **Int. J. Vehicle Design**, 37.

Banhart, J. 2006. "Metal Foams: Production and Stability" **Advanced Engineering Material**, 8: 781-794.

REFERENCES (CONT.)

Banhart, J. 2007. "Metal Foam-Fundamental Research to Application" **Frontiers in The Design of Materials**

Banhart, J. "Production Methods for Metallic Foams" in **Fraunhofer-Institute for Applied Materials Research.** Breman.

Bogdanovic, M., Gajbhiye, R.N. and Kam, S.I. 2009. "Experimental Study of Foam Flow in Horizontal Pipes: Two Flow Regimes and its Implications" **Colloids and Surfaces A.** 344: 56–71.

Cheremisinoff, N.P. 1990. **Handbook of Chemical Processing Equipment**: Butterworth-Heinemann.

Cho, Y.S. and Laskowski, J.S. 2002. "Effect of Flotation Frothers on Bubble Size and Foam Stability" **International of Mineral Processing.** 64: 69-80.

Carrera, J., Parthasarathy, R.N. and Gollahalli, S.R. 2006. "Bubble Formation From a Free-Standing Tube in Microgravity" **Chemical Engineering Science.** 61:7007-7018.

Cingi, C., Niini, E., Orkas, J. 2009. "Foamed Aluminum Parts by Investment Casting" **Colloids and Surfaces A.** 344: 113–117.

Cymat. **Auminium Foam Technology Applied to Automotive Design**

Deshpande, N.S. and Barigou, M. 2000. "The Flow of Gas-Liquid in Vertical Pipes" **Chemical Engineering Science.** 55: 4297-4309.

Deshmukh, N.A., Patil, S.S. and Joshi, J.B. 2006. "Gas Induction Characteristics of Hollow Self-Inducing Impeller" **Chemical Engineers Research and Design.** 84:124-132.

Deqing, W., Weiwei, X. and Ziyuan, S. 2006. "Cell Size Prediction of a Closed Aluminum Foam" **Materials Science and Engineering A.** 431: 298–305.

Deqing, W., Xiangjun, M., Weiwei, X., and Ziyuan, S. 2006. "Effect of Processing Parameters on Cell Structure of an Aluminum Foam" **Materials Science and Engineering A.** 420: 235–239.

REFERENCES (CONT.)

Deqing, W. and Chengxin, S. 2008. "Simulation of Aluminium Foam Formation and Distribution Uniformity" **J Mater Sci,** 43: 2825-2832.

Forrester, S. E., Rielly, C. D. and Carpenter, K. J. 1998. "Gas-Inducing Impeller Design and Performance Characteristics" **Chemical Engineering Science**. 53: 603-615.

Gorain, B.K., Franzidis, J.P. and Manlapig, E.V. 1995. "Studies on Impeller Type, Impeller Speed and Air Flow Rate: Part 1" **Minerals Engineering**. 8: 615-635.

Gergely, V. and Clyne, T.W. 2004. "Drainage in Standing Liquid Metal Foam: Modeling and Experimental Observation" **Acta Materaialia**. 52: 3047-3058.

Grau, R.A. and Heiskanen, K. 2005. "Bubble Size Distribution in Laboratory Scale Flotation Cells" **Minerals Engineering**. 18: 1164-1172.

Gerlach, D., Alleborn, D., Buwa, V. and Durst, F. 2007. "Numerical Simulation of Periodic Bubble Formation at a Submerged Orifice with Constant Gas Flow Rate" **Chemical Engineering Science**. 62:2109-2125.

Hernandez-Aguilar, J.R., Cunningham, R. and Finch, J.A. 2006. "A Test of the Tate Equation to Predict Bubble Size at an Orifice in the Presence of Frother" **Int. J. Miner. Process**. 79: 89– 97.

Higuera, F.J. and Medina, A. 2006. "Injection and Coalescence of Bubbles in a Quiescent Inviscid Liquid" **European Journal of Mechanics B/ Fluids**. 25: 164-171.

Ito, K., and Kobayashi, H. 2006. "Production and Fabrication Technology Development of Aluminium Useful for Automobile Lightweighting" 8: 828-835.

Jamialahmadi, M., Zehtaban, M. R., Mullersteinhagen, H., Sarrafi, A. and Smith, J. M. 2001. "Study of Bubble Formation under Constant Flow Conditions" **Institution of Chemical Engineers**. 79.

REFERENCES (CONT.)

Joshi, K.S., Jeelani, S.A.K., Blickenstorfer, C., Naegeli, I. and Windhab, E.J. 2005. "Influence of fatty alcohol antifoam suspensions on foam stability" **Colloids and Surfaces A.** 263: 239-249.

Khristov, K. and Exerowa, D. 1995. "Influence of the Foam Film Type on the Foam Drainage Process" Colloids and Surfaces A. 94: 303-309.

Kretz, R., Hausberger, K., and Gotzinger, B. 2002. "Energy-Absorbing Behavior of Aluminium Foam: head Impact Test on the A-pillar of a Car" **Advanced Engineering Materials.** 4: 781-785.

Krishna, R., and Ellenberger, J. 2003. "Influence of Low-Frequency Vibration on Bubble and Drop Sizes Formed at a Single Orifice." **Chemical Engineering and Processing.** 42: 15-21.

Koza, E., Leonowicz, M., Wojciechowski, S. and Simancik, F. 2003. "Compressive Strength of Aluminium Foams" **Materials Letters.** 58: 132– 135.

Kantarci, N., Borak, F. and Ulgen, K.O. 2005. "Bubble Column Reactors" **Process Biochemical.** 40: 2263–2283.

Kulkarni, A.A. and Joshi, J.B. 2005. "Bubble Formation and Bubble Rise Velocity in Gas-Liquid Systems: A Review" **Ind. Eng. Chem. Res.** 44: 5873-5931.

Kruglyakov, P.M., Karakashev, S.I., Nguyen, A.V., and Vilkova, N.G. 2007. "Foam Drainage" **Current Opinion in Colloid and Interface Science.** 13: 163-170.

Kogawa, H., Shobu, T., Futakawa, M., Bucheeri, A., Haga, K. and Nao, T. 2008. "Effect of Wettability on Bubble Formation at Gas Nozzle under Stagnant Condition" **Journal of Nuclear Material.** 377: 189-194.

Loubière, K. and Hébrard, G. 2003. "Bubble Formation from a Flexible Hole Submerged in an Inviscid liquid" **Chemical Engineering Science.** 58: 135-148.

REFERENCES (CONT.)

Larmignat, S., Vanderpool, D., Lai, H.K. and Pilon, L. 2008. "Rheology of Colloidal Gas Aphrons (Microfoams)" **Colloids and Surfaces A: Physicochem. Eng. Aspects.** 322: 199–210.

Miyoshi, T., Itoh, M., Mukai, T., Kanahashi, H., Kohzu, H., Tanabe, S. and Higashi, K. 1999. "Enhancement of Energy Absorption in a Closed cell Aluminum by the Modification of Cellular Structures" **Scripta Materialia.** 41: 1055–1060.

Matijasevic, B., and Banhart, J. 2006. "Improvement of Aluminium Foam Technology by Tailoring of Blowing Agent" **Scripta Materialia.** 54: 503–508.

Meloy, J.R., Neethling, S.J. and Cilliers, J.J. 2007 "Geometric Dispersion of Unattached Particles in Foams" **Colloids and Surfaces A.** 309 : 246–253.

1. Malysa, K. and Lunkenheimer, K. 2008. "Foam under Dynamic Conditions" **Current Opinion in Colloid and Interface Science.** 13: 150-162.

Matin, M., Montes, F.J., and Galan, M.A. 2009. "Physical Explanation of the Empirical Coefficients of Gas-Liquid Mass Transfer Equations" **Chemical Engineering Science.** 64: 410-425.

Nahra, H.K. and Kamotani, Y. 2000. "Bubble Formation from Wall Orifice in Liquid Cross Flow under Low Gravity" **Chemical Engineering Science.** 55: 4653-4665.

Nahra, H.K. and Kamotani. 2003. "Prediction of Bubble Diameter at Detachment from a Wall Orifice in Liquid Cross Flow under Reduced and Normal Gravity Conditions" **Chemical Engineering Science.** 58: 55 – 69.

2. Neethling, S.J., Lee, H.T. and Cilliers, J.J. 2003. "Simple Relationships for Predicting the Recovery of Liquid from Flowing Foams and Froths" **Minerals Engineering.** 16: 1123-1130.

Nienow, A.W. and Bujalski, W. 2004. "The Versatility of Up-Pumping Hydrofoil Agitations" **Chemical Engineering Research and Design.** 82: 1073-1081.

REFERENCES (CONT.)

Narsimhan, G. and Wang, Z. 2006. "Rupture of Equilibrium Foam Films due to Random Thermal and Mechanical Perturbations" **Colloids and Surfaces A**. 282-283: 24-36.

Oak, S.M., Kim, B.J., Kim, W.T., Chun, M.S. and Moon, Y.H. 2002. "Physical Modeling of Bubble Generation in Foamed-Aluminum" **Journal of Materials Processing Technology**. 130–13: 304–309.

Pamperin, O. 1995. "Influence of Buoyancy on Bubble Formation at Submerged Orifices" **Chemical Engineering Science**. 50: 3009-3024.

Patwardhan, A.W. and Joshi, J.B. 1999. "Design of Gas-Inducing Reactors" **Ind. Eng. Chem. Res**. 38:49-80.

Pilon, L., and Viskanta. 2004. "Minimum Superficial Gas Velocity for Onset of Foaming" **Chemical Engineering and Processing**. 43: 149-160.

Parkinson, L., Sedev, R., Fornasiero, D. and Ralston, J. 2008. "The Terminal Rise Velocity of 10–100 μm Diameter Bubbles in Water". **Journal of Colloid and Interface Science**. 322: 168-172.

SimanČík, F., Degischer, H.P. and Wörz, H. 1995. "Foamed Aluminium-Light Structural and Insulation Material" In: Euromat '95, Venice/Padua, Italy, 25. - 28 September, Assoziazione Italiana di Metallurgica, Milano, 1995

Sam, A., Gomez, C.O., and Finch, J.A. 1996. "Axial Velocity Profiles of Single Bubbles in Water/Frother Solutions" **International of Mineral Processing**. 47: 177-196

SimanČík, F. and Schoerghuber, F. 1998. "Complex Foamed Aluminum Parts as Permanent Cores in Aluminum Castings" 151-157. in MRS Symposium Proceedings. Pennsylvania: Materials Research Society.

SimanČík, F. 2001. "Metallic Foams – Ultra Light Materials for Structural Applications" **INŻYNIERIA MATERIAŁOWA**. 5: 823-828.

REFERENCES (CONT.)

Ramamurty, U. and Paul, A. 2004. "Variability in Mechanical Properties of a Metal foam" **Acta Materialia**. 52: 869–876.

Ruzicka, M.C., Bunganic, R. and Drahos, J. 2009. "Meniscus Dynamimics in Bubble Formation: Part II: Model". Chemical Engineering Research and Design.

Salman, W., Gavriilidis, A and Angeli, P. 2006. "On the Formation of Taylor Bubbles in Small Tubes" **Cemical Engineering Science**. 61: 6653-6666.

Stevenson, P. 2006. "Dimensional Analysis of Foam Drainage" **Chemical Engineering Science**. 61: 4503 – 4510.

Song, Z., and Nutt, S.R. 2007. "Rheology of Foaming Aluminum Melts" **Materials Science Engineering A**. 458: 108-115.

Srivastava, V.C. and Sahoo, K.L. 2007. "Processing, Stabilization and Applications of Metallic Foams. Art of Science" **Materials Science-Poland**. 25.

Simulescu, V., Angarska, J. and Manev, E. 2008. "Drainage and Critical Thickness of Foam Films from Aqueous Solutions of Mixed Nonionic Surfactants" **Colloids and Surfaces A**. 319: 21-28.

Skurtys, O., Bouchon, P. and Aguilera, J.M. 2008. "Foam of Bubble and Foam in Gelatine Solutions within a Vertical Glass Tube" **Food Hyrocolloids**. 22: 706-714.

Sobrino, C., Acosta-Iborra, A.,Santana, D. and Vega, M.D. 2009. "Bubble Characteristics in a Bubbling Fluidized Bed with a Rotating Distributor" **International Journal of Multiphase Flow**.

Tsuge, H., Terasaka, K., Koshida, W. and Matsue, H. 1997. "Bubble Formation at Submerged Nozzles for Small Gas Flow Rate under Low Gravity" **Chemical Engineering Science**. 52: 3415-3420.

REFERENCES (CONT.)

Tsuge, H., Tezuka, Y. and Mitsudani, M. 2006. "Bubble Formation Mechanism from Downward Nozzle—Effect of Nozzle Shape and Operating Parameters" **Chemical Engineering Science**. 61: 3290 – 3298.

Valencia, A., Cordova, M., and Ortega, J. 2002. "Numerical Simulation of Gas bubbles Formation at a Submerged Orifice in a Liquid." **Int. Comm. Heat Mass Transfer**. 29: 821-830.

Vardar-sukan, F. 1998. "Foaming: Consequences, Prevention and Destruction" **Biotechnology Advances**. 16: 913-948.

Vitankar, V.S., Dhotre, M.T. and Joshi, J.B. 2002. "A Low Reynolds Number k-ε Model for the Prediction of Flow Pattern and Pressure Drop in Bubble Column Reactor" **Chemical Engineering Science**. 57:3235-3250.

Vignes-Adler, M. and Weaire, D. 2008. "New Foam: Fresh Challenges and Opportunities" **Current Opinion in Colloid and Interface Science**. 13:141-149.

Walas, S. M. 1990. **Chemical Process Equipment**: Butterworth-Heinemann.

Warke, V.S., Shankar, S. and Makhlouf, M.M. 2005. "Mathematical Modeling and Computer Simulation of Molten Aluminium Cleansing by the Rotating Impeller Degasser: PartII: Removal of hydrogen gas and solid particles" **Journal of Materials Processing Technology**. 168: 119-126.

Yang, G. Q., Du, B., Fan, L. S. 2006. "Bubble Formation and Dynamics in Gas-Solid-Fluidization-A Review." **Chemical Engineering Science**. 62: 2-27.

Yu, H., Guo, Z., Li, B., Yao, G., Luo, H. and Liu, Y. 2007. "Research into the Effect of Cell Diameter of Aluminum Foam on its Compressive and Energy Absorption Properties" **Materials Science and Engineering A**. 454–455: 542–546.

Yang, D., Hur, B. and Yang, S. 2007. "Study on Fabrication and Foaming Mechanism of Mg Foam using $CaCo_3$ as Blowing Agent" **Journal of Alloys and Compound**.

REFERENCES (CONT.)

Yapici, K., Karasozen, B., Schäfer, M. and Uludag, Y., 2008 "Numerical Investigation of the Effect of the Rushton Type Turbine Design Factors on Agitated Tank Flow Characteristics" **Chemical Engineering and Processing**. 47: 1340-1349.

Zhang, W. and Tan, R.B.H. 2000. "A Model for Bubble Formation and Weeping at a Submerged Orifice" **Chemical Engineering Science**. 55:6243-6250.

Zhang, L. and Shoji, M. 2001. "Aperiodic Bubble Formation From a Submerged Orifice" **Chemical Engineering Science**. 56:5371-5381.

Zhang, Y., Sam, A. and Finch, J.A. 2003. "Temperature effect on Single Bubble Velocity Profile in Water and Surfactant Solution" **Colloids and Surfaces A.** 223: 45 -54.

Zhang, C., Eckert, S., and Gerbeth, G. 2005. "Experimental Study of Single Bubble Motion in a Liquid Metal Column Exposed to a DC Magnetic Field" **International Journal of Multiphase flow**. 31: 824–842.

BIOGRAPHY

Name: Mr. Yok Nusom

Date of Birth: October 2, 1984

Place of Birth: Chumphon

Education:

May 2007 - July 2010	M. Eng in Automotive Engineering (International program), International College, King Mongkut's Institute of Technology Ladkrabang (KMITL)
May 2003 – Mar 2007	B. Eng in Agricultural Machinery Engineering, Department of Agricultural Engineering, Faculty of Engineering, Rajamangala University of Technology Thanyaburi (RMUTT)

Scholarship:

2007-2009	Full scholarship for study in the master degree from National Science and Technology Development Agency (NSTDA)

Experience:

March 2010 - Present	Engineer: National Metal and Material Technology Center (MTEC)
October 2008 – February 2010	Engineer: Excellent Center for EcoProduct (XCEP)

Publications/ Presentation / Patents:

1. Y. Nusom, N. Depaiwa, T. Adachi and S. Srimanosaowapak, "Comparative Study of Bubble Formation between Water and Molten Aluminium for Manufacturing of Aluminium Foam", *ICMAT 2009 - International Conference on Materials for Advanced Technologies*, 28 June - 3 July 2009, Singapore, p. 28 – 29 (Oral).

2. Y. Nusom, N. Depaiwa, T. Adachi and S.

Srimanosoawapak, "Aluminium Foams towards Automotive Industry Implementation in Thailand", Published in CD Proceeding of *ICAE – 5 – International Conference on Automotive Engineering*, 30 March – 2 April 2009, Bangkok, Thailand, 2:1 – 7 (Oral).

3. S. Srimanosaowapak and Y. Nusom, "Foam Generator with Controllable Bubble Feeding Direction", Patent Application No. 0901005077, Thailand Department of Intellectual Property, Filed on 13 November 2009.

4. S. Srimanosaowapak, Y. Nusom and P. Wattanapornphan, "Apparatus for Metallic Foam Component Production in a Multi-Cavity Mold", Patent Application No. 1001000069, Thailand Department of Intellectual Property, Filed on 15 January 2010.